Solution NMR studies of J-domain co-chaperones and bacterial outer membrane permeability

Inauguraldissertation

zur

Erlangung der Würde eines Doktors der Philosophie

vorgelegt der

Philosophisch-Naturwissenschaftlichen Fakultät

der Universität Basel

von

Johanna Viola Ude

aus Freiburg i. Br., Deutschland

Basel, 2023

Originaldokument gespeichert auf dem Dokumentenserver der Universität Basel edoc.unibas.ch

Genehmigt von der Philosophisch-Naturwissenschaftlichen Fakultät

auf Antrag von

Prof. Dr. Sebastian Hiller

Prof. Dr. Anne Spang

Basel, den 02.03.2021

Prof. Dr. Marcel Mayor
Dekan

Table of Contents

List of Abbreviations

%	percent
°	degree
°C	degree Celsius
2D	2-dimensional
3D	3-dimensional
Å	Angstrom, unit of length (10^{-10} m)
α1	α-helix 1
α2	α-helix 2
α3	α-helix 3
α4	α-helix 4
A	alanine
ADP	adenosine diphosphate
Ala	alanine
AprF	alkaline protease secretion protein AprF
Arg	arginine
Asp	aspartic acid
ATP	adenosine triphosphate
ATPase	class of enzymes catalyzing the conversion of ATP to ADP or the inverse reaction
ATPγS	adenosine-5'-(γ-thio)-triphosphate
BiP	binding immunoglobulin protein
C_α	carbon atom in α position
C_β	carbon atom in β position
Cas	CRISPR-associated protein
CcpNmr	Collaborative computational project for NMR / NMR software suite
CFTR	cystic fibrosis transmembrane conductance regulator
CIL	Cambridge Isotope Laboratories
CRISPR	clustered regularly interspaced short palindromic repeats

CSP	chemical shift perturbation
CTDI	C-terminal domain I
CTDII	C-terminal domain II
CYANA	combined assignment and dynamics algorithm for NMR applications software
D	aspartic acid
D_2O	deuterium oxide
DD	dimerization domain
DI/VF motif	protein sequence motif containing Asp-Ile/Val-Phe
DnaJ	heat shock protein of 40 kDa
DnaK	heat shock protein of 70 kDa
DNAJA1	DnaJ heat shock protein family member A1
DNAJB1	DnaJ heat shock protein family member B1
DNAJB2	DnaJ heat shock protein family member B2
DNAJB6	DnaJ heat shock protein family member B6
DNAJB6b	DnaJ heat shock protein family member B6b
DNAJB8	DnaJ heat shock protein family member B8
DNAJC6	DnaJ heat shock protein family member C6
DNAJC13	DnaJ heat shock protein family member C13
DNAJC19	DnaJ heat shock protein family member C19
DSS	2,2-dimethyl-2-silapentane-5-sulfonate
E	glutamic acid
EDTA	ethylenediaminetetraacetic acid
EEVD motif	protein sequence motif containing Glu-Glu-Val-Asp
EPR	electron paramagnetic resonance
ER	endoplasmic reticulum
ERAD	ER-associated degradation
ERdj	endoplasmic reticulum domain j
ERdj1	DnaJ heat shock protein family member C1
ERdj2	DnaJ heat shock protein family member C23
ERdj3	DnaJ heat shock protein family member B11

ERdj3^{J}	J-domain of ERdj3 without the GF-region
ERdj3^{JGF}	J-domain of ERdj3 including the GF-region
ERdj4	DnaJ heat shock protein family member B9
ERdj4^{J}	J-domain of ERdj4 without the GF-region
ERdj4^{JGF}	J-domain of ERdj4 including the GF-region
ERdj5	DnaJ heat shock protein family member C10
ERdj6	DnaJ heat shock protein family member C3
ERdj7	DnaJ heat shock protein family member C79
ERdj8	DnaJ heat shock protein family member C16
F	phenylalanine
FadL	fatty acid outer membrane porin
FpvA	Pseudomonas aeruginosa ferric pyoverdine receptor
g	gram
G	glycine
GF-region	region rich in glycine and phenylalanine
Gln	glutamine
Glu	glutamic acid
GRP78	glucose-regulated protein of 78 kDa
GRP94	glucose-regulated protein of 94 kDa
GrpE	bacterial nucleotide exchange factor
GTP	guanosine triphosphate
HD	high definition
Hdj1	DnaJ heat shock protein family member
Hdj2	DnaJ heat shock protein family member
HEPES	4-(2-hydroxyethyl)-1-piperazineethanesulfonic acid
His	histidine
Hlj1	DnaJ heat shock protein family member B4
HMQC	heteronuclear multiple quantum correlation
HNCACB	triple resonance NMR experiment correlating ^{1}H and ^{15}N amide resonances with intra- and inter-residue $^{13}C_{\alpha}$ and $^{13}C_{\beta}$ resonances

HNCOCACB	triple resonance NMR experiment correlating ^{1}H and ^{15}N amide resonances with $^{13}C_{\alpha}$ and $^{13}C_{\beta}$ resonances of the preceding residue
HPD motif	conserved motif in protein sequence containing His-Pro-Asp
Hsp40	heat shock protein of 40 kDa
Hsp60	heat shock protein of 60 kDa
Hsp70	heat shock protein of 70 kDa
Hsp90	heat shock protein of 90 kDa
Hsp100	heat shock protein of 100 kDa
Hsp110	heat shock protein of 110 kDa
HSQC	heteronuclear single quantum coherence
I	isoleucine
Ile	isoleucine
ILV-labeled	selectively Ile, Leu and Val ^{13}C methyl-labeled
IPTG	isopropyl-β-D-thiogalactopyranoside
IR	infrared
Ire1	inositol-requiring enzyme 1
JDP	J-domain protein
K	lysine
KCl	potassium chloride
K_D	dissociation constant
kDa	kilodalton
KDEL motif	conserved motif in protein sequence containing Lys-Asp-Glu-Leu, ER-retention motif
L	leucine
[L]	concentration of ligand
LamB	Maltose porin
LB medium	lysogeny broth medium / Luria-Bertani medium
LED	light-emitting diode
Leu	leucine
LPS	lipopolysaccharide
Lys	lysine

M	methionine
M / (M)	molarity
M9-medium	M9 minimal medium
µM	micromolar
Mbp	mega base pair
MD	molecular dynamics
MegaX	molecular evolutionary genetics analysis software version X
Met	methionine
mg	milligram
$MgCl_2$	magnesium chloride
min	minutes
mM	millimolar
MST	microscale thermophoresis
NaCl	sodium chloride
NaH_2PO_4	sodium dihydrogen phosphate
NBD	nucleotide binding domain
ND_4Cl	deuterated ammonium chloride
NEB	New England Biolabs
NEF	nucleotide exchange factor
NH_4Cl	ammonium chloride
nm	nanometer
nM	nanomolar
NMR	nuclear magnetic resonance
NMRPipe	nuclear magnetic resonance data processing software
NOE	nuclear Overhauser effect
NOESY	nuclear Overhauser effect spectroscopy
NTA	nitrilotriacetic acid
NUS	non-uniform sampling
Occ	outer membrane carboxylate channel
OccD	OprD-like Occ subfamily
OccK	OprK-like Occ subfamily

OD_{600}	optical density at a wavelength of 600 nm
OmpC	outer membrane porin C (*E. coli*)
Opd	outer membrane protein D family
OprD	outer membrane porin D (*P. aeruginosa*)
OprK	outer membrane porin K (*P. aeruginosa*)
p53	cellular tumor antigen p53
PA7	*Pseudomonas aeruginosa* strain PA7
PA14	*Pseudomonas aeruginosa* strain PA14
PAO1	*Pseudomonas aeruginosa* strain PAO1
PDB	protein data bank
PDI	protein disulfide isomerase
PEP	phosphoenolpyruvate
PG	preparative grade
pH	negative of the base 10 logarithm of the molar concentration of protons in a solution
Phe	phenylalanine
ppm	parts per million
Pro	proline
PseudoCAP	*Pseudomonas aeruginosa* Community Annotation Project
PupA / PupB	ferric pseudobactin receptor
qMDD	quantum multiple-valued decision diagram
QS	quorum sensing
R	arginine
RefSeq	reference sequence
RNQ	rich in asparagine and glutamine
S_b	signal of the bound ligand
SBD	substrate binding domain

SBDα	α-subdomain of the substrate binding domain
SBDβ	β-subdomain of the substrate binding domain
Sec61	heterotrimeric translocon complex
S_f	signal of the free ligand
Sis1	class B JDP from *Saccharomyces cerevisiae*
S_{obs}	signal of the ligand
stdv	standard deviation
SUMO	small ubiquitin-related modifier
SWISS-MODEL	server for automated comparative modeling of 3-dimensional protein structures
T	threonine
TALOS+	software for prediction of protein backbone torsion angles from NMR chemical shift data
TB medium	terrific broth medium
TCI probe	cryogenic, inverse triple resonance probe
TEV	tobacco etch virus
TNFα	tumor necrosis factor α
TOCSY	total correlation spectroscopy
TPR	tetratricopeptide repeat
TRIS	tris(hydroxymethyl)aminomethane
TRX domain	Thioredoxin domain
Tsx	nucleoside-specific porin
U-	uniformly labeled
ULP	SUMO protease / fragment of ubiquitin-like-specific protease 1
UPR	unfolded protein response
V	valine
Val	valine
WT	wild type
XPLOR-NIH	software for structure determination by NMR
Y	tyrosine
Ydj1	yeast homolog of human DNAJA1/DNAJA2

Abstract

The ubiquitous chaperone Hsp70 is a major player in guiding and controlling cellular protein folding processes. It is ATP-dependent and co-chaperoned by individual members of the diverse class of J-domain proteins (JDPs). By synergistic action, these co-chaperones mediate a plethora of versatile functions such as protein maturation, disaggregation, protein translocation and degradation. JDPs bind client proteins and transfer them to Hsp70 while simultaneously stimulating the intrinsically low ATP hydrolysis rate of Hsp70 with their highly conserved J-domain. Here, we compare the structural and functional characteristics of the conserved GF-region of two JDPs from the endoplasmic reticulum (ER), ERdj3 and ERdj4, using NMR spectroscopy. We demonstrate that the GF-region of ERdj3 and ERdj4 forms an α-helix (helix 5) as has been observed for cytoplasmic DNAJB1. However, in stark contrast to their cytoplasmic counterpart, the helix 5 of ERdj3 and ERdj4 populates a conformational equilibrium of the folded helix docked to the J-domain and an undocked disordered conformation. Interestingly, helix 5 occupies the same binding interface involved in binding to the ER-resident Hsp70 BiP during the stimulation of ATP hydrolysis. We then show that the binding of helix 5 to the J-domain is characterized by different binding strengths which results in distinct functional consequences for the interaction of ERdj3 and ERdj4 with BiP. While for ERdj4 helix 5 binds strongly to the J-domain and thereby inhibits the interaction with BiP, it has no impact on the functional synergy between BiP and ERdj3. Therefore, we conclude that the GF-region confers specificity with respect to BiP binding among these two ER-resident JDPs.

Pseudomonas aeruginosa can cause severe infections and constitutes a substantial challenge for human health due to its resistance to antibiotics and disinfectants. An important factor for this intrinsic antibiotic resistance is the remarkably low permeability of the outer membrane of *P. aeruginosa* with respect to the uptake of nutrients and drugs. Translocation of molecules across the outer membrane is tightly regulated by a large number of specific porins. Unlike other Gram-negative bacteria, *P. aeruginosa* simultaneously achieves a high metabolic versatility and a particularly low outer membrane permeability. Herein, we address this paradox by investigating the role of these porins in antibiotic and nutrient uptake. We established an NMR based assay in combination with

genetically modified *P. aeruginosa* strains that allowed us to measure substrate consumption of individual porins under *in vivo* conditions. Our data reveal, that except for the porin OprD, the porins do not constitute an entry for antibiotics into the cell. Systematic *in vivo* NMR spectroscopy-based measurements of the translocatome of the outer membrane porins reveal promiscuous overlapping substrate profiles for 14 tested porins suggesting specificity by exclusion rather than by selective import of substances. Surprisingly, we find that positively charged and hydrophobic substrates can pass the outer membrane in a porin-independent manner. In contrast, the specific porins are required for the transport of molecules with two or more carboxylate groups. These findings elucidate the role of different porins and the outer membrane in antibiotics permeation and provide new insights to improve and develop new antimicrobial compounds for the treatment of infectious diseases

Introduction into NMR spectroscopy

Nuclear magnetic resonance (NMR) spectroscopy is widely used to investigate structural features of molecules ranging from small organic compounds to macromolecules such as proteins or DNA. In the field of protein structural biology, NMR spectroscopy offers a vast variety of experiments that can be used to address specific topics such as structure elucidation, protein dynamics, biochemical features of a protein and protein interactions with other molecules such as proteins, DNA or small molecules.

NMR spectroscopy is based on the nuclear spin angular momentum I, an intrinsic property characteristic for nuclei. Nuclei with a spin I = ½ are of major importance in NMR spectroscopy, however most chemical elements do not have a spin I = ½. Luckily for structural biologists, one of the most abundant chemical elements, hydrogen (^{1}H) has this favourable property and so-called NMR-active isotopes of nitrogen (^{15}N) and carbon (^{13}C) can easily be incorporated into recombinantly expressed proteins by the use of minimal media containing these isotopes as sole nitrogen or carbon source (Fig I).

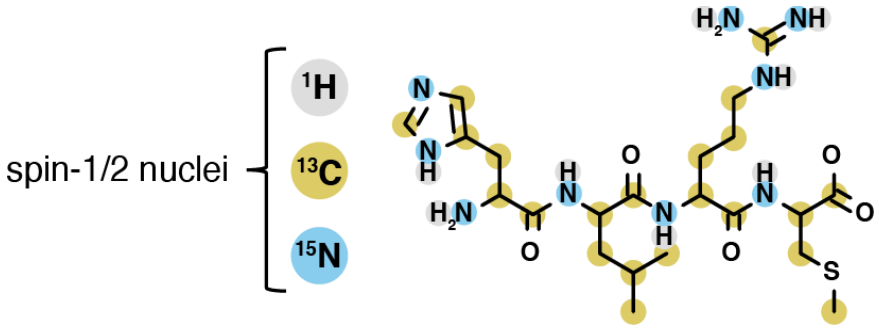

Figure I: NMR-active nuclei with spin I = ½. The most abundant isotope of carbon is ^{12}C and that of nitrogen is ^{14}N, respectively. Their spin angular momentum is I = 0 which renders these nuclei NMR-invisible. Therefore, protein NMR spectroscopy requires the incorporation of ^{13}C and ^{15}N into the respective protein sample by recombinant expression in minimal media enriched with these isotopes.

When placed in an external magnetic field, the spin angular momentum of NMR-active nuclei (I≠0) can transition between (2I +1) spin energy levels. For spin I =1/2 nuclei this results in 2 energy levels, E_α and E_β. This splitting between spin energy levels is called the nuclear Zeeman splitting and the transition between these energy levels is associated to a frequency, ν_0:

$$\begin{aligned} \Delta E_{\alpha\to\beta} &= E_\beta - E_\alpha \\ &= \frac{h}{2\pi}\gamma B_0 \\ &= h\upsilon_0 \end{aligned} \tag{1}$$

B_0: magnetic field strength

γ: gyromagnetic ratio

h: Planck's constant, h = 6.62607015 e^{-34} J s

The gyromagnetic ratio γ is a unique property of each nucleus, it is the proportionality constant that relates the intrinsic spin angular momentum I to the intrinsic magnetic moment of a nucleus. ν_0 is called the Larmor frequency, it is unique for each nucleus and it is this frequency giving rise to the typical peaks in an NMR spectrum. A sample containing solely one sort of nuclei results in an NMR spectrum showing one peak at the Larmor frequency ν_0 (Fig II).

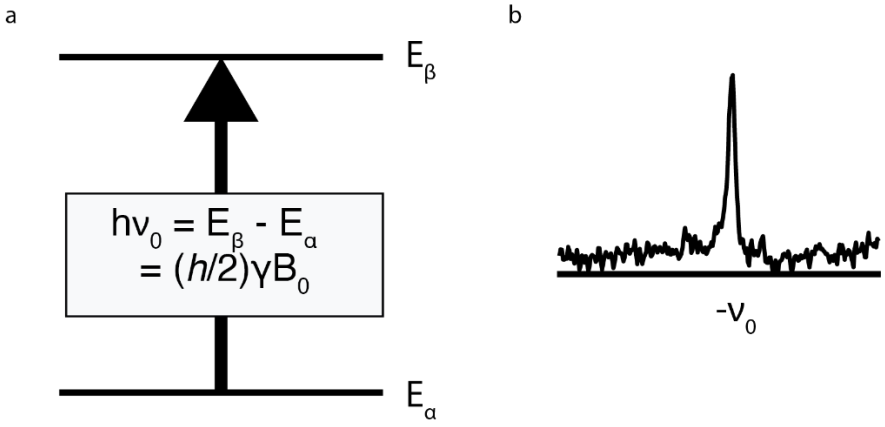

Figure II: The Zeeman effect leads to two distinct energy levels for nuclei with a spin I = ½. The Larmor frequency is the frequency associated with the transition between the two energy levels E_α and E_β (a), giving rise to the characteristic peaks in an NMR spectrum (b).

As can be seen from equation (1), the Larmor frequency ν_0 depends on the strength of the external magnetic field B_0. Therefore, NMR spectroscopy requires the use of strong magnets with large field strengths in order to increase the energy difference between the two levels and thereby enhance the sensitivity. However, the applied magnetic field is not the only field a nucleus in a molecule experiences. In a molecule each nucleus is surrounded by other atoms. These atoms by themselves generate a magnetic field by the circulation of electrons around the nucleus and the intrinsic magnetic moments of the electrons and the nuclei. Therefore, each nucleus in a molecule is affected by a unique magnetic field which results in a unique Larmor frequency. The influence of the local electronic environment on the Larmor frequency is called the chemical shift of a nucleus. The presence of the magnetic moment of other nuclei accounts for an effect called nuclear spin-spin coupling. This effect appears for nuclei that are either coupled through a chemical bond (J-coupling) or through space (dipole-dipole coupling). Both effects further add to the uniqueness of the Larmor frequency for each nucleus. This leads to what is commonly called the NMR fingerprint of a molecule and can be used to derive structural information about the molecule.

NMR spectroscopy is a method with very low sensitivity compared to other spectroscopic methods. This is due to the small difference between the populations p_α and p_β of the two energy E_α and E_β levels which populate according to the Boltzmann distribution.

$$\frac{p_\beta}{p_\alpha} = e^{\frac{\Delta E_{\alpha\beta}}{k_B T}} \quad (2)$$

k_B: Boltzmann constant, k_B = 1.380640 e^{-23} J/K

T: temperature

However, technical and methodological advances such as the development of high field magnets[1], cryogenic probes[2], methods for the suppression of the water signal[3,4] and most importantly the development of higher dimensional correlation spectra[5] have led a to large set of diverse experiments suitable for the investigation of proteins. Experiments that have been used during the studies of this theses will be shortly described in the following sections.

1D [^{1}H] spectra

1D [^{1}H] spectra are mainly suited for small organic molecules because distinct and clearly separated signals allow the structural analysis of the molecule. For proteins the high number of protons giving rise to signals leads to very crowded spectra with limited information content (Fig III). The use of NMR spectroscopy for the exploration of protein structures began with the development of multidimensional NMR spectra.

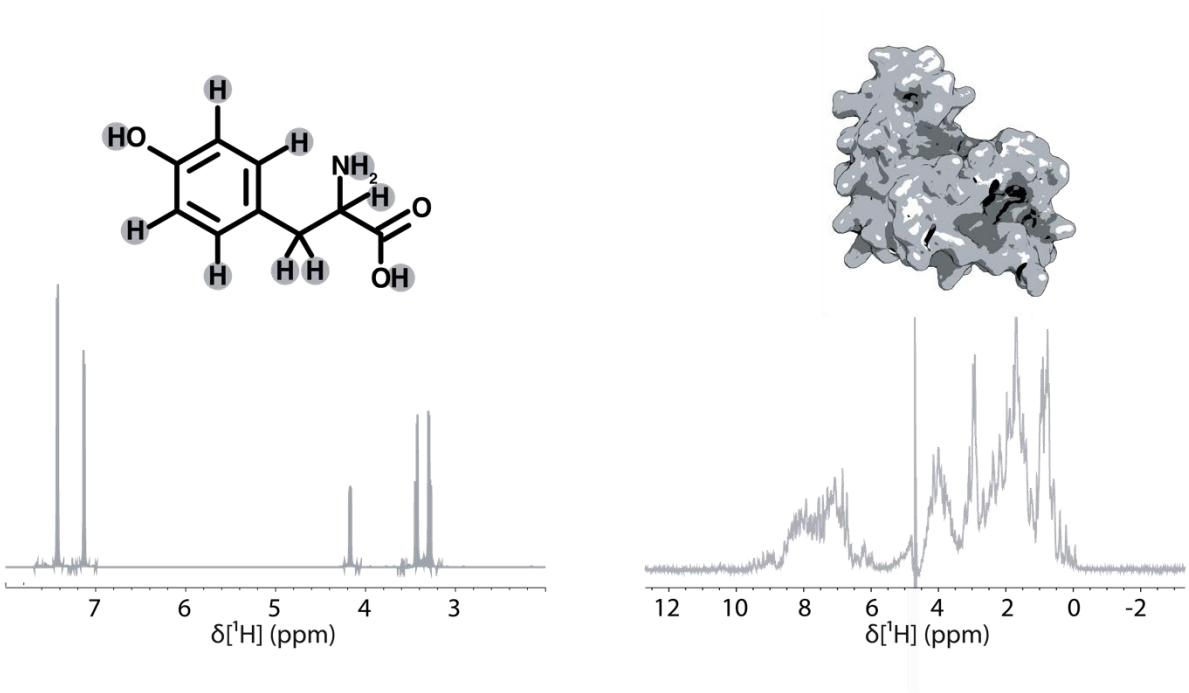

Figure III: 1D ^{1}H NMR spectra of tyrosine and a protein. While the limited number of protons give rise to distinct signals in small molecules such as tyrosine, protein 1D [^{1}H] spectra are very crowded.

2-dimensional Heteronuclear single quantum correlation (HSQC) spectra

HSQC spectra are based on the exploitation of the scalar coupling (J coupling) between two nuclei connected via a chemical bond. Most HSQC spectra used in protein NMR spectroscopy correlate ^{1}H nuclei either with ^{15}N or ^{13}C nuclei. The resulting 2D spectra show a peak for each ^{1}H that is connected via one bond to either a ^{15}N or a ^{13}C nucleus. Here, on one axis of the spectrum the chemical shift of the ^{1}H nucleus is given and on the other axis the chemical shift of the connected ^{13}C/^{15}N nucleus. 2D [^{15}N,^{1}H]-HSQC spectra belong to the most used spectra in protein NMR because each amide of the protein backbone gives rise to one distinct signal (side chain amines and amides can result in additional signals). The only exception is proline where the peptide bond is a tertiary amide. Thereby 2D [^{15}N,^{1}H]-HSQC spectra reveal a unique fingerprint for each protein[6]. Even without the assignment of the individual peaks to the amino acid residue they origin from, these spectra can give information about structural and biochemical properties of a protein such as the degree of structured and unstructured regions, the presence of secondary structural elements, protein stability in specific buffers and at specific temperature ranges as well as interaction with ligands (Fig IV).

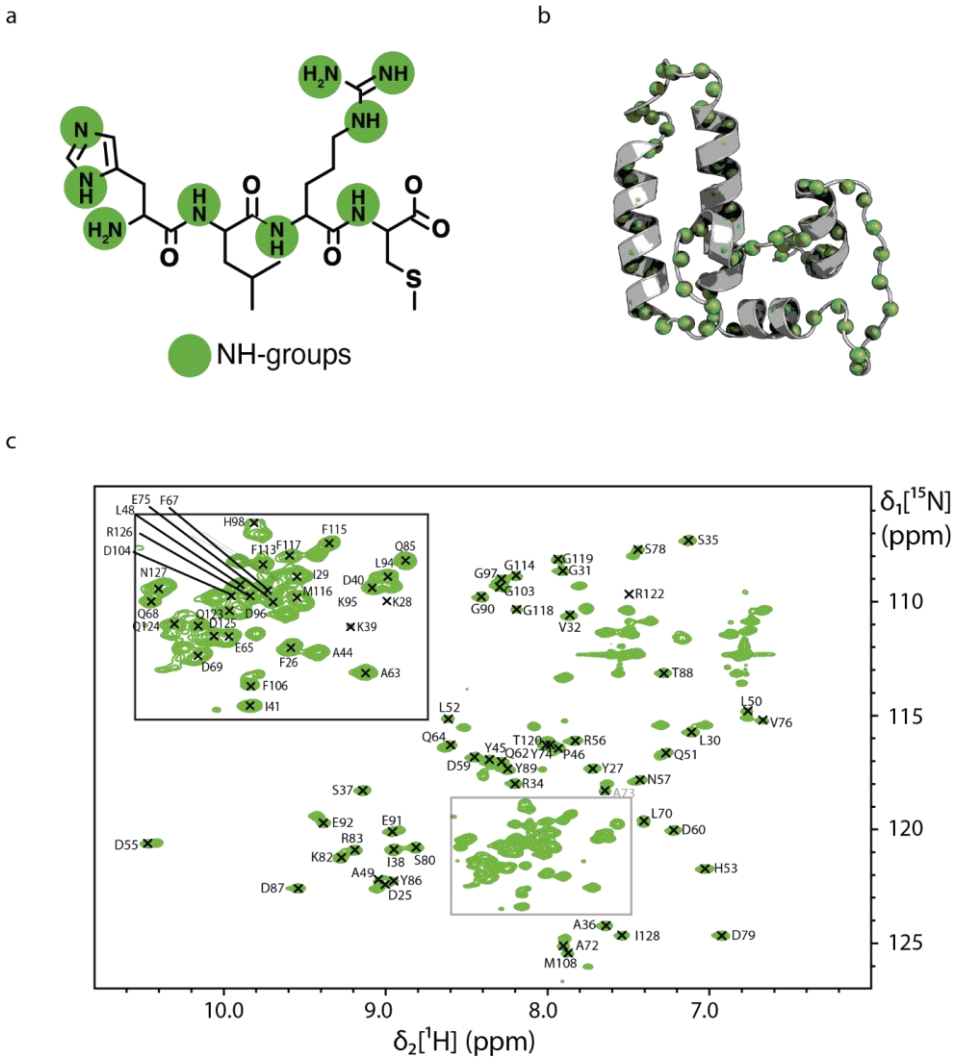

Figure IV: The 2D [^{15}N,^{1}H]-HSQC spectrum. a: NH-groups giving rise to NMR signals in a 2D [^{15}N,^{1}H]-HSQC spectrum. b: Backbone amides in a protein depicted by green circles. c: a 2D [^{15}N,^{1}H]-HSQC spectrum of a protein with the assignment of its 128 residues.

Chemical shift perturbations (CSPs)

With the assignment of 2D HSQC spectra detailed structural information about interactions of a protein with other proteins or other ligands can be gained[7]. If a protein binds to a ligand the chemical environment of nuclei in the vicinity of the binding site of the ligand changes. This results in perturbations of chemical shifts (CSPs) and allows for the identification of residues involved in binding of the ligand. If a titration experiment with increasing amounts of the ligand is performed, CSPs can also be used to calculate dissociation constants (K_D) for the binding event[8].

3-dimensional correlation spectra for the assignment of protein signals

The concept of correlating bonded nuclei via their J-coupling can easily be expanded to correlate more spins in a spin system. Each spin type can then be resolved in an additional frequency axis yielding higher dimensional NMR spectra. A combination of these 3D correlation spectra can be used to assign a peak to the nucleus it origins from[9]. The most commonly used assignment spectra correlate the amide proton and nitrogen with the C_α ,C_β or CO nucleus. The resulting peak positions are characteristic for each residue and appear at the chemical shift of the proton in one dimension, the coupled nitrogen in the second dimension and the respective coupled carbon nucleus in the third dimension. Because correlations do not only occur within the same residue but can also be extended to the adjacent amino acid residue, these spectra give information about the connectivity between adjacent amino acids in the protein chain and allow the unambiguous assignment of protein signals[10].

Secondary chemical shifts

The chemical shifts of C_α and C_β nuclei have characteristic values for carbons either within α-helices or β-sheets. This effect is used to determine the secondary structural content of a protein[11]. The difference between the observed $C\alpha$ and $C\beta$ chemical shifts and averaged values obtained from random coil structures[12] (unstructured polypeptide chains) are used to calculate secondary chemical shift differences ($\Delta\delta C_\alpha$ - $\Delta\delta C_\beta$) with

$$\delta C_\alpha = C_{\alpha,observed} - C_{\alpha,random\ coil}$$
$$\delta C_\beta = C_{\beta,observed} - C_{\beta,random\ coil}$$

Positive values for secondary chemical shift differences are representative for α-helices whereas negative value characterize β-sheets.

Heteronuclear Nuclear Overhauser effects (hetNOEs)

hetNOEs are a measure of the dynamic properties of a coupled spin pair. They are mainly used to characterize dynamics in the ns – ps range of backbone amides[13]. They are acquired by the comparison of two 2D [^{15}N,^{1}H]-HSQC spectra, one with a presaturation in which the NOE is present and a control spectrum without the NOE. Attenuated signal intensities in the spectrum with presaturation reveal dynamic elements within a protein.

Nuclear Overhause effect Spectroscopy (NOESY)

NOESY spectra are used to identify through space interactions between nuclei[14]. In protein NMR spectroscopy they are usually used in form of 3D HSQC-NOESY spectra that first select protons attached to either nitrogen or carbon by the J-coupling in an HSQC[15]. . In the third NOE dimension they detect which protons are in close proximity to the previously selected HX pair interacting via through space dipole-dipole couplings. These NOE contact allow to derive information about the 3D structure of the molecule and are a very important input for structure calculations using NMR based restraints[16,17]

Chapter 1:

The functional role of the GF-region of two ER-resident J-domain co-chaperones for the regulation of Hsp70

1. Chapter 1 - Introduction

Protein folding and the role of chaperones

Proteins are the workhorses that enable the cell and a whole organism to exert the various functions needed to sustain itself and reproduce. Proteins are composed of linear chains of amino acids of unique sequence. However, to be biologically functional, most of the proteins need to adopt its correct three-dimensional structure and, in many cases, assemble into a complex consisting of several proteins. Apart from simply missing its function, a protein that is misfolded or damaged can cause enormous stress for the cell through the formation of protein aggregates that are toxic and can lead to aggregation diseases[18–20]. Therefore, each organism ranging from bacteria to complex cellular organisms has developed mechanisms that ensure the integrity of the proteome starting from correct protein maturation, the assembly of protein complexes, the rescue of misfolded proteins to the disassembly of protein aggregates and the correct disposal of ultimately damaged proteins. At the heart of this quality control mechanism lies a complex network of a protein class called chaperones, a large group of various proteins, each tackling fundamental tasks to maintain protein homeostasis.

Chaperones are functionally and structurally very heterogenous and therefore are divided into further highly conserved classes. The processes they are involved in are folding of nascent protein chains (de novo folding)[21,22], un- and refolding of misfolded proteins, prevention of protein aggregation[23], disaggregation[24,25], assembly of protein oligomers[26,27], protein trafficking[28–30] and facilitation of protein degradation[31–33]. Many chaperones need energy in the form of ATP to exert their functions whereas others work without the cost of ATP hydrolysis. These ATP-independent chaperones are often considered as “holdases”, they bind un- and misfolded proteins without subsequent refolding of their client in order to prevent misfolding, binding to other proteins and aggregation[34]. They also can function as “translocases” that escort their client proteins to a specific cellular destination[35]. While ATP-independent chaperones merely hold their client proteins, energy released from ATP hydrolysis can be used to actively unfold, refold and remodel proteins[36]. These ATP-

dependent chaperones recognize and bind hydrophobic amino acid sequences exposed by non-native proteins, thereby keeping the client protein from aggregation or even unfolding the it[37]. Well studied ATP-dependent chaperone systems are the Hsp60, Hsp70, Hsp90 and Hsp110 families[38–41]. In most of the cases, chaperones do not act on their own but in complex networks requiring simultaneous and sequential interactions in a highly orchestrated manner[42–45]. One of the most versatile key hubs is the network generated by Hsp70, together with the ATP-independent J-domain proteins (JDPs) and its specific Nucleotide exchange factors (NEFs). This network provides assistance in all aforementioned processes for a large fraction of expressed proteins[46]. It is one of the first chaperones a nascent chain is in contact with and might be one of the last ones accompanied to final degradation[21–23,29,31].

The Hsp70-co-chaperone system

As one of the most ubiquitous chaperones, Hsp70 (Heat Shock protein of 70 kDa) is highly conserved among all kingdoms of life[47]. There are 13 homologues of Hsp70 in humans found in all organelles[48], the cytoplasm, the nucleus, the endoplasmic reticulum (ER) and the mitochondria underlining its fundamental role. Hsp70 consists of a nucleotide binding domain (NBD) and a substrate binding domain (SBD) made of two subdomains, SBDα and SBDβ, the NBD and the SBD are connected by a short interdomain linker[49]. The structural arrangement of the NBD and the SBD differs depending on the nucleotide bound to the NBD. While bound to ATP SBDα and SBDβ are docked onto the NBD, in this closed conformation the affinity to clients is low and the association and dissociation rates high[49,50]. ATP hydrolysis to ADP follows a conformational rearrangement, now SBDα closes onto SBDβ and the bound client like a lid and the NBD detached from both SBD subunits[51]. This leads to an increase of the affinity to client protein and thereby trapping the client within the SBD[50,52]. Polypeptide binding triggers ATP hydrolysis by a network of residues coupling these two events resulting in a tight allosteric control of the activity of Hsp70[53,54]. However, the efficient exertion of ATP hydrolysis requires binding of a J-domain protein to the interface of NBD and SBD, in order to enhance the transmission of conformational changes[53,55,56] (Fig 1).

Hsp70 assist the folding of proteins by promiscuously recognizing and binding hydrophobic amino acid sequences[37,57–59] in non-natively folded proteins[60] and thereby reducing the

likelihood of aggregation of the client[60,61]. It has been suggested that Hsp70 unfolds parts of the protein around the binding site and simultaneous binding of many Hsp70s results in unfolding of the client protein[62]. This process is thought to rescue client proteins from misfolded states they got trapped in, eventual release from Hsp70 offers a new chance to find the correct folding route[36,63]. Although more information is required to fully understand the functional details of the Hsp70 activity, its simple holdase/unfoldase mechanism opens the question about how Hsp70 is able to exert such diverse function as *de novo* protein folding[21], protein complex assembly[64,65], disassembly of protein aggregates[66–71], protein trafficking[29,72] and facilitation of degradation[31]. These numerous different Hsp70 functions can only be understood in the context of its complex interaction network with other chaperones and Co-chaperones. A tremendous part of navigating Hsp70 along its versatile functions is achieved by J-domain proteins (JDPs), a large and diverse protein family represented in each organism[73–75].

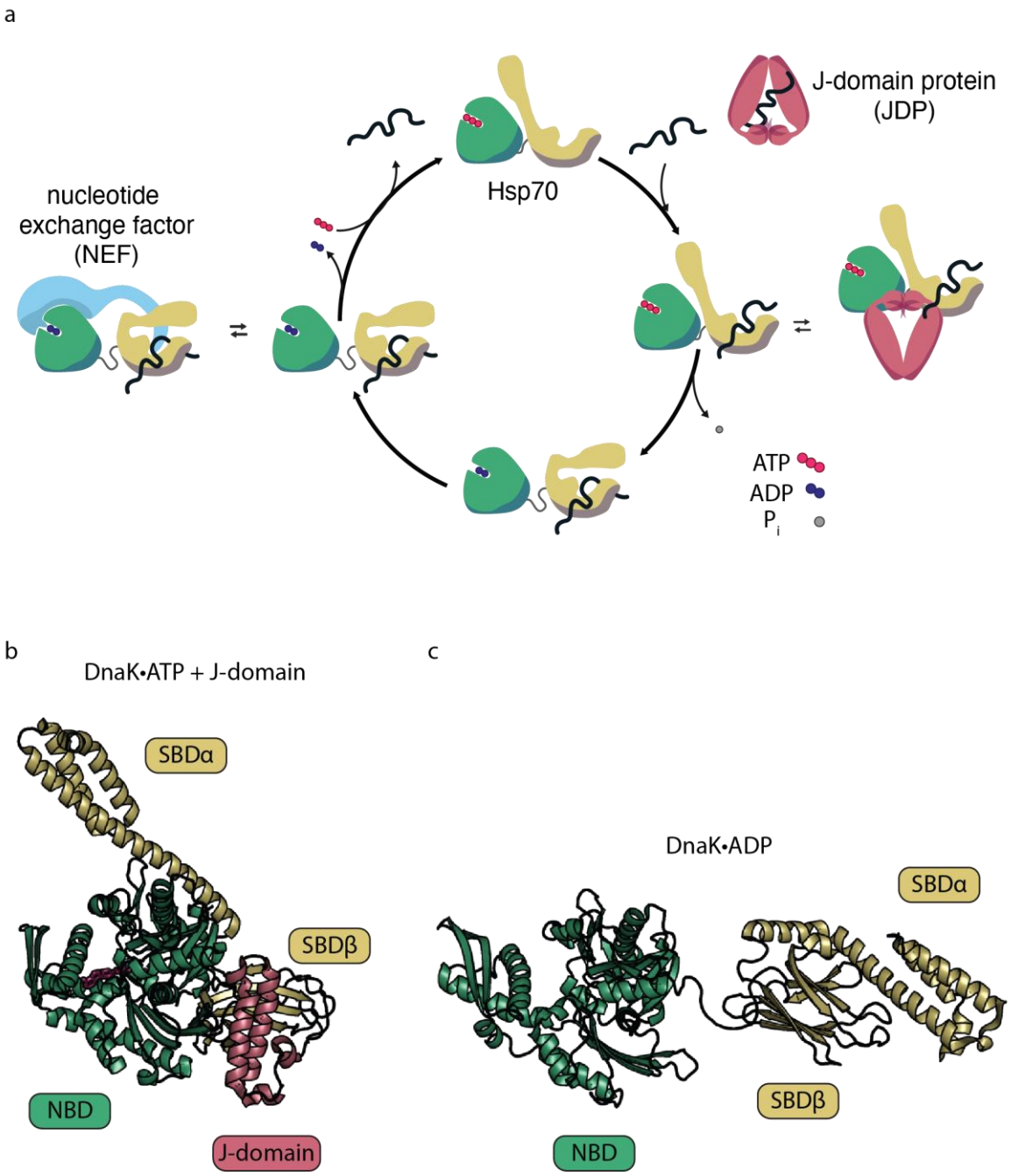

Figure 1: The functional cycle of the chaperone Hsp70 a: In the ATP-bound closed state, the SBDα and SBDβ are docked onto the NBD. A JDP delivering the client protein stimulates hydrolysis of ATP and during an associated conformational change the SBDα closes onto the SBDβ trapping the client protein. Release of ADP by a NEF triggers the subsequent release of the client protein and if necessary, it can be rebound in a following cycle. b: structure of DnaK (Hsp70 from E. coli) in the STP-bound state in complex with the J-domain of DnaJ (pdb: 5NRO). c: DnaK in the ADP bound state (pdb: 2KHO).

J-domain proteins

To each Hsp70 homologue comes a subset of different JDPs, in total the human organism comprises 53 to date known J-domain proteins forming the largest chaperone family in humans[75,76]. Apart from the crucial function to stimulate the intrinsically low ATP hydrolysis of Hsp70[55,56], J-domain proteins deliver client proteins to Hsp70[77–82] and recruit Hsp70 to specific locations within the cell. Combined, these actions are key in the navigation of the manifold functions of Hsp70. JDPs act in sub-stoichiometric ratios compared to Hsp70, their concentration in-vivo has been found typically around 10-fold lower than the concentration of Hsp70[63,75].

Classification of J-domain proteins

JDPs exert a large variety of functions in collaboration with Hsp70 but also independent from the ubiquitous chaperone. This variety is explained by the vast diversity of JDP structures, the only common feature is the J-domain. J-domain proteins are grouped into three classes, class A, B and C. Class A is the group with the highest sequence conservation, the members are homologues of the bacterial DnaJ and of approximately 40 kDa, they are also named Hsp40. In this class, the N-terminal J-domain is followed by a region rich in glycine and phenylalanine (GF-region) and two C-terminal domains (CTDI with a zinc binding site and CTDII) that harbor the client binding sites[80,83,84]. Class A J-domain proteins form dimers mediated by the C-terminal dimerization domain (DD)[80,85]. The class B of J-domain proteins is more heterogenous compared to class A and can be divided into two subgroups. Members of subgroup I (canonical class B JDPs) have the same domain organization as class A proteins, however their CTDI lacks the zinc-binding site[86]. Subgroup II (non-canonical JDPs) comprises proteins containing a substrate binding domain unrelated to the conserved CTDI and CTDII[87]. In both cases class B J-domain protein have a N-terminal J-domain with the subsequent GF-region which is extended by glycine/methionine rich region[88]. Like class A JDPs canonical class B JDPs form dimers by their dimerization domain[89]. Class C J-domain proteins are all those proteins having a J-domain but lacking a fixed domain organization as well as domain conservation. Here, the J-domain can be found at any position within the protein. It is the largest group of J-domain proteins with the highest domain variety additional to the J-domain reflecting their high degree of specialization[73,75,76,90] (Fig 2).

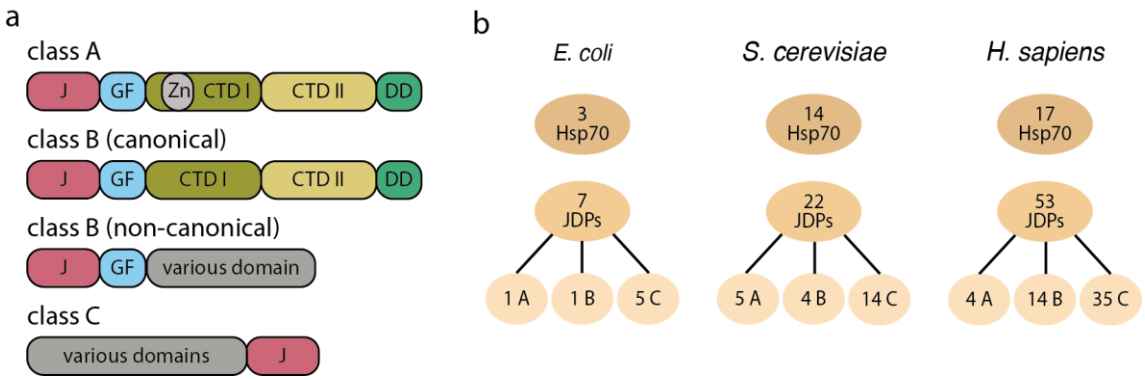

Figure 2: JDP classification a: domain organization of class A, B, and C JDPs. Class B JDPs are further categorized into canonical class B JDPs and non-canonical JDPs, the latter do not comprise a client binding domain homologous to the CTDI and CTDII of class A and canonical class B JDPs. b: number of different Hsp70 chaperones and JDP in *E. coli*, *S. cerevisiae* and *H. sapiens*. In all organisms, JDPs outnumber Hsp70s, with class C containing the most numbers of different JDPs.

Functions of JDPs

JDPs participate in manifold processes, in the simplest case, the J-domain alone is serving solely to recruit Hsp70 to a certain cellular localization. Yeast Hlj1 consists of a J-domain that is anchored at the ER membrane by a single transmembrane spanning helix where it recruits cytosolic Hsp70 to assist proteins exiting the ER for degradation[91]. Similarly, the human JDP DNAJC19 resides at the mitochondrial translocon increasing the local concentration of Hsp70 in order to facilitate folding of nascent protein chains[92].

Many JDPs act like "holdases" in an ATP-independent way to prevent misfolding and aggregation of client proteins[93,94]. Class A and canonical class B JDPs, as well as several members of class C JDPs have been found to bind to similar peptide patterns as Hsp70 and thereby can bind a broad range of diverse un- or misfolded client proteins to finally hand them over to Hsp70 during *de novo* protein folding[76,82,83,95]. Whereas this process requires the recognition of generic motifs with the sequence of every protein, some JDPs bind to destabilized proteins as has been shown for DNAJA1 and a misfolded mutant of p53 in order to prevent their misfolding[96]. The non-canonical class B DNAJB6 and DNAJB8 specifically bind to aggregation-prone proteins to inhibit toxic accumulation of protein aggregates[97–99]. A few JDPs selectively bind specific folded proteins, for example DNAJC6 (auxilin) which remodels clathrin coated vesicles[100] and DNAJC20, a JDP involved in the correct folding of proteins contain an Fe-S cluster[101]. If the maintenance of correct protein folding has gone awry, large

protein complexes known as disaggregase machineries solubilize protein aggregates. These complexes include the ATP-dependent Hsp100, Hsp70 and JDPs, combined actions lead to threading and pulling forces that disentangle trapped polypeptides[102]. To highlight the immense role JDPs play during these processes, a synergistic formation of transient heterocomplexes of class A and class B JDPs has been found to increase the disaggregase function of Hsp70[66,71]. Finally, if all attempts to send a protein back on track fail, the cell has no other option than to remove it to prevent further damage. In this context, several JDPs have been found to drive protein degradation. A striking example is DNAJB2, a non-canonical class B JDP which has 2 ubiquitin-interacting motifs and thereby demonstrating a link to the proteosome[103]. Human DNAJA1 has been shown to increase the degradation of the CFTR anion channel[104] and several ER-resident JDPs are involved in the ER-associated degradation of proteins (see below).

The importance of a functional J-domain protein network is highlighted by the knowledge about protein aggregation diseases linked to mutations in JDPs. These disease include cardiomyopathy (DNAJC19[105]), motor neuropathy (DNAJB2[106]), Parkinson's disease (DNAJC6[107], DNAJC13[108]), and Amyotrophic Lateral Sclerosis (DNAJB6)[109]. Due to their specificity JDPs also have been suggested for novel opportunities to clinically target the chaperone network without interfering with basic chaperones such as Hsp70, Hsp60 or Hsp90[110].

Structural elements of JDPs

J-domain

The structure of the isolated J-domain of various J-domain proteins has been solved[111–113], it is a small domain of approximately 8 kDa and consists of 4 α-helices ($\alpha1 - \alpha4$) connected by small loops. In the small loop between $\alpha2$ and $\alpha3$ a short three amino acid long motif of aspartate, proline and histidine (HPD motif is found, crucial for the stimulation of ATP hydrolysis of Hsp70 (Fig 3 c). The J-domain is highly conserved among all species and organelles, however the sequences of class A, B and C J-domain proteins differ slightly[114]. Despite high sequence and structural similarity, the J-domains of class A, class B and class C JDPs can be distinguished[48].

Substrate binding domains

Obtaining information about full-length structures by X-ray crystallography of especially class A and B JDPs has been hampered by the presence of the GF-region connecting the J-domain with the CTDs introducing flexibility into the protein[80,85,115]. Truncated structures revealed that the CTDs form double β-sandwich domains, the DD consists of two α-helices (Fig 3 a). Lately, the structure of a class B J-domain protein bound to a client protein has been solved by NMR spectroscopy showing that the client protein binds in an unfolded flexible state with interchanging binding sites to CTDI and CTDII (Fig 3 b). Neither the J-domain nor the GF-linker participate in this interaction[93]. Structures of few members of class C JDPs have been elucidates, they include TRX domains[116], tetratricorepeats[117] (TPR), cysteine rich[116,118] regions and GTP-binding[119] sites.

GF-region

Unlike the J-domains and the substrate binding domains of JDPs, the GF-region found in canonical class A and B JDPs has gained less attention. The GF-region is a sequence rich in glycine and phenylalanine and its length varies from 20 to approximately 50 amino acids depending on the JDP, its function remains largely enigmatic. Due to its low degree of structural order, it has been believed to mainly serve as a linker between the J-domain and the substrate binding domains[90]. However, within this region which shows little sequence similarity, there is a short sequence of six to nine amino acids that are highly conserved among class A and canonical class B JDP among all organisms[120]. The core of this region forms a DI/VF motif. Intrigued by this feature, several studies have been conducted in order to unravel the function of the GF-region. Remarkably, it is not possible to draw a unified conclusion from their results since they attribute manifold functional roles to the GF-linker (Fig 3 d). In one of the earliest investigations, it has been shown that the GF-region is not required for the stimulation of Hsp70 ATPase activity, but it is involved in modulating the substrate binding activity of Hsp70. Furthermore, deletion of the complete GF-region from the *E. coli* DnaJ reduced cell growth and resulted in a deficient down regulation of the heat shock response[120]. The toxic effect on cell growth was also found by another group by mutating the conserved DI/VF motif to alanine and glycine. They rationalized that the effect was dependent on Hsp70 because overexpression of the NEF GrpE or mutations of the HPD motif fundamental for efficient ATP hydrolysis could reverse it. This observation lead to the

conclusion that the GF-region plays crucial role in the regulation of the Hsp70 chaperone cycle subsequent to ATP hydrolysis[121]. Another study showed that deletion of the GF-region impairs the ability of *E. coli* DnaJ to bind natively folded and partially unfolded substrates but not completely unfolded substrate proteins. Therefore provides the co-chaperone with a tool to distinguish between different substrates[122]. The GF-region from Sis1, a canonical class B JDP from *Saccharomyces cerevisiae* has been shown to be crucial for cell growth and [RNQ^+] prion maintenance and additionally, the effect could be bypassed by mutations in the HPD motif[123]. Since chimera proteins of Sis1 substituted with the GF-region of Ydj1 had the same effect as deletion of the GF-region, the authors claimed that GF-region provides JDP with functional specificity[124]. As already mentioned above, mutations in JDPs have been linked with aggregation diseases and in the case of dominantly-inherited myopathy, the mutations were found in the GF-region of DNAJB6 directly before the conserved DI/VF motif[109,125] underlining the importance of this protein domain.

On a structural level it has early been shown that the GF-region of DnaJ was not entirely disordered, however no structural details could be provided[111]. Later a combined X-ray and EPR-study of DnaJ from *Thermus thermophilus,* a class B JDP, revealed an α-helical element within the GF-region. Furthermore, mutations within the α-helix were associated with higher client refolding[115]. Only recently NMR studies of the human DNAJB6b[87] and DNAJB1[126] also showed that their GF-regions contain a α-helix. However, when comparing their structures with DnaJ from *Thermus thermophilus* a difference in the position this helix occupies becomes clear. In human DNAJB6b and DNAJB1, the helix folds back onto the J-domain whereas in DnaJ it is not attached to the J-domain and found at the opposite site of the J-domain[115]. For DNAJB1 the α-helix has been proved to act as a regulatory element for the interaction with Hsp70. Only recently, a new role of the GF-region has been discovered for the human JDPs Hdj1 and Hdj2 as well as yeast Sis1 and Ydj1. These proteins have been shown *in vivo* and *in vitro* to undergo phase separation and assemble on membrane less organelles, a process which was mainly driven by the GF-region of the JDPs[127].
Summarizing the results of these studies it becomes clear that the GF-region is an important element of class A and class B JDPs. The functional characteristics of it are attributed to an involvement in client binding and regulation of the interaction with Hsp70, however, a clear understanding is still missing.

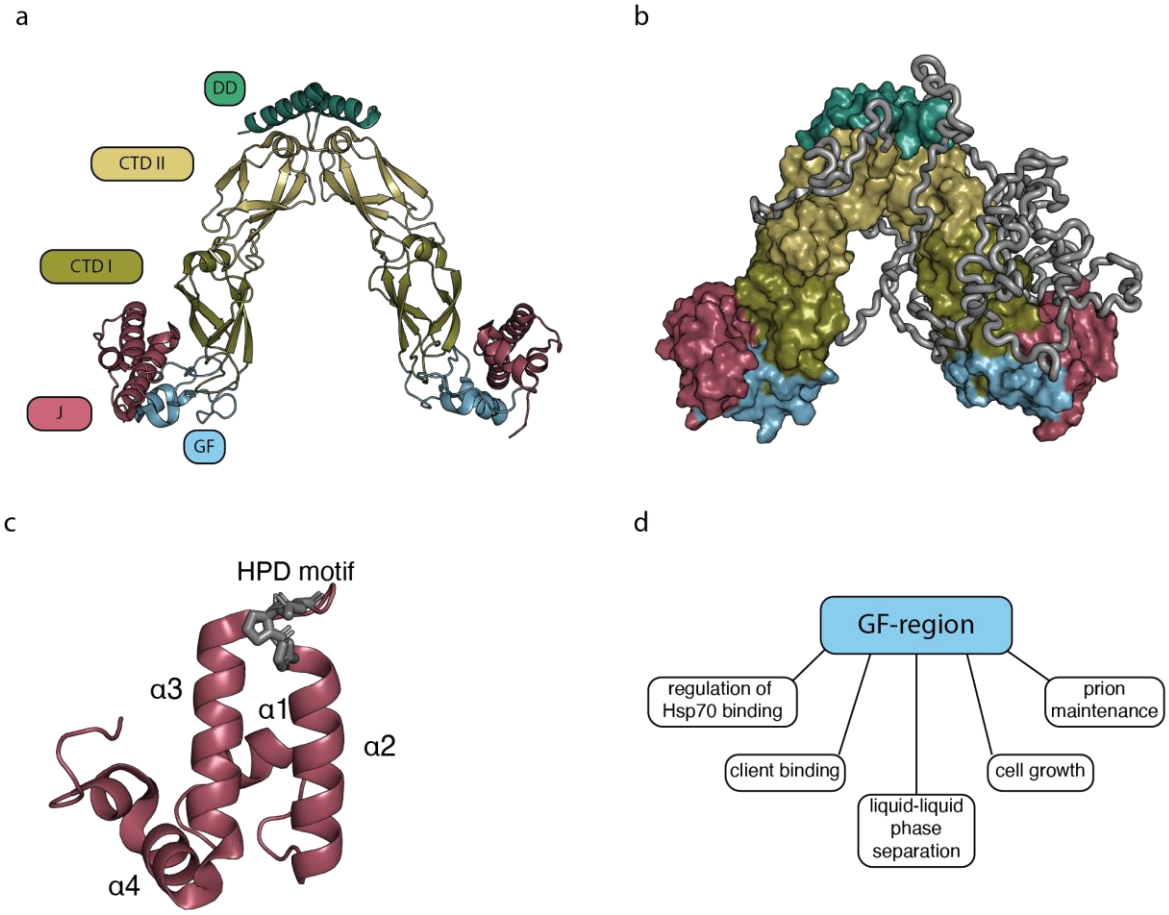

Figure 3: JDP structures a: Structure of the class B DnaJ from *T. thermophilus* with single domains highlighted. The J-domain is shown in red, the GF-region in bright blue, CTDI and CTDII in green and yellow respectively and the DD in dark green (pdb:4J80). b: structure of *T. thermophilus* DnaJ with bound client protein (PhoA). The client protein binds in an unstructured conformation to CTDI and CTDII (pdb: 6PSI). c: J-domain of the class B JDP Sis1 from S. cerevisiae with α-helices 1 – 4 and the HPD-motif highlighted (pdb: 4RWU). d: different functional roles associated with the GF-region.

Protein folding in the endoplasmic reticulum

While cytosolic proteins get synthesized and folded in the cytosol secretory and membrane proteins which constitute one third of the human proteome[128], mature in the endoplasmic reticulum[129]. Surrounded by a lipid membrane this organelle forms a protective compartment distinct from the cytosol with respect to ion concentration and redox conditions.[130]. Here, secretory and membrane proteins get folded and subsequently packaged into vesicles to be targeted to their final destination. These classes of proteins

distinguish from cytosolic proteins by distinct features: Membrane proteins contain numerous hydrophobic residues on their surface and many secretory proteins require unique co- and posttranslational modification such as glycosylations[131] and disulfide bridges[132]. A N-terminal signal sequence in their nascent polypeptide chain directs the ribosome to the ER membrane where it attaches to the Sec61 translocon complex in order to release the nascent polypeptide chain in to the ER lumen[133]. Once in the ER, the nascent polypeptides are received by chaperones that have evolved to meet the special needs of membrane and secretory proteins. Most of these chaperones belong to one of the four major chaperone groups in the ER. The first group are the lectin-like chaperones calnexin and calreticulin, both recognize and process glycosylated proteins[134,135]. The second group are the Protein disulfide isomerases (PDIs)[136,137], required for the correct formation of disulfide bridges. The third group comprises the peptidyl-prolyl cis/trans isomerases that catalyze cis/trans isomerization of peptide bonds[138]. The last major group comprises chaperones belonging to the heat shock family (ER resident Hsp70 BiP, ER-resident Hsp90 GRP94 and the ER-resident JDPs)[139–141].

The unfolded protein response

As in the cytoplasm, correct maturation, folding and assembly of proteins and protein complexes in the ER is of utmost importance and therefore the ER homeostasis is tightly monitored by a collection of highly conserved signaling pathways collectively termed unfolded protein response (UPR)[142]. In case of any disruption of the ER homeostasis, UPR activation increases the protein folding capacity by the upregulation of chaperone expression in order to combat an increased amount of improperly folded proteins[143]. Causes for a disruption of the ER homeostasis are manyfold including protein amino acid mutations, oxidative stress, faulty protein quality control, environmental toxins, viral infection, heat, pH, drugs, inflammatory cytokines, Ca^{2+} depletion, metabolic starvation and aging. If correct folding of proteins fails, these proteins are delivered outside of the ER and targeted to the proteasome in the cytosol for degradation during a process called ER- associated degradation (ERAD)[144,145].

ER-resident Hsp70 and J-domain proteins

The ER is equipped with one Hsp70 variant, BiP (Binding immunoglobulin protein, or GRP78, glucose regulated protein of 78 kDa) and eight J-domain proteins. In addition to chaperoning newly synthesized proteins BiP is fundamental for several other processes such as maintaining the permeability barrier of the ER during protein translocation[146], targeting irreparably misfolded proteins to the ERAD[147,148], contribution to the control of calcium storages[149,150], and sensing conditions of stress in this organelle to activate the mammalian unfolded protein response (UPR)[151–156].

Of the eight to date known ER-resident JDPs, ERdj1 – 8 (Endoplasmic Reticulum domain j), four are membrane spanning class C JDPs with either cytosolic or luminal J-domains (ERdj1, 2, 7, 8). The other four are soluble proteins with client binding domains directly contributing to protein binding and folding. ERdj1 (DNAJC1) and ERdj2 (DNAJC23) are both associated with the Sec61 translocon and facilitate the translocation of nascent polypeptide chains[157–160]. ERdj8 has been suggested to play a role in autophagosome formation[161] but the role of ERdj7 (DNAJC79) remains unclear to date[162].

Two of the soluble JDPs in the ER belong to the class C JDP, ERdj5 (DNAJC10) and ERdj6 (DNAJC3). ERdj5 (DNAJC10) is a protein disulfide isomerase and most likely acts as a reductase[163]. It is constitutively expressed, only mildly upregulated during ER-stress and additionally has been linked to ERAD[118]. ERdj6 (DNAJC3) is ubiquitously expressed in the ER lumen under normal physiological conditions, however, during stress, it translocates to the cytoplasm where it acts as a modulator of translation in response to cellular stress[82]. This co-chaperone selectively binds unfolded client proteins and additionally has been suggested to be involved in ERAD[164]. It is a monomer consisting of nine consecutive tetratricopeptide repeat (TPR) motifs and a C-terminal J-domain. Typically for class C JDPs, it lacks the GF-region[164,165].

Two members of class B JDPs are found in the ER, the canonical class B JDP ERdj3 (DNAJB11) and the non-canonical class B JDP ERdj4 (DNAJB9). No member of class A JDPs is represented in the ER, however, ERdj3 has been found to be referenced as a class A JDP despite the lack of a zinc-binding cluster[166]. This classification is most probably due to the presence of two disulfide bridges at a position where the zinc binding cluster is found in class A JDPs[167]. ERdj3 is constitutively expressed at high levels, especially in cells with a high secretory load[168]. Although having the same domain organization ERdj3 differs from other class B JDPs by

forming a tetramer instead of a dimer[169]. However, a high-resolution structure neither of the full-length protein nor of single domains could yet be obtained. ERdj3 binds a broad range of unfolded clients[95,167,170] and it has been found to interact with the Sec61 translocon where it transfers client proteins to BiP for further maturation[171]. Furthermore, a role linked to protein degradation is discussed[172]. Due to the lack of a canonical ER-retention motif ERdj3 can be found outside of the cell where it maintains its chaperone function[173,174].
ERdj4 is a non-canonical class B JDP, it comprises the conserved J-domain and a GF-region of approximately 40 residues, however its substrate binding domain shows no homology to any other protein and its structure has not been solved to date. ERdj4 is expressed at low level under non-stress conditions[175], it gets upregulated by agents that induce ER stress as well as by several mechanisms known to activate the UPR such as early hematopoietic stem cell differentiation[176], angiogenesis[177], macrophage activation, TNFα-induced proinflammatory responses, and plasma cell differentiation[178]. ERdj4 binds unfolded proteins and has been shown to be involved in ERAD[179], furthermore it binds to Ire1, a UPR transducer residing in the ER membrane[180,181]. A study that compared binding epitopes of BiP, ERdj3, ERdj4 and ERdj5 could show that BiP and ERdj3 bound to similar motifs that frequently occur within polypeptide chains. On the other side, ERdj4 and ERdj5 rather bound to sequences displayed by aggregation-prone proteins[153].

It becomes clear that besides from the specialized class C JDPs in the ER, also the two class B JDPs ERdj3 and ERdj4 have evolved ER-specific features and thereby differentiate from their cytosolic family members. They are interesting targets to study the JDP network in the context of protein folding and quality assurance in the ER.

1. Chapter 1 - Aim of the study

The protein family of J-domain proteins is, with its high functional versatility, a great example for an intriguing balance between conserved and uniquely evolved protein features. The ER-resident Hsp70-JDP network illustrates this balance comprising six highly specialized class C JDPs and two class B JDPs which also demonstrate exclusive characteristics when compared to other class B family members. To gain insights into the specialized and conserved intricacies of the JDP-Hsp70 network within the ER, this study includes the structural and functional characterization of three ER-resident JDPs, ERdj3, ERdj4 and ERdj6. While there is an increasing amount of structural and functional information about the J-domain of JDPS, at the beginning of this study, only little data was available about the functional relevance of the GF-region and its structural impact. With a length ranging from 20 to 40 amino acids, it contains a highly conserved stretch of 6 to 9 residues, at its center a characteristic DI/VF motif[120] (Fig 4 b). First having been seen as an unstructured linker without functional relevance, evidence accumulates that the GF-region plays a role in several molecular processes ranging from the regulation of the functional cycle of Hsp70[121], client binding[120,122], prion maintenance[123,124] to liquid-liquid phase separation[127]. Interestingly, differing functions were attributed to this part of the protein leading to the hypothesis that the GF-region contributes to JDP specificity. Besides unique features such as the tetramer formation and the disulfide bridges of the ER-resident JDPs ERdj3 as well as the unique client binding domain of ERdj4, these two class B JDPs comprise a GF-region including the highly conserved DI/VF motif (Fig 4 a, b). This study aims at the structural and functional elucidation of the GF-region of ERdj3, a canonical class B JDP and ERdj4, a non-canonical class B JDP by NMR spectroscopy and additional biophysical methods. NMR spectroscopy was chosen because it is particularly well suited to investigate dynamic and possibly disordered protein domains as well as protein interactions. The project started with the design of several constructs of ERdj3, ERdj4 and ERdj6 for recombinant protein expression and purification. Once stable protein constructs were obtained, they were characterized by biophysical and NMR spectroscopical methods including their full backbone assignment. To complement the knowledge about the J-domain fold, the structure of the J-domain of ERdj3 was solved by

NMR spectroscopy. With all characterizations set, the impact of the GF-region on the functional Hsp70-cycle was investigated by interaction studies with the JDPs and the ER-resident Hsp70 BiP.

a

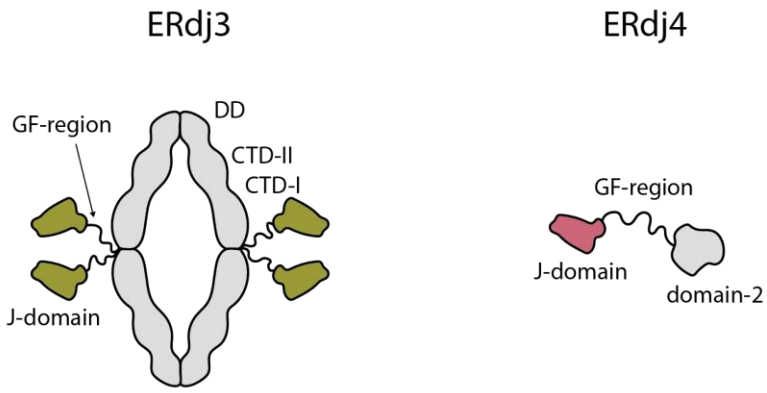

b

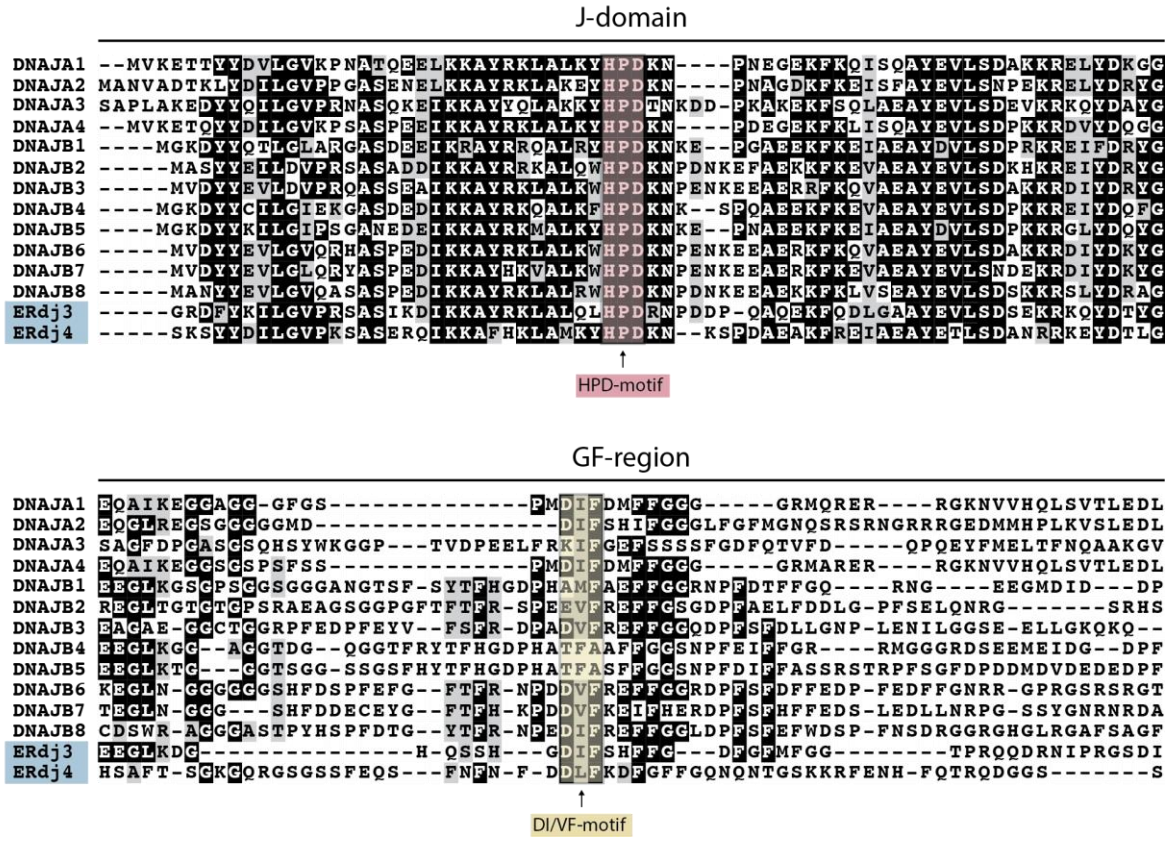

Figure 4: Domain organization of the ER-resident JDPs ERdj3 and ERdj4 and sequence alignment of the J-domain and the GF-region of human class A and class B JDPs. a: Domain organization of ERdj3 and ERdj4. ERdj3 forms as only known canonical class B JDP a tetramer, however, a high-resolution structure is not available. The J-domain of ERdj4 is the only domain of that protein that has been solved, its client binding domain (here domain-2) is of unknown structure. b: Sequence alignment of the J-domain and the GF-region of human class A and class B JDPs. The sequences of ERdj3^{JGF} and

ERdj4^{JGF} are shown at the bottom, highlighted in blue. The HPD motif in the J-domain is highlighted in red and the DI/VF motif in the GF-region is highlighted in yellow. The sequences of the J-domains were aligned with the alignment software MegaX[182] using the ClustalW algorithm[183], the alignment of the GF-region was edited manually.

2. Chapter 1 - Results

The GF-region of ERdj3 and ERdj4 forms a small α-helix that is in contact with the J-domain

To investigate the structural role the GF-region plays in the JDPs ERdj3 and ERdj4 we used NMR spectroscopy to compare their isolated J-domains with and without the GF-region. 2D [^{15}N,^{1}H]-HSQC spectra provide information about the position of the GF-region with respect to the J-domain. In case both domains are in close vicinity to each other, they would influence their peak positions in the 2D [^{15}N,^{1}H]-HSQC spectra since the individual residues of both domains experience a change on their chemical environment due to contacts to the other domain. This effect is named chemical shift perturbation (CSP) and is commonly used to investigate interactions of a protein with any kind of ligand by NMR spectroscopy[8]. A comparison of 2D [^{15}N,^{1}H]-HSQC spectra of their isolated J-domains with (ERdj3^{JGF}, ERdj4^{JGF}) and without the GF-region (ERdj3^{J}, ERdj4^{J}) reveals large chemical shift perturbations (CSPs) demonstrating an interaction between the GF-region and the J-domain for ERdj3 and ERdj4 (Fig 5 a - d). For both JDP constructs, the involved residues belong to α-helices 2 and 3 of the J-domain, however less residues were strongly affected in ERdj3^{JGF} by the adjacent GF-region compared to ERdj4^{JGF}. Remarkably, His31 from the highly conserved HPD motif of ERdj4 showed large CSPs, whereas the same residue in ERdj3 was only moderately affected. The HPD motif is found in every J-domain and is crucial for the stimulation of the ATPase activity of Hsp70, mutation results in complete loss of the stimulatory interaction[95,188]. These results clearly show that the GF-region is bound to the J-domain of ERdj3 and ERdj4, but the exact structural detail might vary for different J-domain proteins.

To further understand the structural characteristics of the GF-region we recorded secondary chemical shift differences. Secondary chemical shifts differences are derived from the chemical shifts of the C_α and C_β-atoms and give information about the secondary structure of a protein. Positive secondary chemical shifts differences are characteristic for α-helices whereas negative values are usually found for β-sheets[11]. The analysis of the secondary chemical shift differences of ERdj3^{JGF} and ERdj4^{JGF} reveals a stretch of positive values within the GF-region that demonstrate the formation of an α-helical element, here named helix 5

(Fig 5 d). This α-helix 5 is formed around the highly conserved signature DI/VF motif of the GF-region[120,121] (Fig 1 b) and recently has been found to form an α-helix in the non-canonical class B JDP DNAJB6b and the canonical class B JDP DNAJB1[87,126]. However, for ERdj3^{JGF} and ERdj4^{JGF} the secondary chemical shifts differences for helix 5 are reduced by a factor of three when compared to values of helices 1-4 showing a less pronounced α-helical nature, which is in contrast to DNAJB1 and DNJB6b where helix 5 is fully formed[87,126]. These data show that α-helix 5 or ERdj3^{JGF} and ERdj4^{JGF} is transiently formed in an equilibrium with an disordered state.

In order to complement our data with information about the dynamics of the GF-region, we measured ^{1}H-{^{15}N} NOEs. These give information about the flexibility of the protein backbone. Values close to 1 are representative for rigid regions of the backbone, while reduced values indicate increased mobility on the ps-ns timescale[189]. In both ERdj3^{JGF} and ERdj4^{JGF} helix 5 displays a moderate level of rigidity as shown by ^{1}H-{^{15}N} NOEs, because the values for helix 5 are slightly attenuated compared to helix 1 – 4 which indicates that helix 5 exhibits residual flexibility (Fig 5 e). Taking together the reduced helicity and rigidity observed for helix 5, we confirm that this helix is of transient nature. The absence of unambiguous NOE contacts between helix 5 and helix 2 and 3 confirm this idea as through-space NOE signals can only be captured if the lifetime of the complex is long enough. We interpreted this as an exchange between a folded state of helix 5 and a disordered conformation for both, ERdj3^{JGF} and ERdj4^{JGF} and therefore concluded that helix 5 of ERdj3^{JGF} and ERdj4^{JGF} resides in an equilibrium between a docked conformation in which helix 5 is bound to helix 2 and 3 and a disordered undocked conformation. We used the structure of DNAJB6b[87] to model structures of the J-domains of ERdj3 and ERdj4 together with the GF-regions (Fig 5 f, g). The position of helix 5 in the models of ERdj3-JGF and ERdj4-JGF reveals an overall congruence with the observed CSPs, however, especially for ERdj3-JGF, they do not match entirely. We observe Glu53 which is positioned towards the end of helix 3 to be involved in the interaction with helix 5 suggesting a slightly more diagonal position of helix 5 in ERdj3 (Fig 1f). In summary, we find that the GF-region of the ER-resident JDPs ERdj3 and ERdj4 can adopt an helical conformation what has been reported recently[115,126,190]. The position at which this helix fold back onto the J-domain is overall similar, however slight differences are revealed for ERdj3 by CSP experiments. While helix 5 of ERdj4 is more shifted

toward the HPD motif, helix 5 in ERdj3 adopts a more diagonal position moved towards the C-terminal end of helix 3. Most interestingly and in stark contrast with the studies on DNAJB1 and DNAJB6b we reveal that helix 5 of the ER-resident JDPs only shows 30 % of helical propensity proposing a first insight into a differential mechanism of regulation by an order to disorder equilibrium.

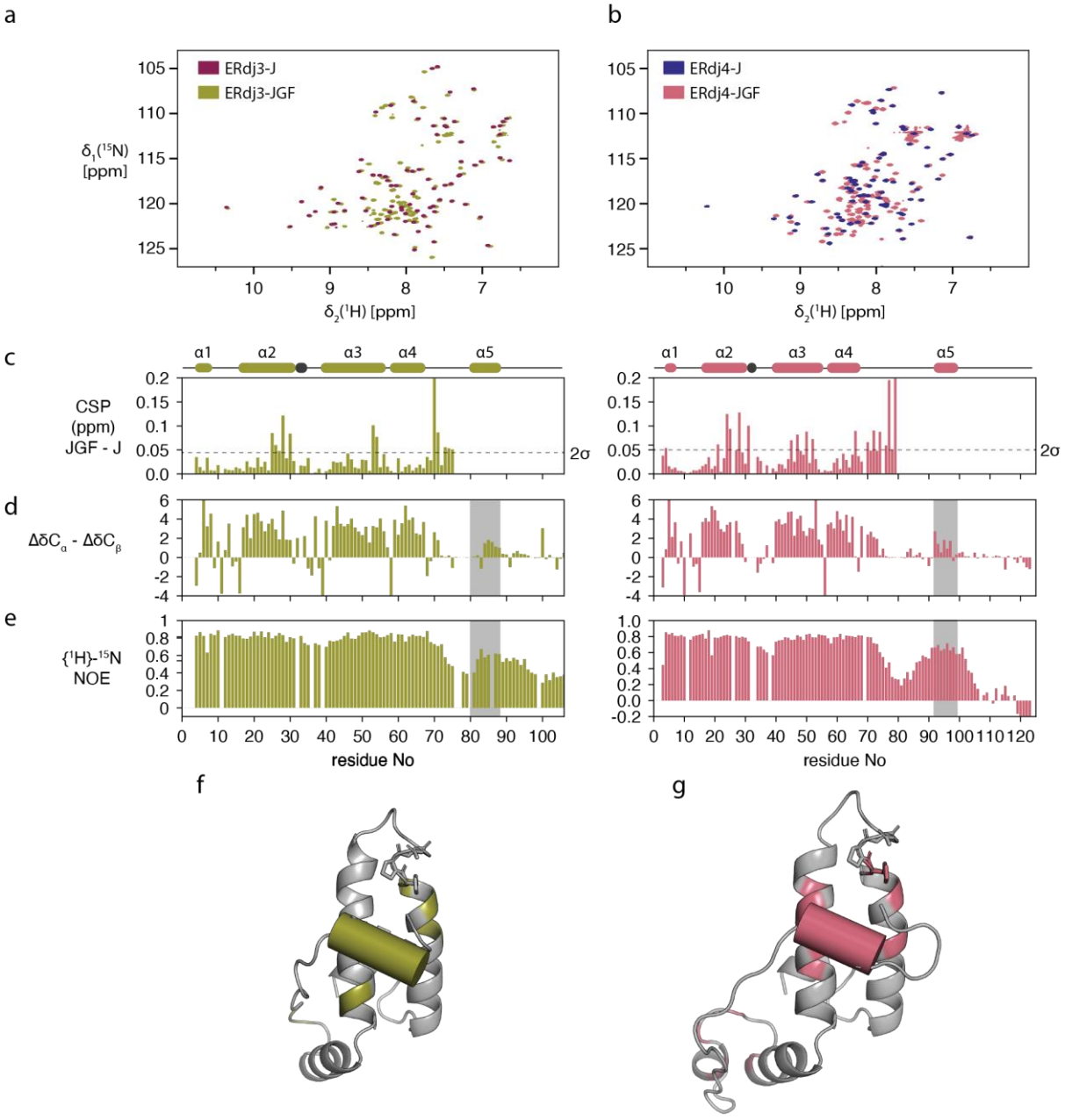

Figure 5. The conserved GF-linker is a structural part of the J-domains of ERdj3 and ERdj4 a, b: Overlay of 2D [^{15}N,^{1}H]-HSQC spectra of ERdj3 (a) and ERdj4 (b) constructs without and with their GF-region. Spectra were recorded at a protein concentration of 50 µM. c: Chemical shift perturbations

(CSPs) on the J-domains of ERdj3 (left panel) and ERdj4 (right panel) upon removal of the GF-region. d: secondary chemical shift differences of ERdj3- and ERdj4-constructs including the GF-region. Residues belonging to helix 5 are highlighted by a grey box. e: ^{1}H-{^{15}N} NOEs of ERdj3- and ERdj4-constructs including the GF-region. Residues belonging to helix 5 are highlighted by a grey box. f, g: CSPs > 2*stdv mapped on the modelled structures of the J-domains of ERdj3-JGF (f) and ERdj4 -JGF (g) in green and red respectively. Structural models were generated using SWISSMODEL[191] (template pdb: 6U3R).

The binding interface of the J-domain with Hsp70 is highly conserved

Interestingly, the interaction interface between helix 5 and the J-domain overlaps with the binding site for Hsp70 shown for the bacterial homologues DnaK and DnaJ[53] and human Hsc70 with the J-domains of DNAJA1 and DNAJB1[126]. As already described, helix 5 is also observed in DNAJB1 to fold back onto the Hsp70 binding site, here it inhibits an interaction of the two chaperones. However, in contrast to our results, helix 5 in DNAJB1does not show exchange between a bound and a disordered conformation, but regulation occurs in an on/off model triggered by allosteric events through preceding binding of Hsc70 to the CTDII of the JDP[126]. We therefore wanted to investigate if helix 5 of ERdj3 and ERdj4 has a similar regulatory role as DNAJB1.To elucidate the role of helix 5 for ERdj3 and ERdj4 with respect to its interaction with Hsp70, we first set to identify and confirm the binding site for the ER-resident Hsp70 BiP by NMR spectroscopic titration experiments. The structure of the J-domain of ERdj4 has been determined (pdb: 2CTR), however, no structure of ERdj3 is available. In order to accurately map the BiP binding interface onto the J-domain of ERdj3, we determined its structure using NMR spectroscopy with a backbone RMSD of 0.62 ± 0.27 Å (Fig 6).

a

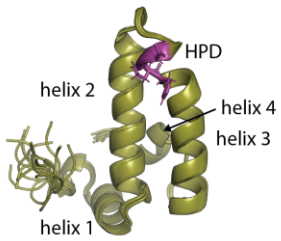

b

NOE distance restraints:

All:		
Intraresidue, |i-j|=0:	1706	100%
Sequential, |i-j|=1:	410	24.0 %
Short-range, |i-j|<=1:	447	26.6%
Med-range, 1<|i-j|<5:	857	50.2%
Long-range, |i-j|>=5:	424	24.9%

Restraints violated in 6 or more structures:
2 violated distance restraints.
2 violated van der Waals restraints.
0 violated angle restraints

Ramachandran statistics:

Residues in most favored regions:	90.9 %
Residues in additionally allowed regions:	9.1 %
Residues in generously allowed regions:	0.0 %
Residues in disallowed regions:	0.0 %

RMSDs for residues 1 to 76:
backbone RMSD: 0.62 ± 0.27 Å
Heavy atom: 1.02 ± 0.27 Å

Figure 6: NMR structure of the J-domain of ERdj3. Overlay of the 20 conformers with the lowest target function. Helices 1 – 4 are indicated, the HPD motif between helices 2 and 3 is highlighted in purple. NMR structure elucidation statistics. The structure was calculated using CYANA[17] and further refined in implicit water with XPLOR-NIH[187].

As discussed in the previous section, we used CSPs to identify J-domain residues directly involved in the binding interface. Upon addition of increasing amounts of unlabeled BiP, CSPs of interacting residues increase allowing to identify the binding site and estimate the binding affinity between the J-domains and BiP. In addition to CSPs, reduced peak intensities are also an indicator of residue-specific interactions and can be used for K_D estimations.

It has been established that Hps70 interacts with the J-domain in its ATP-bound state. To be able to observe this interaction between the J-domains and BiP, we used a BiP-variant deficient in ATP hydrolysis that comprised a mutation in its nucleotide binding domain (NBD, T229G) in presence of 5 mM ATP to trap BiP in its ATP-bound state. To expand the structural diversity of investigated J-domains, we incorporated the J-domain of the class C JDP ERdj6 into our investigations. For all J-domains, residues of the His-residue belonging to the HPD motif show large CSPs and a strong decrease in signal intensity confirming its importance for HSP70/JDP interactions. In addition, all J-domains show an interaction for residues in helix 2 and 3 (Fig 7 a - i). Furthermore, we could confirm that BiP interacts with the J-domain of ERdj3 via lobe IIA of the nucleotide binding domain by using an IV-labeled sample of wildtype BiP supplemented with ATPγS in order to trap the protein in its ATP-bound state upon addition of unlabeled ERdj3-J (Fig 8 a, b). The residues identified for the interaction were Met196, Ile199, Ile207 and Ile220 all belonging to the NBD of BiP.

Using the bacterial DnaK-DnaJ complex[53] to model the interaction between BiP and the J-domains, we identified several conserved pairs of interacting residues. A hydrophobic patch consisting of Ala and Leu/Met in all three J-domains experiences strong CSPs ($Ala27^{3J}$/$L28^{3J}$, $A27^{4J}$/$M28^{4J}$, $A28^{6J}$/$M29^{6J}$). These residues can form contacts with the sidechains of $V415^{BiP}$

and L417^{BiP} belonging to the interdomain-linker of BiP. Furthermore, the sidechain nitrogen of His33 from the HPD motif of all J-domains interacts with the carbonyl-group from L416^{BiP} (interdomain-linker). Both interactions confer allosteric changes withing BiP important for ATP hydrolysis[53].

We observe strong CSPs from G49^{3J}, A50^{4J} and I52^{6J}. At the corresponding position in *E. coli* DnaJ Lys51 is found, interacting with T420 from the SBD of DnaK. Although T445 in BiP is homologous to T420^{DnaK}, based on our model, we rather think that these hydrophobic J-domain residues interact with V442 in BiP.

In the DnaK-DnaJ complex, a salt bridge between the Arg22 of the J-domain and E206^{DnaK} from lobe II of the NBD is observed. From our data, we do not see a strong CSP from the corresponding Lys of the J-domains (K20^{3J}, K20^{4J}, I21^{6J}), however we observe the subsequent Lys21 from ERdj4^{J} being strongly affected by BiP binding, similar residues in ERdj3 and ERdj6 show moderate effects. We rationalized that these Lys residues interact rather with E217^{BiP} from lobe II rather than with T236^{BiP} which is found at the corresponding position of E206^{DnaK}. This would result in a slight rotation of the J-domain towards the SBD of BiP.

A corresponding residue to E498 in BiP has been reported to be fundamental for the Hsp70-J-domain interaction (D477^{DnaK}). E498^{BiP} contact can form salt bridges with R45^{4J} in ERdj4-J, however, in ERdj3-J we find a Gln46^{3J} at this position, possibly weakening this interaction. Finally, in ERdj6-J the positively charged residue is substituted by Ile50^{6J}. We therefore conclude that for the interaction between BiP and its subset of J-domains, this residue is not as fundamental as in the bacterial Hsp70-JDP complex.

These data confirm that the binding interface of Hsp70 and different J-domains is highly conserved among the species but also among the organelles of the eukaryotic cell and different classes of JDPs. However, changes in residues establishing this interaction might confer the specificity of each Hsp70-JDP subset.

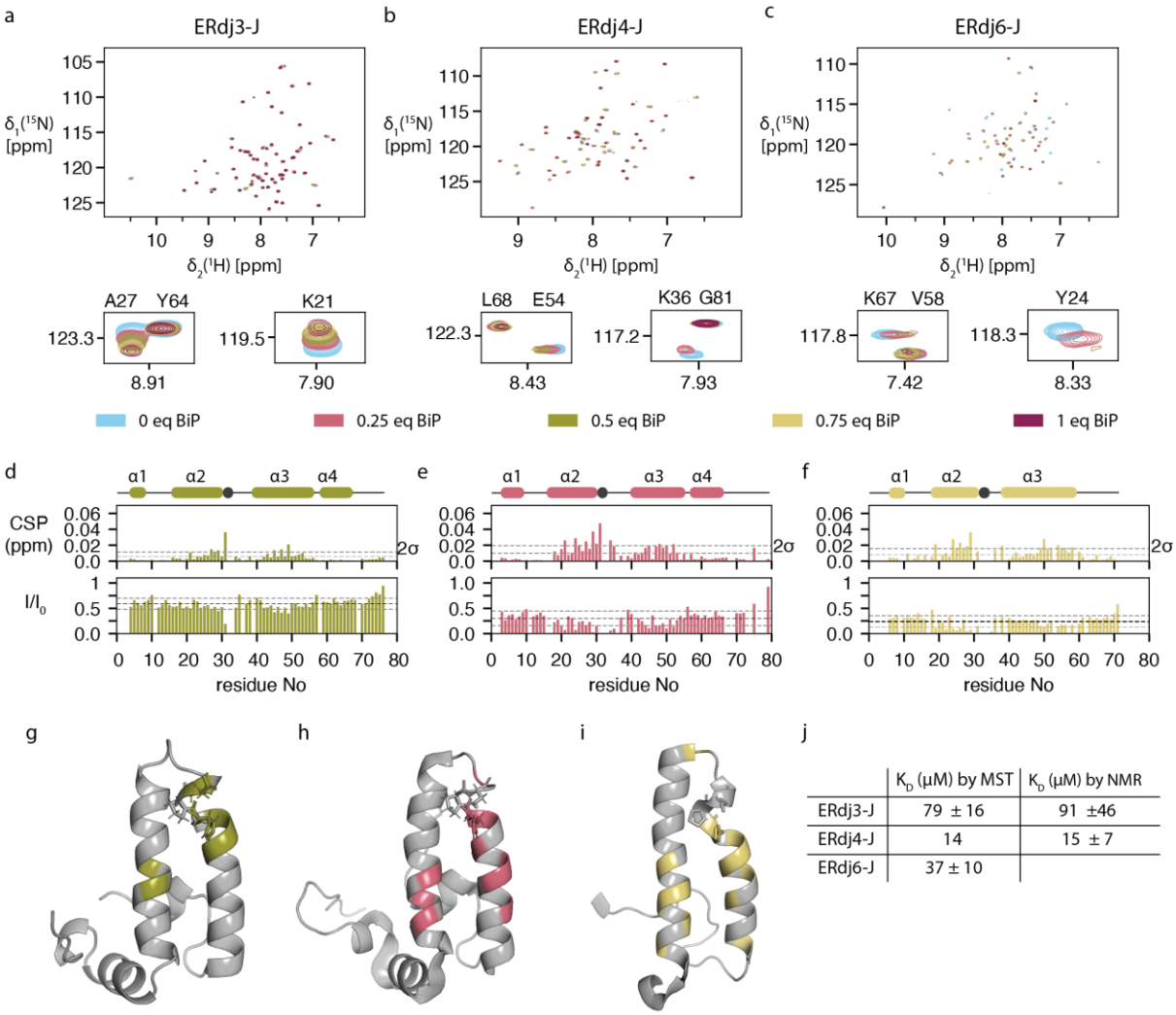

Figure 7. BiP binding interface on the J-domains of ERdj3, ERdj4 and ERdj6 a - c: 2D [^{15}N,^{1}H]-HSQC spectra of a titration of the Hsp70 chaperone BiP to the J-domains of ERdj3 (a), Erdj4 (b) and ERdj6 (c). The spectra were recorded at a concentration of J-domain constructs of 50 μM and with the BiP equivalents titrated as indicated at 30 °C in NMR buffer supplemented with 5 mM ATP in presence of an ATP regeneration system. d - f: Chemical shifts perturbations and relative intensity changes caused by 0.5 eq BiP. G – I: CPSs > 2*stdv caused by addition of 0.5 eq of BiP mapped onto the structures of ERdj3 (structure determined by NMR spectroscopy, see Fig 6), ERdj4 (pdb: 2CTR) and ERdj6 (pdb: 2Y4U) in green, red and yellow respectively. j: K_D values determined by MST and NMR of the interaction of respective J-domains with BiP. For the calculation of K_D values from NMR spectra, binding curves from peaks of those residues involved in binding were taken.

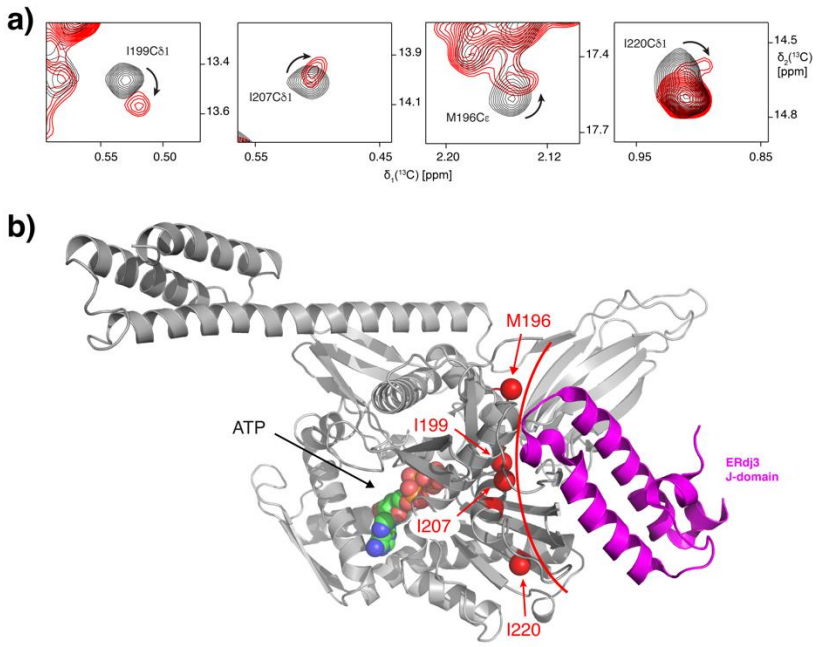

Figure 8: The binding interface of the J-domain of ERdj3 on BiP. a: Overlay of a section of a 2D of [^{13}C, ^{1}H]-HMQC spectra of U-[^{2}H^{14}N], Ile-[^{13}CH$_3$], Leu-[^{13}CH$_3$]proS, Met-[^{13}CH$_3$] methyl-labelled BiP without (black) and with four equivalents of ERdj3 J-domain (red). The spectra were recorded at a BiP concentration of 50 μM at 30 °C in NMR buffer supplemented with 5 mM ATP in presence of an ATP regeneration system. Assignment of the residues I199, I207, M196 and I220 in BiP ATP bound state is indicated next to the corresponding signals. b: Residues showing chemical shift perturbations upon titration of 4 equivalents of ERdj3 J-domain are mapped on BiP structure in red. The complex between ERdj3 J-domain and BiP in the ATP bound state (pdb 5E84) has been aligned to the crystal structure of its bacterial homolog, the Dnak/DnaJ complex (pdb 5NRO).

In addition to residue specific reductions in peak intensities, the formation of large protein complexes leads to a decrease of all signal intensities due to larger tumbling times of large molecules. The averaged overall decrease in relative intensity of ERdj3-J (about 60% upon addition of 0.5 eq of BiP, Fig 7 d) is less than that of ERdj4-J and ERdj6-J (approximately 20%, Fig 7, e, f) indicating different affinities for these J-domains to BiP. We determined K_D values by microscale thermophoresis to be 79 ± 16 μM for ERdj3-J, 14 μM for ERdj4-J and 37 ± 10 μM for ERdj6-J (Fig 7 j and Fig 9 a, c, e). The values were confirmed by estimating the K_D from the normalized peak intensities of the NMR spectra (Fig 9 b, d, f). These values lie within

the same range and both methods give lower values for ERdj4-J and ERdj6-J compared to ERdj3-J suggesting a differential interaction of BiP with the J-domains of different JDPs.

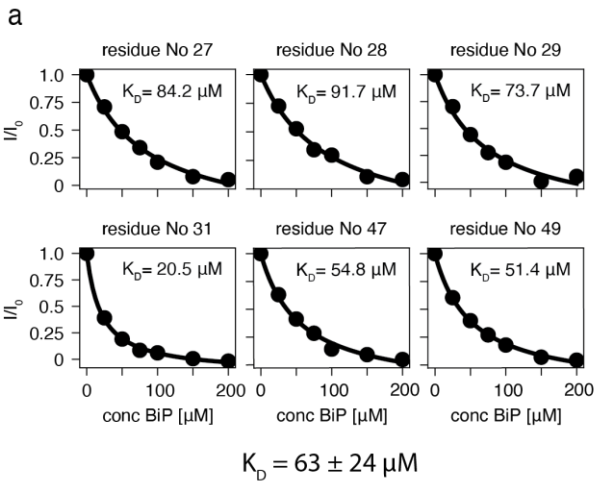
a
residue No 27
residue No 28
residue No 29
residue No 31
residue No 47
residue No 49
K_D= 84.2 µM
K_D= 91.7 µM
K_D= 73.7 µM
K_D= 20.5 µM
K_D= 54.8 µM
K_D= 51.4 µM
I/I_0
conc BiP [µM]
K_D = 63 ± 24 µM

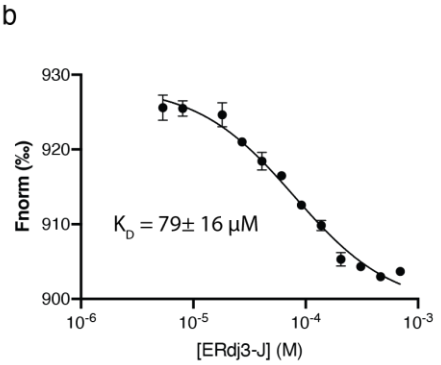
b
Fnorm (‰)
K_D = 79± 16 µM
[ERdj3-J] (M)

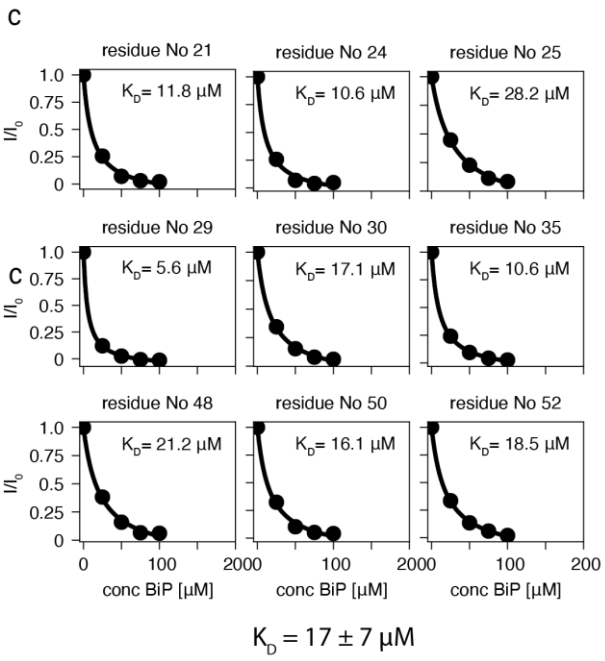
c
residue No 21
residue No 24
residue No 25
residue No 29
residue No 30
residue No 35
residue No 48
residue No 50
residue No 52
K_D= 11.8 µM
K_D= 10.6 µM
K_D= 28.2 µM
K_D= 5.6 µM
K_D= 17.1 µM
K_D= 10.6 µM
K_D= 21.2 µM
K_D= 16.1 µM
K_D= 18.5 µM
I/I_0
conc BiP [µM]
K_D = 17 ± 7 µM

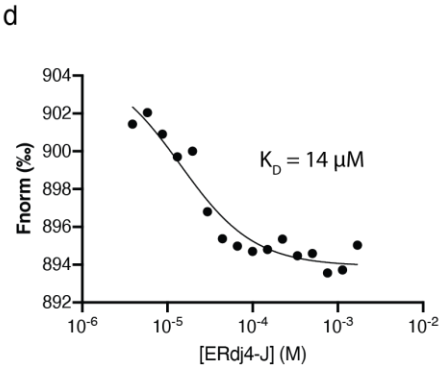
d
Fnorm (‰)
K_D = 14 µM
[ERdj4-J] (M)

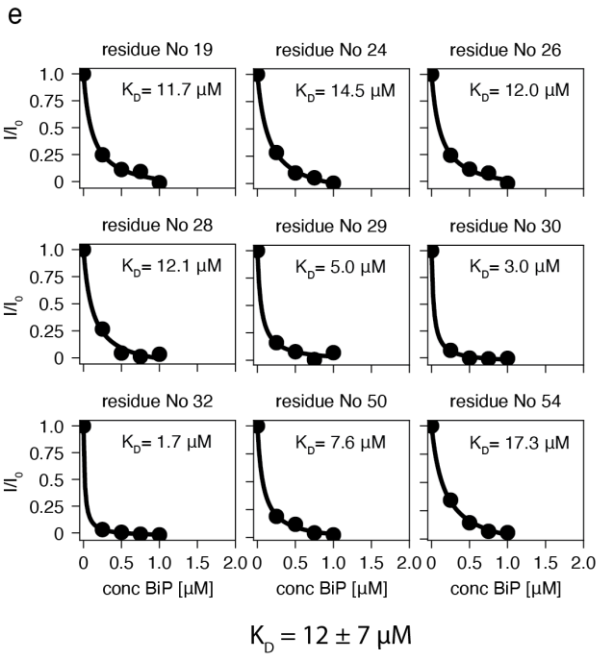
e
residue No 19
residue No 24
residue No 26
residue No 28
residue No 29
residue No 30
residue No 32
residue No 50
residue No 54
K_D= 11.7 µM
K_D= 14.5 µM
K_D= 12.0 µM
K_D= 12.1 µM
K_D= 5.0 µM
K_D= 3.0 µM
K_D= 1.7 µM
K_D= 7.6 µM
K_D= 17.3 µM
I/I_0
conc BiP [µM]
K_D = 12 ± 7 µM

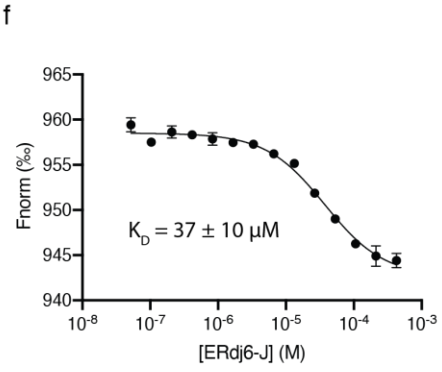
f
Fnorm (‰)
K_D = 37 ± 10 µM
[ERdj6-J] (M)

Figure 9: Affinities of the isolated J-domain to BiP. a, c, e: K_D values estimated from peak intensities of NMR titrations for ERdj3-J, ERdj3-JGF, ERdj4-J, ERdj4-JGF respectively. For the calculation of the K_D, binding curves from peaks of those residues involved in binding were taken. Measurements were performed at 30°C in NMR buffer supplemented with 1 mM ATP and an ATP regeneration system. b, d, f: Microscale Thermophoresis (MST) measurements to determine the Dissociation constant (K_D) of the J-domains of ERdj3, ERdj4 and ERdj6 respectively to BiP. Measurements were performed at 30°C in NMR buffer supplemented with 1 mM ATP at a constant concentration of fluorescently labelled BiP of 250 nM.

In Summary, we showed that the interaction of the ER-resident Hsp70 BiP with the J-domains of three different J-domains is highly conserved. It involves the HPD motif, helix 2 and 3 from the J-domain and the interface between the NBD and SBD on Hsp70 which is in line with observations for other pairs of Hsp70s and J-domain proteins.
Furthermore, different affinities of the three different J-domains to BiP were found which might suggest that the specific roles each JDP plays in collaboration with BiP are also defined by their strength of the interaction between the J-domain and the NBD of BiP.

Helix 5 of ERdj4 reduces the stimulatory effect of JPD on the ATP hydrolysis by BiP

After confirming the conserved Hsp70 binding interface, it becomes clear that helix 5 of the GF-region from ERdj3 and ERdj4 occupies the Hsp70 binding site. This observation calls for an investigation of the functional role of helix 5 for the stimulation of the ATPase activity of BiP. We therefore compared the relative ATP hydrolysis rates of BiP alone and upon addition of the J-domain constructs with and without the GF-region. The presence of helix 5 of ERdj4^{JGF} resulted in a significant decrease of the ATP hydrolysis stimulation (1.5-fold stimulation) compared to ERdj4^{J} (4-fold, Fig 10). Remarkably, the GF-region of ERdj3^{JGF} did not show a similar reducing effect, the stimulation of the ATP hydrolysis was comparable to the J-domain alone (3-fold). Furthermore, the data reveals a slight difference in the stimulatory effect on the ATPase activity between the J-domains or ERdj3 (three-fold) and ERdj4 (four-fold) which could be explained by the described differences in their affinities to BiP as shown in Fig 7 j and Fig 9.

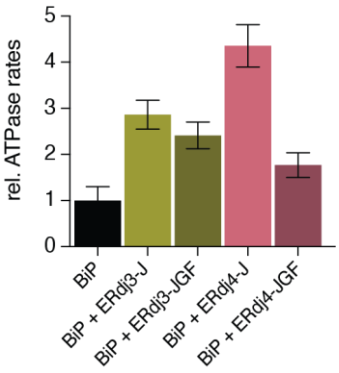

Figure 10. Stimulation of BiP ATPase activity by cochaperone variants. Normalized ATP hydrolysis rates of full length BiP upon addition of 5 equivalents of J-domain constructs as indicated. ATP hydrolysis rates of BiP were measured by spectrophotometric quantification of the complex formed by malachite green, molybdate and free orthophosphate. BiP WT was used in a concentration of 2 µM in 25 mM HEPES, 150 mM KCl, 10 mM $MgCl_2$, 1 mM ATP, the incubation time was 60 min at 37°C.

To gain further structural insights into the interaction of BiP with J-domain and to evaluate the effect of the GF-region on this interaction, we recorded 2D [^{15}N,^{1}H-]-HSQC spectra of ERdj3^{JGF} and ERdj4^{JGF} upon titration with BiP. These experiments demonstrated the same binding interface to BiP as has been shown for the J-domain only constructs for both ERdj3 and ERdj4 (Fig 7, Fig 11). This can only be explained by BiP binding to the J-domain while helix 5 is not bound. Furthermore, these data suggest a possible involvement of the GF-region in binding to BiP since CSPs and intensity decreases could be observed for residues from helix 5. However, it remains to be determined if they origin from an increased detachment of helix 5 upon BiP binding or on additional subsequent binding to BiP (Fig 11).

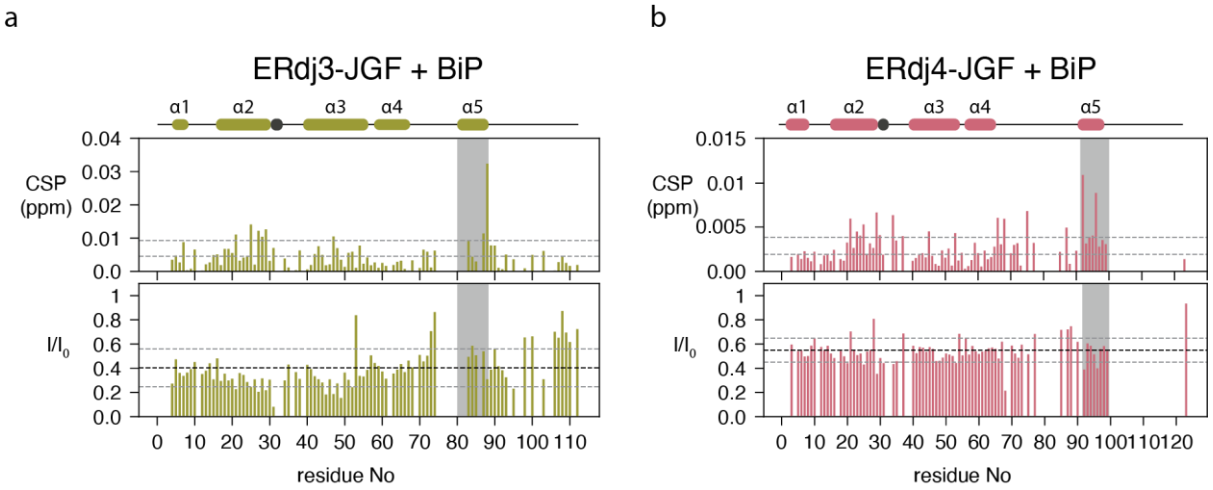

Figure 11. Interaction of ERdj3^{JGF} and ERdj4^{JGF} with BiP. a, b: Chemical shift perturbations (CSPs) and intensity changes of ERdj3-JGF (a) and ERdj4 (b) upon addition of 0.5 eq of BiP. The spectra were recorded at a concentration of J-domain constructs of 100 μM and with the BiP equivalents titrated as indicated at 30 °C in NMR buffer supplemented with 5 mM ATP in presence of an ATP regeneration system.

Since the binding interface to BiP on the J-domain constructs lacking and including the GF-region remains the same, we rationalized that the inhibitory effect of the GF-region in ERdj4 origins from an occupation and thereby blocking of the BiP binding site. We thus confirm that the GF-region of ERdj4 has a role in the regulation of an functional Hsp70-JDP interaction as has been recently shown for DNAJB1[126]. On the contrary, we did not see the same inhibitory effect for the GF-region of the canonical class B JDP ERdj3, although it also occupies the BiP binding interface. We therefore conclude that the regulatory effect of interaction of the GF-region with the BiP-binding site on the J-domain is not highly conserved among class B JDPs as has been suggested by Faust et al[126]. Furthermore, the observation of a slightly lower stimulatory effect of the isolated J-domain (without GF-region) of ERdj3 when compared to the effect of ERdj4 mirrored the differences in affinity to BiP. Although the differences are small, they might represent a fine-tuning mechanism for the specific interaction of BiP with distinct JDPs as has been suggested earlier for the BiP homologue in *S. cerevisiae*[192].

Helix 5 of ERdj4 is binding stronger to the J-domain

Next, we sought to explain different effects that the GF-region exerts on ERdj3^{JGF} and ERdj4^{JGF} in the context of their interaction with BiP on a structural level. An inspection of the modeled structures of ERdj3^{JGF} and ERdj4^{JGF} including the GF-region reveal a conserved phenylalanine in the center of helix 5 of both proteins (F84 in ERdj3^{JGF} and F96 in ERdj4^{JGF}). This phenylalanine inserts between two other aromatic residues of helix 2 and helix 3 (Y23, F45 in ERdj3^{JGF} and F23, F45 in ERdj4^{JGF}) allowing for hydrophobic interactions and possible π-stacking to stabilize the interaction between helix 5 and the J-domain (Fig S4a, b). These two aromatic residues of the J-domain are conserved in class B JDPs, in class A JDPs however, only the aromatic residue on helix 3 is conserved (Fig 12).

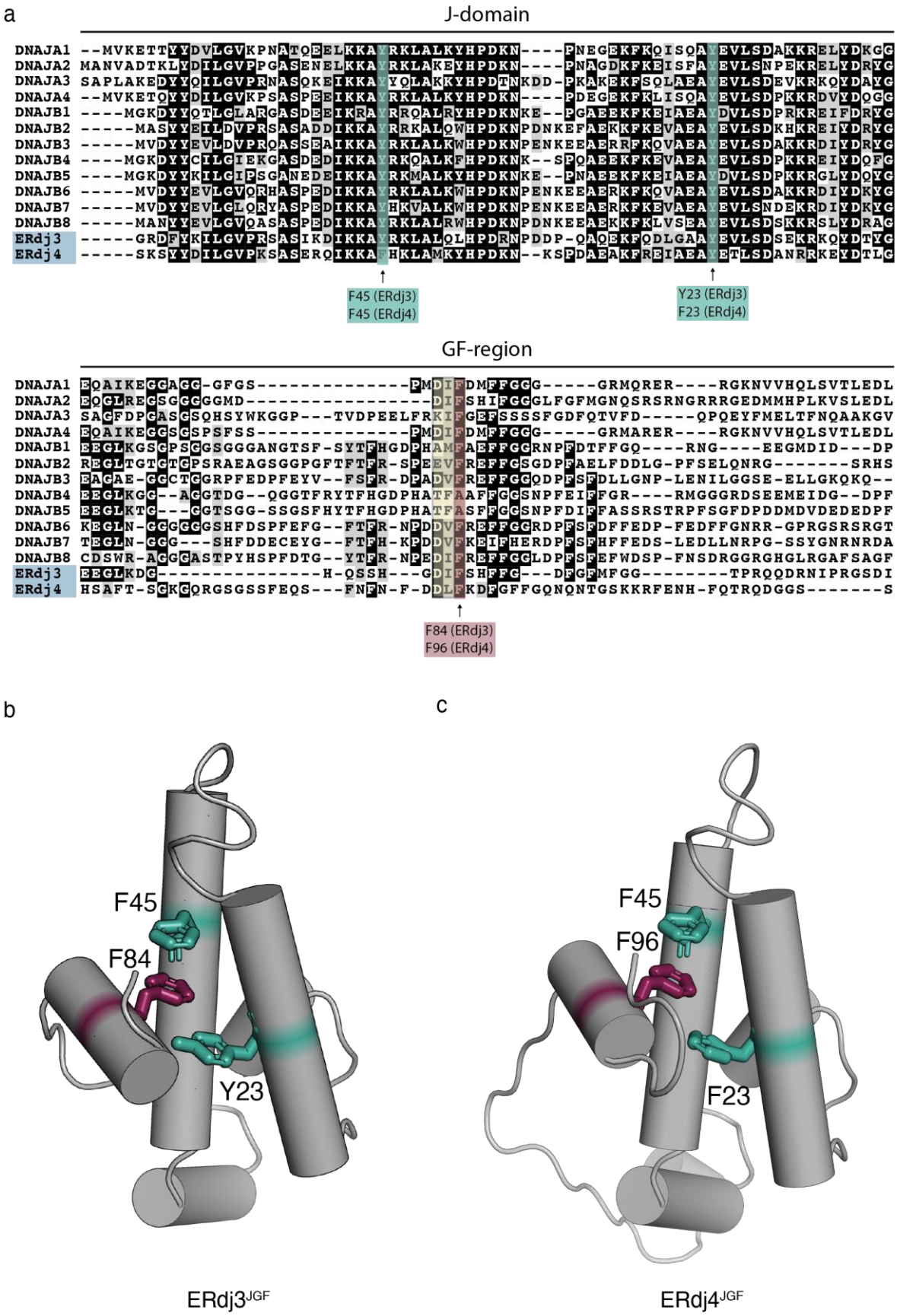

Figure 12: Conserved aromatic residues in ERdj3 and ERdj4 that establish interaction between J-domain and GF-region. a: Sequence alignment of all class A and class B (canonical and non-canonical)

JDPs. The three aromatic residues that might be important for the interaction between the J-domain and the GF-region are highlighted in teal (on the J-domain) and in purple (in the conserved part of the GF-region which is highlighted in yellow). b, c: Models of ERdj3^{JGF} and ERdj4^{JGF}. The described aromatic residues are highlighted on the structure in teal and purple. The models were generated using SWISSMODEL (template 6U3R).

To examine the differences between the J-domains of ERdj3^{JGF} and ERdj4^{JGF} regarding their interaction with helix 5, we mutated the central phenylalanine in helix 5 to an aspartate (F84D in ERdj3^{JGF} and F96D in ERdj4^{JGF}) and investigated the influence of the mutation on the structure of both JDPs by 2D [^{15}N,^{1}H-]-HSQC spectra (Fig 13 a, b). The signal positions of residues assigned to helix 2 and 3 of ERdj3^{JGF} F84D significantly differ from the signal positions of WT ERdj3^{JGF} indicating an altered conformation of the ERdj3^{JGF} F84D (Fig 13 a). We identified CSPs of exactly those residues that are involved in binding to helix 5 in WT ERdj3^{JGF}. A comparison with spectra of ERdj3^{J} reveal that all peak positions of ERdj3^{JGF} F84D are shifted towards or overlap with peak positions of the isolated J-domain, indicating that the equilibrium between the docked and the open conformation is shifted towards the open form by a detachment of helix 5 from the J-domain. Furthermore, the F84D mutation increased the relative signal intensities of the C-terminal region including helix 5 when compared to WT ERdj3^{JGF} (Fig 13 c). This change in signal intensities is characteristic for an increased flexibility which again can be explained by the detachment of helix 5. These observations prove the importance of the central conserved phenylalanine in helix 5 of ERdj3 for the interaction of the GF-region and the J-domain because the F84D mutation could significantly weaken this interaction.

In contrast, mutation of the Phe residue at the same position in helix 5 (F96D) of ERdj4^{JGF} did not significantly disrupt the interaction between helix 5 and helix 2 and 3 as can be seen from chemical shift positions and signal intensities (Fig 13 b, e, f). Here, the peak positions of the F96D mutant lie much closer to or overlap with those of residues belonging to WT ERdj4^{JGF} and the relative peak intensities of the C-terminal region including helix 5 did not increase. They showed similar values as helices 1 – 4 from the J-domain as it is also observed for WT ERdj4^{JGF} (Fig 13 e, f). These data suggest the phenylalanine centrally placed in helix 5 of ERdj3 and ERdj4 establishes the interaction with helices 1 – 4 from the J-domain, probably

by hydrophobic interactions and π-stacking. However, in ERdj4 more interacting residues must contribute since the F96D mutation did not detach helix 5 from the J-domain.

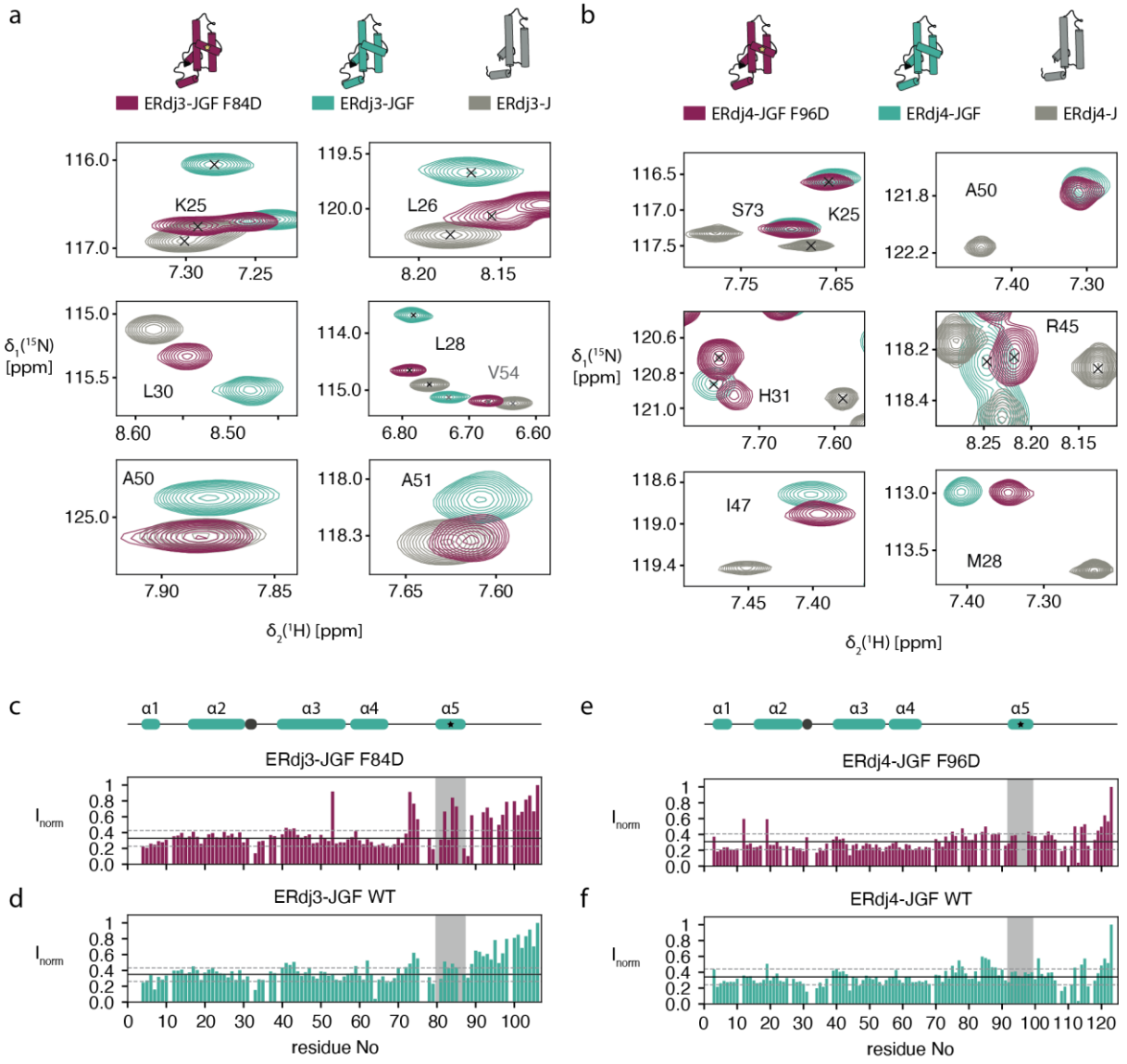

Figure 13: Effect of the central phenylalanine in helix 5. a, b: sections of 2D [^{15}N,^{1}H]-HSQC spectra of ERdj3^{JGF} F84D and ERdj4^{JGF} F96D (dark red) compared to WT ERdj3/4^{JGF} (green) and ERdj3/4^{J} (gray) (left and right panel respectively). The spectra were recorded at a concentration of J-domain constructs of 50 µM at 30 °C in NMR buffer. c, d: Normalized peak intensities of ERdj3-JGF F84D (c) and ERdj4-JGF F96D (d) (normalization to the peak with the highest intensity within the same spectrum). e, f: Normalized peak intensities of WT ERdj3^{JGF} and WT ERdj4^{JGF} (normalization to the peak with the highest intensity within the same spectrum).

Closer examination of the model of ERdj4-JGF reveals contacts that could stabilize the interaction between the J-domain and the GF-region in addition to the central phenylalanine in helix 5 (Fig 14 a, b). H24 on helix 2 could form π-stacking with F99 at the outer edge of helix 5 and R45 on helix 3 can be involved in a polar interaction with D93 at the beginning of helix 5. These interactions cannot be established in ERdj3^{JGF} due to differences within the sequence regarding residues at comparable positions (93D→81G, 45R→46N). Additionally, the linker connecting helix 5 to the J-domain of ERdj3 is 20 residues shorter introducing a tension into the GF-region that might counteract the attracting forces between helix 5 and the J-domain. These details could also explain our observation that helix 5 adopts a more diagonal position along the J-domain.

ERdj3^{JGF} F84D stimulated similarly the ATP hydrolysis by BiP as compared to WT ERdj3^{JGF} confirming that the observed interaction between helix 5 and the J-domain of ERdj3 does not block the interaction between the J-domain and BiP (Fig 14 c). In contrast, ERdj4-JGF F96D has a similar inhibitory effect on ATP hydrolysis as WT ERdj4^{JGF}, demonstrating the tighter interaction between helix 5 and the J-domain of ERdj4^{JGF} (Fig 14 c) compared to ERdj3^{JGF}. We therefore conclude that the equilibrium between the docked and the open conformation is different for the two ER-resident class B chaperones (Fig 14 d, Fig 15). While the BiP binding site of ERdj3 is easily accessible, the interaction between ERdj4 and BiP is regulated by the GF-region.

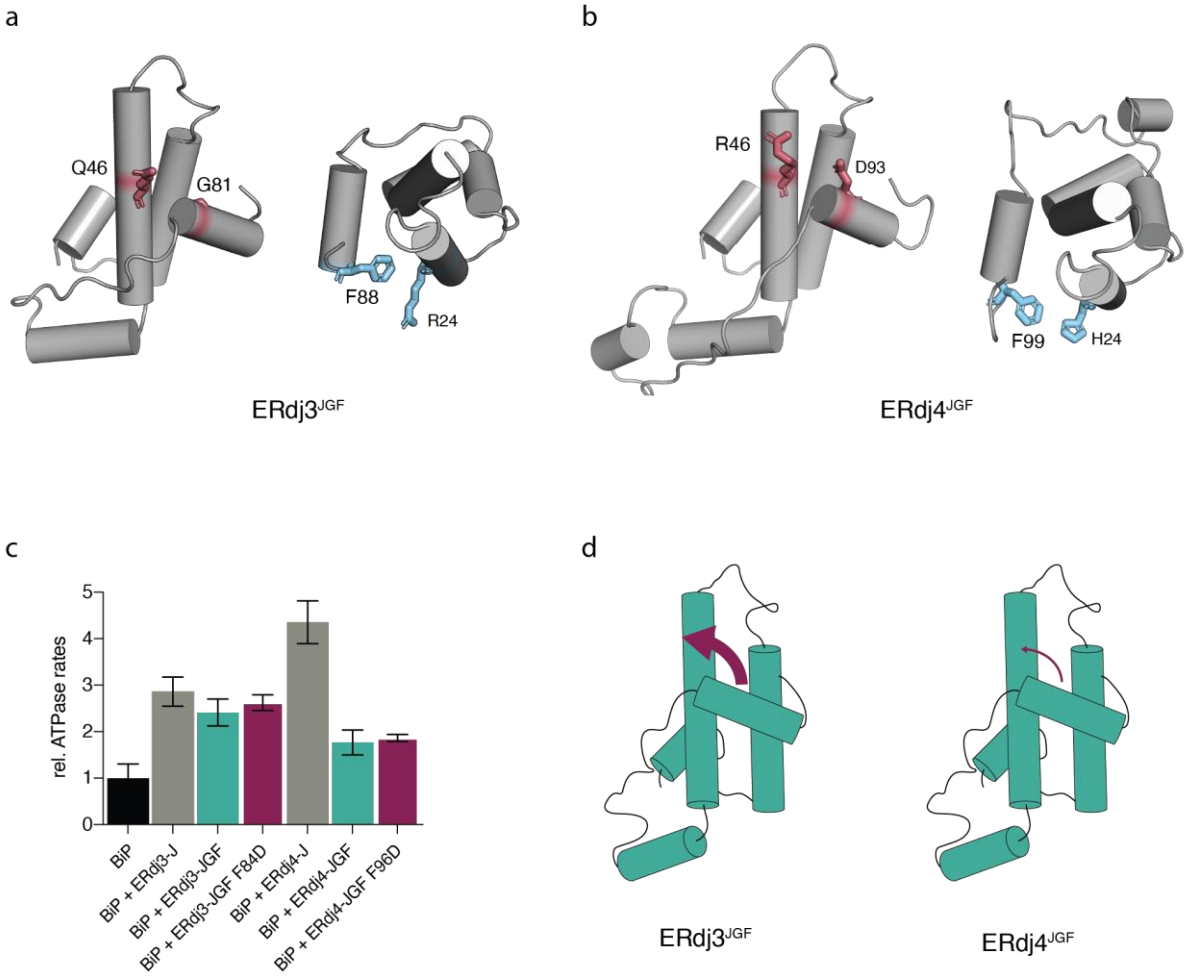

Figure 14: Sequence differences of ERdj3 andERdj4 determine the affinity between the J-domain and helix 5. a, b: comparison between residues in ERdj3^{JGF} (a) and ERdj4^{JGF} (b) that might strengthen the interaction between the J-domain and helix 5 from the GF-region. c: Normalized ATP hydrolysis rates of full length BiP upon addition of 5 equivalents of J-domain constructs as indicated. H: schematic model of the equilibrium between the docked and undocked conformation of ERdj3^{JGF} and ERdj4^{JGF}.

Overall, these results suggest that, although conserved among all class A and B J-domain proteins, helix 5 might not exhibit the same strength of interaction with the J-domain in all members of this protein class leading to different roles it plays for their interaction with Hsp70. This offers a mechanism for the distinction and differential regulation in the interaction of BiP with its two class B JDPs in particular and for Hsp70 with JDPs in general (Fig 12).

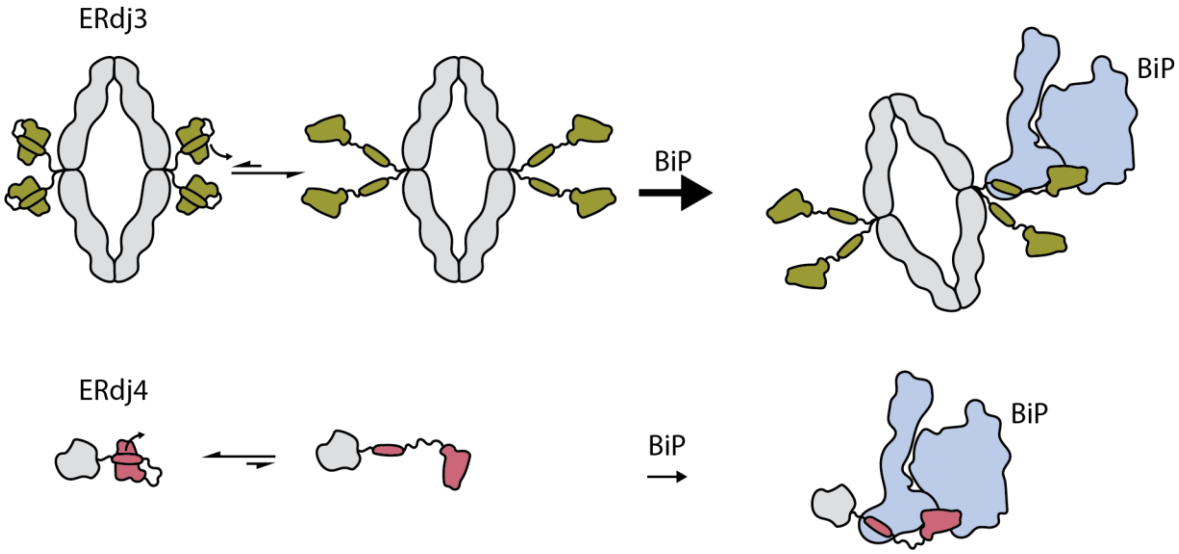

Figure 15: Model for BiP interaction with cochaperones. The GF-region of ERdj3 is not regulatory with respect to the interaction with BiP and allows stimulation of ATP hydrolysis rates. In contrast, for ERdj4, the GF-region binds tighter to the J-domain and thereby regulates its interaction with BiP.

3. Chapter 1 – Discussion and Outlook

In this study we did a comparative structural analysis of 3 ER-resident JDPs ERdj3, ERdj4 and ERdj6 and investigated the influence of the GF-region of the class B JDPs ERdj3 and ERdj4. For both cochaperones, the conserved DI/VF motif adopts an α-helical fold (helix 5) that binds perpendicular to helix 2 and 3 of the J-domain thereby occupying the highly conserved binding site for Hsp70. This fold has been shown recently for the human class B JDPs DNAJB6b[87] and DNAJB1[126] and it is therefore likely a conserved feature of the GF-region in class B JDPs. In *T. thermophilus* DnaJ, a class B JDP, the GF-region also forms a small α-helix, however its position was defined as a parallel alignment to helix 3 of the J-domain[115]. It therefore remains to be determined if the engagement of the Hsp70 binding site in the positioning of helix 5 is only conserved among humans or eukaryotes. Our NMR data demonstrates that helix 5 is not confined in a rigid conformation, but rather resides in an equilibrium between a folded docked state and a disordered open state where the Hsp70-binding interface is accessible. This differentiates both ER JDPs from the cytosolic DNAJB1 and DNAJB6b for which helix 5 adopts a unique rigid conformation[87,126]. Most interestingly, this equilibrium is differently balanced for ERdj3 and ERdj4 (Fig 15). While in ERdj4, the GF-region efficiently blocks the BiP binding site resulting in a reduced stimulatory effect on the ATPase activity of BiP, the BiP binding site is easily accessible in ERdj3. We therefore can confirm a regulatory role for the GF-region of ERdj4 as has been found for DNAJB1[126]. However, the GF-region of ERdj3 did not interfere with the stimulation of ATPase activity indicating that this regulatory role is not conserved among all class B JDPs. The differences in their ability to block BiP binding can be explained by distinct amino acid sequences of the GF-region and the J-domain of the two JDPs. Polar and aromatic residues convey stabilizing interactions between the J-domain and the GF-region of ERdj4 that are not possible in ERdj3 due to differences in the amino acid sequence. Furthermore, the region before the DI/VF motif is shorter in ERdj3 compared to ERdj4 that might introduce a counteracting tension. As shown for the human full length DNAJB1, its Hsp70 binding site is released upon an interaction of the C-terminal EEVD motif of Hsp70 with the CTDII of DNAJB1. This motif is highly conserved among cytosolic Hsp70s and has already earlier shown to bind to the CTDII of class B JDPs and thereby regulates their interaction with Hsp70[86,188,193,194]. However, BiP,

residing in the ER, has the C-terminal ER-retention motif KDEL and its disordered C-terminus does not contain a sequence similar to the EEVD motif. Therefore, a similar release mechanism might not be found for the ER-resident Hsp70 BiP and the canonical class B JDP ERdj3. ERdj3 has been identified as a pro-folding co-chaperone[195] residing at the translocon[78,196] where it assists during *de novo* folding of nascent polypeptides. Considering that the translocation of membrane and secretory proteins into the ER and their subsequent folding is an elementary and steady process, during which a regulation of the co-chaperoning of BiP by ERdj3 might not be necessary, we hypothesize that ERdj3 might have lost its regulatory element within the GF-region. ERdj3 already shows other features such as the tetramer formation and disulfide bridges that distinguish this JDP from other class B members, which might origin from an adaptation to the requirements and conditions of protein folding within the ER. The GF-region of the class A JDP DNAJA1 does not adopt an α-helix folding back onto the J-domain and therefore does not serve as a regulatory element in contrast to DNAJB1[126]. The authors therefore conclude that the structural fold and mechanistic role of the GF-region is a conserved difference between class A and class B JDPs. ERdj3 frequently is described as class B JDP because of its lack of the zinc binding cluster. However, it is also found to be referenced as a class A JDP, supposedly because its disulfide bridges are approximately at the same position as the zinc binding cluster in class A JDPs and might be relict of the latter due to adaptions to the oxidizing environment of the ER[197]. Due to the proven formation of α-helix 5 in ERdj3 but the lack of the regulatory function, one possibility is that the differentiation between class A and canonical class B JDPs based on the functional role of the GF-region is not as strict as proposed by Faust et al[126] and "hybrid" JDPs such as ERdj3 might exist.

On the contrary ERdj4, a non-canonical class B JDP, which is upregulated during ER-stress, has been shown to bind aggregation-prone sequences within proteins[195] and to play a role during ERAD[179] and the UPR[198]. These delicate processes require a high regulation[199] and therefore it is highly plausible, that the specialized cochaperone ERdj4 kept its regulatory motif in the GF-region. Especially because both, BiP and ERdj4 have been found to form a complex with the UPR signaling protein, Ire1[181]. The mechanism by which the BiP binding site gets released from the GF-region is not known yet. We show that the dynamic nature of the interaction between GF-region and J-domain still allows BiP binding, although to lower

extent. It might be sufficient accomplish its specialized chaperoning tasks. However, other events such as client binding or post-translational modifications that alter the J-domain-GF-region interplay could be an alternative regulation mechanism. Indeed, ERdj4 contains a conserved serine in its GF-region which has been proven as phosphorylation site in DNAJB1. This serine is located between the J-domain and helix 5, phosphorylation might change the dynamics of the GF-region and thereby release helix 5 from the J-domain.

Although not representing a regulatory element for the interaction with Hsp70[126], the conserved DI/VF motif is present in ERdj3 as well as in human class A JDPS, the elucidation of its role remains an intriguing challenge. Our results might suggest an involvement of the GF-region in binding to BiP, however the analysis of these data is difficult since the handling of protein samples of constructs containing the GF-region is particularly challenging. These constructs tend to acquire viscous gel-like properties during measurement which requires the preparation and use of several fresh samples for one titration experiment. However, these changes probably happen already within the first hours of measurement and therefore our data on BiP binding might be obscured by the gel-formation of GF-region containing protein samples. These observations are reminiscent of the formation of liquid droplets during liquid liquid phase separation and just recently, this process has been demonstrated for the human JDPs DNAJA1 and DNAJB1 as well as for the yeast JDPs Ydj1 and Sis 1[127]. An obvious next step is therefore to test ERdj3 and ERdj4 for the formation of liquid droplets and their participation in liquid liquid phase separation. The formation of membrane-less organelles is plausible, especially for ERdj3 which is involved in the folding of nascent polypeptides at the translocon, and therefore an increased accumulation of folding chaperones appears beneficial for this process.

JDPs have long been seen as side kick of the well-known and noted chaperones of the Hsp70 and the Hsp90 family. However, it becomes more and more apparent that this diverse chaperone family is as important and interesting as their ubiquitous “bigger” sisters. Much remains to be discovered such as client hand-over to Hsp70 but also individual and independent functions of JDPs.

4. Chapter 1 - Materials and Methods

Expression and purification of J-domain constructs

The constructs for ERdj3-J, ERdj4-J, ERdj4-JGF, ERdj4-JGF F96D and ERdj6-J were cloned with an N-terminal His-tagged SUMO-fusion-protein. ERdj3-JGF and ERdj3-JGF F84D were cloned with a C-terminal-His-Tag preceded by a TEV-cleavage site into a pET28a vector by GenScript.

All proteins were expressed in *E. coli* BL21-(λ DE3)-Lemo cells (New England Biolabs (NEB)) in LB medium or M9-medium supplemented with either ^{15}N NH_4Cl (for interaction studies by NMR (Cambridge Isotope Laboratories; CIL)) or ^{15}N NH_4Cl and U-^{13}C glucose (for assignments and structure determination, (Cambridge Isotope Laboratories; CIL)). Expression was induced at an OD_{600} = 0.8 by addition of 0.5 mM IPTG and took place at 25 °C during 5 hours. All constructs were purified via nickel-affinity chromatography using buffer A (25 mM HEPES, 200 mM NaCl, 20 mM imidazole, pH = 7.5) for washing. Before elution with buffer B (25 mM HEPES, 200 mM NaCl, 500 mM imidazole, pH = 7.5), a washing step with buffer C (25 mM HEPES, 1 M NaCl, 20 mM imidazole, pH = 7.5) was included. After tag removal by addition of the respective protease (ULP for SUMO-fusion protein constructs and TEV for ERdj3-JGF and ERdj3-JGF F84D) and subsequent reverse Nickel-affinity chromatography, the proteins were further purified by size exclusion chromatography (Superdex-75 16/600 PG) using a buffer containing 25 mM HEPES, 150 mM KCl, 10 mM $MgCl_2$, pH = 7.5.

Expression and purification of BiP constructs

BiP WT and BiP T229G were cloned with an N-terminal His_6-tag preceded by a TEV-cleavage site and expressed in in *E. coli* BL21-(λ DE3)-Lemo cells (New England Biolabs (NEB)) in TB medium to obtain unlabeled proteins. For the expression of U-[^{2}H, ^{14}N], Met-[$^{13}CH_3$], Val-[$^{13}CH_3$]$^{proS/proR}$ BiP, M9 medium $^{15}ND_4Cl$ (1 g/liter, Sigma-Aldrich) and d-glucose-d_7 (2 g/liter; Sigma-Aldrich) was supplemented with 80 of mg 3,3-[$^{2}H_2$],4-[^{13}C]-2-ketobutyrate (NMR-Bio), 100 mg of 2-oxo-3-[^{2}H]-3-[$^{2}H_3$]methyl-4-[^{13}C]-butanoate (a-ketoisovalerate, Sigma-Aldrich) (, 40 mg of L-leucine-d_{10} (Sigma-Aldrich) and 100 mg of [α,β,γ-$^{2}H5$, e13C]- L-methionine

(Cambridge Isotope Laboratories; CIL). Expression was induced at an OD_{600} = 0.6 by addition of 1 mM IPTG and took place at 25 °C during 5 hours. The protein constructs were purified via nickel-affinity chromatography using buffer A (25 mM HEPES, 500 mM NaCl, 20 mM imidazole, pH = 7.5) for washing and buffer B (25 mM HEPES, 500 mM NaCl, 500 mM imidazole, pH = 7.5) for elution. After purification, the buffer was exchanged by dialysis to 25 mM HEPES, 300 mM NaCl, pH = 7. Subsequently, the protein was unfolded in buffer A containing 6 M urea and a nickel-affinity chromatography under denaturing conditions was performed using buffers A to B each containing additionally 6 M urea. After refolding of the protein by dialysis against 4 L of 25 mM HEPES, 300 mM, KCl, pH=7.5, the His_6-tag was removed by addition of TEV protease and a subsequent reverse nickel-affinity chromatography. Buffer exchange to 20 mM TRIS, pH = 8.0 was followed by ion-exchange chromatography using an elution buffer containing 20 mM TRIS, 1 M NaCl, pH = 8.0. The protein was further purified by size exclusion chromatography (Superdex S200, preparative grade) using a buffer containing 25 mM HEPES, 150 mM KCl, 10 mM $MgCl_2$, pH = 7.5.

NMR experiments

All NMR spectra were recorded on a Bruker Avance III spectrometers operating at 600 and 700 MHz proton frequency, each equipped with a cryogenic triple-resonance TCI probe.

For the interaction experiments of the J-domain protein constructs with BiP, 2D [^{15}N,^{1}H-]-HSQC spectra with 2048 points in the direct dimension and 400 points in the indirect dimension were recorded. Prior to Fourier transformation, the spectra were multiplied with a 75°-shifted squared sine bell and zero-filled to 4096 points and 1024 points respectively. The samples contained 100 μM of [*U*-^{15}N]-labeled J-domain constructs and 0, 0.25, 0.5, 0.75 and 1.0 equivalents of BiP T229G in 25 mM HEPES, pH = 7.5 150 mM KCl, 10 mM $MgCl_2$, 1 mM ATP, in presence of an ATP regeneration system (REF) (0.01 mM PEP, 3 Units of pyruvate kinase from *Bacillus stearothermophilus*), 100 μM DSS and 5% D_2O. Measurements were performed at 30 °C.

2D [^{15}N,^{1}H]-HSQC spectra for the comparison of the constructs with and without helix 5 were recorded with 2048 points in the direct dimension and 512 points in the indirect dimension.

Prior to Fourier transformation, the spectra were multiplied with a 75°-shifted squared sine bell and zero-filled to 4096 points and 1024 points respectively. The samples contained 50 μM of [*U*-^{15}N]-labeled J-domain constructs in 10 mM NaH_2PO_4, 100 mM NaCl, 1 mM EDTA, pH = 6.4, 100 μM DSS, 5% D_2O. Measurements were performed at 25 °C.

The samples for the assignment of all used constructs and for the structure calculation of the J-domain of ERdj3 contained 0.3 mM (linker constructs) and 1 mM (J-domains without linker) of [*U*-^{13}C, ^{15}N]-labeled J-domain constructs in 10 mM NaH_2PO_4, 100 mM NaCl, 1 mM EDTA, pH = 6.4, 100 μM DSS, 5% D_2O, all spectra were measured at 37 °C. The proton chemical shifts were referenced to an internal DSS standard and those for ^{13}C and ^{15}N were indirectly referenced. The backbone assignment of ERdj3-J, ERdj3-JGF, ERdj4-J, ERdj4-JGF and ERdj6 was performed using a 3D [^{13}C,^{15}N,^{1}H-]-HNCACB in combination with a 3D [^{13}C,^{15}N,^{1}H-]-HNCOCACB. Sidechain assignment of the aliphatic residues of ERdj3-J was achieved using a 3D [^{15}N,^{1}H-]-HSQC-TOCSY, a 3D [^{13}C,^{15}N,^{1}H-]-hCcoNH -TOCSY, a 2D [^{13}C,^{1}H-]-HSQC together with a 3D [^{13}C,^{1}H-]-HcCH-TOCSY, a 3D [^{13}C,^{1}H-]-hCCH-TOCSY for aliphatic residues. Aromatic sidechains were assigned with a 2D [^{13}C,^{1}H-]-HMQC and a 3D [^{13}C,^{1}H-]-NOESY-HSQC. Distance restraints were obtained from a 3D [^{15}N,^{1}H-]-NOESY-HSQC-HSQC and a 3D [^{13}C,^{1}H-]-NOESY. A list of all recorded spectra as well as the relevant measurement and processing parameters is given in table A1 in the appendix.

Calculation of secondary structure elements ($\Delta\delta C_\alpha$ - $\Delta\delta C_\beta$)

Secondary chemical shifts were obtained by subtracting values of averaged random coil from the observed chemical shifts for C_α and C_β of each residue obtained from the 3D assignment spectra:

$$\delta C_\alpha = C_{\alpha,observed} - C_{\alpha,random\ coil}$$
$$\delta C_\beta = C_{\beta,observed} - C_{\beta,random\ coil}$$

The values C_α and C_β of random coil structures were obtained from Schwarzinger et al[12].

Measurement of ^{15}N{^{1}H} Nuclear Overhauser Effects of ERdj3-JGF and ERdj4-JGF

The samples used for the measurement of ^{15}N{^{1}H} NOEs contained 100 μM ERdj3-JGF or ERdj4-JGF in 10 mM NaH_2PO_4, 100 mM NaCl, 1 mM EDTA, pH = 6.4, 100 μM DSS, 5% D_2O.

Two 2D [^{15}N,^{1}H-]-HSQC spectra at equilibrium and with proton saturation during the relaxation delay prior to the starting 90 ^{15}N pulse were recorded in an interleaved manner. Proton saturation was achieved by a series (600) of hard 120° pulses with a delay of 5 ms between each pulse. The recycle delay was set to 2 s to ensure complete relaxation of water magnetization at the beginning of each scan. The information about the motion of the N-H bond vector is calculated by the ratio of the peak intensities from the saturated and the not-saturated spectra:

$$^{15}N\{\,^{1}H\,\}\mathrm{NOE} = {I_{saturated}}/{I_{equilibrium}}$$

Data analysis

All spectra were processed using NMRPipe[184] and qMDD[185] for the reconstruction of non-uniformly sampled spectra. Spectra analysis and assignments were done with CcpNmr Analysis (Version 2.4.2[186]). Chemical shift perturbations were calculated using a scaling factor of 0.14 for ^{15}N shifts. Chemical shift perturbations larger than 2 times the value of the standard deviations were considered to be significantly involved in binding and mapped on the respective structures.

Structure calculation of ERdj3-J

The structure of ERdj3^{J} was calculated with ^{1}H, ^{13}C and ^{15}N chemical shifts, together with NOE restraints and dihedral angle constraints (calculated with TALOS+) as input. Initial NOE assignments and structure calculations for ERdj3^{J} were done iteratively using Cyana 3.98.5[17]. The structures were further refined with an implicit water model using XPLOR-NIH v2.44[187].

Estimation of K_D values from NMR peak intensities

KD values were estimated from normalized peak intensities, which are given by the ratio of the peak intensities from samples with and without ligand (BiP) at given concentrations. Peaks belonging to residues within the binding site were taken for K_D estimation. Decrease in normalized peak intensities was fitted with the formula for simple binding assuming that the binding is saturated:

$$I/I_0 = \frac{B_{max} * [L]}{K_D + [L]}$$

With

B_{max}: maximal number of binding sites

[L]: concentration of ligand

Microscale thermophoresis (MST) experiments

For the determination of the dissociation constants by MST His_6-tagged BiP T229G was labeled with a fluorescent dye (RED-tris-NTA 2nd generation, Nanotemper) at its N-terminal His_6-tag. The samples contained 250 nM of labeled BiP T229G with increasing amounts of the respective J-domain constructs in 25 mM HEPES, 150 mM KCl, 10 mM MgCl2, 1 mM ATP, prepared by serial dilution. Prior to loading into capillary tubes, the samples were incubated during 30 min at 30 °C. For all thermophoretic experiments, premium treated capillary tubes were used (NanoTemper, LLC, Munich, Germany). The LED power (i.e., the power supplied to the excitation LED) was 100% and the MST power (i.e., the power supplied to the IR laser) was medium. (What does it mean?). The pre-MST period was 5 s, the MST-acquisition period was 30 s, and the post-MST period was 5 s. Measurements were performed in duplicates at a Monolith NT.115 (NanoTemper). The curves were fitted to calculate the dissociation constant with the following formula:

$$S_{obs} = S_f + (S_b - S_f)\left(\frac{(C_p + C_L + K_D) - \sqrt{(C_p + C_L + K_D)^2 - 4C_P C_L}}{2C_L}\right)$$

With

S_{obs}: signal of the ligand

S_f: signal of the free ligand

S_b: signal of the bound ligand

C_L: total concentration of ligand

C_P: total concentration of protein

K_D: dissociation constant

Determination of ATP hydrolysis rates

ATP hydrolysis rates of BiP were determined by the measurement of the liberation of free orthophosphate from ATP by spectrophotometric quantification of the complex formed by malachite green, molybdate and free orthophosphate (Malachite Green Phosphate Assay Kit, Sigma-Aldrich).

BiP WT was used at a concentration of 2 μM in 25 mM HEPES, 150 mM KCl, 10 mM $MgCl_2$, 1 mM ATP. To resolve the contribution of the J-domain, 5.0 equivalents of the respective J-domain constructs in the same buffer were added. The samples were incubated at 37 °C during 60 min to ensure sufficient ATP hydrolysis and diluted four-fold to keep the ATP concentration below 0.25 mM prior to addition of malachite green. The formation of the complex was followed by absorption measurements at a wavelength of 620 nm.

5. Chapter 1 - Appendix

Table A1: NMR spectra and spectroscopic parameters used for backbone assignment, sidechain assignment and structure calculation of J-domain constructs. Zero filling to double the number of points was applied to all spectra in all dimension. All spectra were processed with a square sine bell function with a sine bell shift of 2 and a baseline correction.

Protein sample	spectrum	Number of scans	Number of points
ERdj3-J, 1.2 mM	2D [^{1}H-^{15}N]-HSQC	4	512 x 2048 ($\omega1(^{15}N)$, $\omega2(^{1}H)$)
	3D [^{13}C, ^{15}N,^{1}H-]-HNCACB	32 with 25% NUS	180 x 128 x 2048 ($\omega1(^{13}C)$, $\omega2(^{15}N)$, $\omega3(^{1}H)$)
	3D [^{13}C, ^{15}N,^{1}H-]-HNCOCACB	32 with 25% NUS	180 x 128 x 2048 ($\omega1(^{13}C)$, $\omega2(^{15}N)$, $\omega3(^{1}H)$)
	2D [^{13}C,^{1}H-]-HSQC	8	480 x 2048 ($\omega1(^{13}C)$, $\omega2(^{1}H)$)
	3D [^{15}N,^{1}H-]-HSQC-TOCSY	8	152 x 128 x 2048 ($\omega1(^{15}N)$, $\omega2(^{1}H)$, $\omega3(^{1}H)$)
	3D [^{13}C, ^{15}N,^{1}H-]-hCccoNH -TOCSY	8	152 x 128 x 2048 ($\omega1(^{13}C)$, $\omega2(^{15}N)$, $\omega3(^{1}H)$)
	3D [^{13}C,^{1}H-]-HcCH-TOCSY	8	56 x 128 x 2048 ($\omega1(^{13}C)$, $\omega2(^{1}H)$, $\omega3(^{1}H)$)
	3D [^{13}C,^{1}H-]-hCCH-TOCSY	8 with 25% NUS	56 x 128 x 2048 ($\omega1(^{13}C)$, $\omega2(^{13}C)$, $\omega3(^{1}H)$)
	2D [^{13}C,^{1}H-]-HMQC	32	400 x 2048 ($\omega1(^{13}C)$, $\omega2(^{1}H)$)
	3D [^{15}N,^{1}H-]-NOESY	8	96 x 320 x 1024 ($\omega1(^{15}N)$, $\omega2(^{1}H)$, $\omega3(^{1}H)$)
	3D [^{13}C,^{1}H-]-NOESY for aliphatic residues	8	128 x 328 x 1024 ($\omega1(^{13}C)$, $\omega2(^{1}H)$, $\omega3(^{1}H)$)
	3D [^{13}C,^{1}H-]-NOESY	8	128 x 328 x 1024

	for aromatic residues		(ω1(^{13}C), ω2(^{1}H), ω3(^{1}H))
ERdj3-JGF, 50 µM	3D [^{13}C, ^{15}N,^{1}H-]-HNCACB	48 with 25% NUS	128 x 264 x 2048 (ω1(^{13}C), ω2(^{15}N), ω3(^{1}H))
	3D [^{13}C, ^{15}N,^{1}H-]-HNCOCACB	48 with 25% NUS	128 x 264 x 2048 (ω1(^{13}C), ω2(^{15}N), ω3(^{1}H))
ERdj4-J, 1 mM	2D [^{1}H-^{15}N]-HSQC	4 with 25% NUS	400 x 2048 (ω1(^{15}N), ω2(^{1}H))
	3D [^{13}C, ^{15}N,^{1}H-]-HNCACB	32 with 25% NUS	128 x 180 x 2048 (ω1(^{13}C), ω2(^{15}N), ω3(^{1}H))
	3D [^{13}C, ^{15}N,^{1}H-]-HNCOCACB	32 with 25% NUS	128 x 180 x 2048 (ω1(^{13}C), ω2(^{15}N), ω3(^{1}H))
ERdj4-JGF, 300 µM	2D [^{1}H-^{15}N]-HSQC	16 with 25% NUS	400 x 2048 (ω1(^{15}N), ω2(^{1}H))
	3D [^{13}C, ^{15}N,^{1}H-]-HNCACB	48 with 25% NUS	128 x 264 x 2048 (ω1(^{13}C), ω2(^{15}N), ω3(^{1}H))
	3D [^{13}C, ^{15}N,^{1}H-]-HNCOCACB	48 with 25% NUS	128 x 264 x 2048 (ω1(^{13}C), ω2(^{15}N), ω3(^{1}H))
ERdj6-J, 1 mM	2D [^{1}H-^{15}N]-HSQC	4 with 25% NUS	400 x 2048 (ω1(^{15}N), ω2(^{1}H))
	3D [^{13}C, ^{15}N,^{1}H-]-HNCACB	32 with 25% NUS	128 x 180 x 2048 (ω1(^{13}C), ω2(^{15}N), ω3(^{1}H))
	3D [^{13}C, ^{15}N,^{1}H-]-HNCOCACB	32 with 25% NUS	128 x 180 x 2048 (ω1(^{13}C), ω2(^{15}N), ω3(^{1}H))

Chapter 2 - Outer membrane permeability: Antimicrobials and diverse nutrients bypass porins in *Pseudomonas aeruginosa*

6. Chapter 2 - Introduction

Pseudomonas aeruginosa

With 144 species, the genus *Pseudomonas* is currently the genus of gram-negative bacteria with the largest number of known species[200]. Many of the 144 *Pseudomonas* species are opportunistic bacteria infecting different types of host such as animals, plants, fungi and algae[201], but with the exception of *Pseudomonas aeruginosa*, they rarely cause disease. Pathogenicity within Pseudomonas strain is conferred by the expression of virulence factors and regulatory elements and the genotypic differentiation between the pathogenic or beneficial strains is subject of many investigations[202]. As all members of the genus, *P. aeruginosa* is equipped with a versatile metabolic capacity and broad potential for adaptation to their environment[203], enabling the bacterium to live in various biotic and abiotic environments such as soil, water and air[204]. It has been detected in many habitats contaminated with human activity such as medical equipment[205] leading to a high rate of nosocomial infections[206,207]. *Pseudomonas aeruginosa* infections are a tremendous danger to the healthcare system because of their intrinsic resistance to antibiotics and disinfectants[208,209] and increasing numbers of multidrug- and pan-drug-resistant strains[210–212]. The most common *P. aeruginosa* strains, PAO1, PA14 and PA7 cause an array of life-threatening acute and chronic infections including ventilator-associated pneumonia[213], central line-associated bloodstream infection[214], urinary catheter-related infection[215] and surgical/transplantation infections. These infections are a particular danger to immuno-compromised patients and the leading cause for morbidity and mortality in cystic fibrosis patients[216]. Antibiotic treatment of infected patients usually includes cephalosporins, carbapenems, or anti-pseudomonal β-lactam-containing antibiotics[217], however the emergence of strains that are resistant to last resort antibiotics like carbapenems increase mortality rates[218]. Due to its intrinsic antibiotic resistance mechanisms, increasing numbers of emerging multidrug- and pan-drug-resistant strains and its high environmental adaptability, *P. aeruginosa* belongs to the group of the so-called “ESKAPE” bacteria which urgently demand the development of new methods for the effective treatment of infections[219]. Development of new treatment strategies and novel antiobitics[220–224] are

targeted by academic and industrial research, however, pharmaceutical research is continuously reduced due to low profit[225]. With a size of approximately 5 to 7 Mbp *P. aeruginosa* has a comparatively large genome (*E. coli* genome 4.5 Mbp) encoding genes responsible for its extraordinary capability of survival. The core adaptation mechanisms include a high metabolic versatility, quorum sensing (QS), motility-sessility switch, biofilm formation, antibiotic resistance mechanisms, adaptive radiation for persistence, stringent response and the CRISPR-Cas system[226]. The purposeful design and development of new antimicrobials and treatment approaches require an accurate understanding of these adaption mechanisms, a trail-and-error approach is too costly.

Antibiotic resistance mechanisms

For many Gram-negative bacteria intrinsic, acquired and adaptive resistance mechanisms against specific classes of antibiotics have been discovered and by the combination of multiple resistance mechanisms*, P. aeruginosa* is capable to survive even harsh antibiotic treatment. A big part of the intrinsic resistance is achieved by the expression of proteins protecting the bacteria against toxic substances. These proteins include efflux-pumps that transport harmful molecules out of the cell and enzymes deactivating antibiotics such as β-lactamases[227]. *P. aeruginosa* acquires further protection through mutations of exactly these genes involved in intrinsic resistance. The mutations lead to increased promoter activity or decreased negative control resulting in overexpression of β-lactamases and efflux pumps[227]. Additionally to mutations, plasmids that are gained by horizontal gene transfer encode genes for extended-spectrum β-lactamases and carbapenemases[228].

However, one of the first barriers one has to pass when applying antibiotics against bacteria in general is the cell membrane. With a comparatively low permeability, the outer membrane of *P. aeruginosa* represents an exceptional protection for the bacterium and therefore contributes immensely to its intrinsic antibiotic resistance[229,230].

The low outer membrane permeability of *P. aeruginosa*

The outer membrane of Gram-negative bacteria in general is composed of a phospholipid inner face and a lipopolysaccharide outer face and constitutes a barrier against passive

diffusion into the cell (Fig. 1). For the uptake of nutrients and contact with the environment, the outer membrane contains various proteins for the transport of molecules, ions or signaling molecules into and out of the cell. The main representative classes of these proteins are specific transporters, efflux-pumps and non-selective and substrate-specific porins[231]. The low permeability of the outer membrane of *P. aeruginosa* which is only 8% of that of *E. coli* [232] is achieved by a reduced number of non-specific porins usually found in other Gram-negative bacteria such as OmpF and OmpC in *E. coli*. These are large porins known for the unselective uptake for nutritional compounds and antibiotics[233,234]. In contrast to other Gram-negative bacteria, only one general non-specific porins can be found in the outer membrane on *P. aeruginosa*, OrpF[235]. For efficient nutrient uptake in fluctuating diverse environments, the large genome *P. aeruginosa* contains genes encoding for numerous specific porins that equip the bacterium with a mechanism for the tight control of substance entry into the cell[236]. These porins are water-filled channels with a narrow pore that allow diffusion-based transport of molecules across the membrane.

Porin families in the outer membrane of *P. aeruginosa*

The outer membrane porins of *P. aeruginosa* can be divided into three main families: the TonB-dependent gated porins, the OprM efflux/secretions family and the OprD-specific porin family[231] (Fig 16).

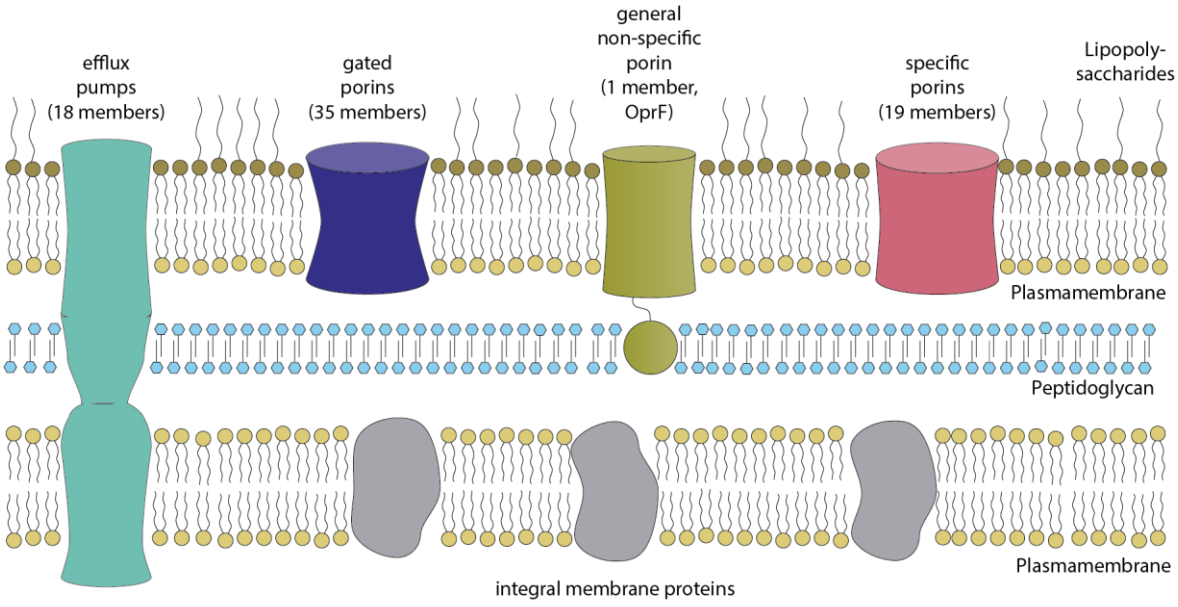

Figure 16: Schematic representation of the cell wall of *P. aeruginosa* with the asymmetric outer membrane, the peptidoglycan layer, the symmetric plasma membrane and the four classes of outer membrane porins. With OprF as the only general non-specific porin and a large subset of specific porins, *P. aeruginosa* has a remarkably low outer membrane permeability.

Gated porins

P. aeruginosa comprises a large number of TonB-dependent gated porins involved in ion uptake, mainly iron, a crucial component for aerobic metabolism[237]. By conformational changes which are exerted by energy provided by the periplasm spanning inner membrane resident protein TonB, gated porins take up iron-binding compounds such as siderophores. Important and well characterized members are FpvA[238], PupA[239], PupB[240], and the FptA/PfeA/Heme complex[241]. These gates porins form 22-stranded β-barrel with a lid composed of a 4-stranded β-sheet[242].

Efflux systems

As already mentioned, active efflux of toxic compounds is a major mechanism in antibiotic resistance. In *P. aeruginosa* the four main efflux pumps are MexAB-OprM[243], MexCD-OprJ[244], MexEF-OprN[245], and MexXY[246]. These are large protein complexes composed of a transporter protein translocating the compound across the inner membrane (MexB, MexD, MexF, and MexY), a membrane fusion protein (MexA, MexC, MexE, and MexX) which connects the transporter protein with a porin residing in the outer membrane responsible for releasing the compound out of the cell (OprM, OprJ, and OprN). Other efflux systems are AprF, OpmH, OpmF, OmpK and OpmL[247].

The general non-specific porin OprF

OprF is the only non-specific porin in the outer membrane of *P. aeruginosa*. This homologue to the *E. coli* outer membrane protein A (OmpA) is the most abundant non-lipoprotein in the outer membrane of P. aeruginosa[248]. It has been suggested that OprF resides in 2 distinct conformations that can convert into each other, a closed form composed of three domains: A N-terminal eight-stranded β-barrel residing in the outer membrane, a cysteine-rich linker connecting the β-barrel to the C-terminal domain which attaches the protein to the

peptidoglycan layer. The open conformation is represented by a single β-barrel consisting of 14 to 16 strands, which accounts for approximately 5% of observed OprF in the outer membrane[249,250] (Fig 17). Conductivity experiments confirm the small conformation with a weak conductivity, however, values for the open conformation remain controversial[235]. OprF has been subject of many studies and has been shown to be involved in many processes such as outer membrane integrity[251], biofilm formation[252], adhesion to mammalian cells[253], outer membrane vesicle formation[254], the quorum-sensing response[252], perception of environmental cues and acute and chronic infections[255].

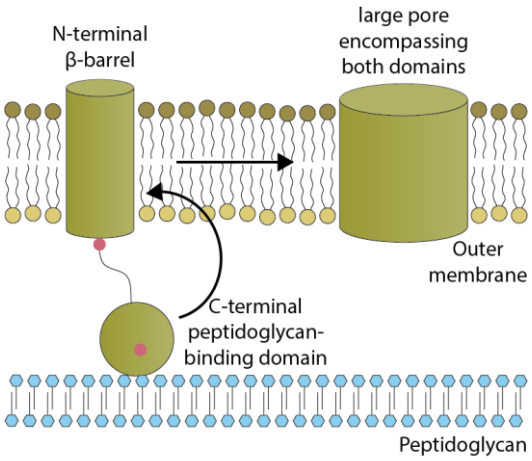

Figure 17: The two suggested conformations of OprF. A large barrel is formed when the N-terminal peptidoglycan-binding domain and the C-terminal domain fuse into the outer membrane, this conformation is found to be represented to 5%[250].

Specific porins

As part of its extremely protective outer membrane, the genome of *P. aeruginosa* comprises a large set of substrate-specific porins[231,255]. These porins comprise low-affinity binding sites in the μM to mM range that allow diffusion of substrates along a very shallow concentration gradient[256,257], a schematic representation of common representatives id shown in Fig 3. Several family members have been characterized regarding their substrate specificity and structure and identified to mediate nutrient and ion uptake[258]. However, many of them have only been predicted from the genome and information on their expression and specificity still remains elusive (see Pseudomonas Genome DataBase[259]). Members of this porin family form β-barrels of 8 to 18 β-strands with several extracellular loops which fold into the β-

barrel to form a unique substrate-specific restriction pore[258]. A summary of all subclasses of specific porins found in *P. aeruginosa* is given in table 2. Table 3 gives on overview about all to date known specific porins.

Table 2: Subclasses of the specific porins from *P. aeruginosa*.

Porin subclass	Number of members	Substrate class
OprB	3	monosaccharides
Tsx	3	nucleosides
FadL	3	Fatty acids
OprP, OprO	2	Phosphate, pyrophosphate
OprG	1	Amino acids?
OprD family	19	Amino acids, small nutritional compounds
SphA-like proteins	5	Involved in sphingosine metabolism[260]
Hypothetical proteins (predicted proteins)	5	

Table 3: All currently known specific porins of *P. aeruginosa*. The alternative name includes the Occ nomenclature for Opr family members. PseudoCAP was the first complete internet- and community-based genome annotation system[261]. The PA14 reference represents the entry in the Pseudomonas Genome DataBase for the P. aeruginosa PA14 strain[259]. The UniProt code references to its entry in the Universal Protein Resource[262]. The REfSeq code links to the porin entry in the Reference Sequence (RefSeq) collection[263].

gene name	**alternative name**	**subclass**	**PseudoCAP/ PA01**	**PA14 reference**	**UniProt**	**RefSeq**
oprB	OprB	OprB	PA3186	PA14_23030	Q51485	NP_251876.1
opbA	OprB2	OprB	PA2291	PA14_34960	Q9I1I4	NP_250981.1

	OprB3	OprB	PA4099	PA14_10870	Q9HWS9	NP_252788.1
	Tsx	Tsx	PA0165	PA14_02060	Q9I6W7	NP_248855.1
		Tsx	PA0234	PA14_02890	Q9I6Q4	NP_248925.1
		Tsx		PA14_01770		
fadL	FadL	FadL	PA1288	PA14_47540	Q9I456	NP_249979.1
	FadL2	FadL	PA1764	PA14_41750	Q9I2X5	NP_250455.1
	FadL3	FadL	PA4589	PA14_60730	Q9HVJ6	NP_253279.1
oprP	OprP	OprP	PA3279	PA14_21620	P05695	NP_251969.1
oprO	OprO	OprO	PA3280	PA14_21610	P32977	NP_251970.1
oprG	OprG	OmpW	PA4067	PA14_11270	Q9HWW1	NP_252756.1
oprD	OccD1	OprD sub1	PA0958	PA14_51880	P32722	NP_249649.1
opdC	OccD2	OprD sub1	PA0162	PA14_02020	Q9I6X0	NP_248852.1
opdP	OccD3	OprD sub1	PA4501	PA14_58410	Q9HVS0	NP_253191.1
opdT	OccD4	OprD sub1	PA2505	PA14_32270	Q9I0X7	NP_251195.1
opdI	OccD5	OprD sub1	PA0189	PA14_02370	Q9I6U5	NP_248879.1
oprQ	OccD6	OprD sub1	PA2760	PA14_28400	Q9I083	NP_251450.1
opdB	OccD7	OprD sub1	PA2700	PA14_29220	Q9I0E2	NP_251390.1
opdJ	OccD8	OprD sub1	PA2420	PA14_33410	Q9I161	NP_251110.1
opdK	OccK1	OprD sub2	PA4898	PA14_64720	Q9HUR5	NP_253585.1
opdF	OccK2	OprD sub2	PA0240	PA14_02980	Q9I6P8	NP_248931.1
opdO	OccK3	OprD sub2	PA2113	PA14_37260	Q9I202	NP_250803.1
opdL	OccK4	OprD sub2	PA4137	PA14_10440	Q9HWP4	NP_252826.1
opdH	OccK5	OprD sub2	PA0755	PA14_54520	Q9I5H4	NP_249446.1
opdQ	OccK6	OprD sub2	PA3038	PA14_24790	Q9HZH0	NP_251728.1
opdD	OccK7	OprD sub2	PA1025	PA14_51070	Q9I4U9	NP_249716.1
oprE	OccK8	OprD sub2	PA0291	PA14_03800	G3XDA5	NP_248982.1
opdG	OccK9	OprD sub2	PA2213	PA14_36090	Q9I1Q4	NP_250903.1
opdN	OccK10	OprD sub2	PA4179	PA14_09850	Q9HWK2	NP_252868.1
opdR	OccK11	OprD sub2	PA3588	PA14_17890	Q9HY38	NP_252278.1
sphA		SphA-like	PA5325	PA14_70300	Q02E37	NP_254012.1
		SphA-like		PA14_32640		
		SphA-like		PA14_33380		
	FapF	SphA-like	PA1951	PA14_39270		
FapF		SphA-like	PA1763	PA14_41760		
			PA1974	PA14_39000	Q9I2D1	NP_250664.1

	PA0696	PA14_55320	Q02HI7	NP_249387.1
lptF	PA3692	PA14_16630	Q9HXU8	NP_252382.1
	PA3497	NA	Q9HYB2	NP_252187.1
qbdB	PA3772	PA14_15280		

OprB – the sugar transporter

OprB is a close homologue to the *E. coli* porin LamB which is selective for oligosaccharides. However, contrary to LamB, liposome swelling assays demonstrated that OprB is only selective for monosaccharides. This selective porin forms a monomeric 16-stranded β-barrel with a pore restriction mediated by its long extracellular loops 2 and 3 (L2 and L3). In contrast to LamB, OprB does not contain a so-called "greasy-slide" which mediates oligosaccharide transport. This missing feature is proposed as an explanation for its specificity to monosaccharides as opposed to oligosaccharides[264].

OprP and OprO – phosphate transporters

OprP and OprO show a high level of sequence similarity (76% identity), they both form 16-stranded β-barrels, however they have distinct substrate specificities. OprP prefers monophosphates whereas OprO is more selective for di- and polyphosphates. Both porins are upregulated during conditions of limited phosphate as well as in bacteria colonizing epithelial cells. Both porins reveal a row of arginines forming a basic ladder leading to the constriction zone, but the constriction zones themselves differs in two residues (Y62 and Y114 in OprP opposed to F62 and D114 in OprO). Interconverting these residues exchanged the substrate specificities of both porins[265,266].

Tsx

Tsx is a specific nucleoside channel which forms a 12-stranded β-barrel containing two binding sites for the base and the sugar moiety of the nucleoside respectively. Diffusion based transport of the substrate proposedly happens by consecutive binding to these binding sites[267].

FadL

FadL is involved in the specific uptake of long-chain fatty acids across the outer membrane of gram-negative bacteria. FadL of *P. aeruginosa* has a low sequence identity with its *E. coli* homologue. However, it is structurally very similar to it except for the position of some extracellular loops. Both proteins are composed of 14-stranded β-barrels, a strand number which is unique for outer membrane porins and the N-terminus forms three α-helices resulting in a small compact "hatch" inserting into the barrel. For *E. coli* FadL it has been shown that hydrophobic substrates are taken up by lateral diffusion from the barrel into the outer membrane and the crystal structure of *P. aeruginosa* FadL shows the same structural features important for this uptake mechanism. It can therefore be concluded that a mechanism by lateral opening is conserved among FadL homologues[268,269].

OprG

OprG is the second smallest porin described so far, it forms a β-barrel of only 8 β-strands but with long extracellular loops, its closest *E. coli* homologue is OmpW[66]. It reveals a distinct hydrophobic patch in the lumen wall at the extracellular side composed of approximately 45 residues. Additionally, between strands 3 and 4 a lateral opening can be observed. Both structural features are conserved among OmpW homologues and it has been suggested that they are functionally important, however, the precise function of this small porin remains to be determined. Since the hydrophobic patch and the lateral opening are also present in FadL proteins, it has been proposed that OprG is involved in the uptake of small hydrophobic molecules. However, it also has been shown by liposome swelling assays that OprG transports small amino acids including glycine, alanine, valine, serine and threonine across the outer membrane[67]. Other studies suggest a role in ion uptake, biofilm formation and outer membrane vesicle formation[255].

The OprD family

The large OprD protein family, named after its prototype OprD, comprises to date 19 members that show sequence similarity and common structural characteristics (4 Opr proteins and 14 Opd proteins). The high number of family members is one of the reasons

for *P. aeruginosa's* high metabolic versatility while being highly restrictive regarding membrane permeation[231,255].

Structural characteristics and biophysical properties

All members for which crystal structures have been determined form 18-stranded β-barrels with seven extracellular loops (L1-L7). For most members extracellular loops L3 and L7 fold into the barrel and thereby form a constriction pore and a gate region at the entry to the pore (Fig18). Sequence alignment of all OprD family members reveals only three conserved regions, (1) the periplasmic end of β-strands S2, S3 and S4, (2) extracellular loop L3 and (3) the interface of L7 and the barrel wall. Conservation of regions (2) and (3) indicate that the architecture of the constriction pore is invariant among the family members. However, the residues lining the pore are less conserved offering a possibility for varying substrate specificities[270]. A stretch of arginine and lysine residues forms a basic ladder leading to the constriction pore on the extracellular side of the porin and away from the pore on the periplasmic side[271–273]. Among all OrpD family members, the number of these basic residues ranges from three to six[270]. Mutational studies have shown for OprD that those residues of the basic ladder within the restriction are fundamental for substrate transport whereas the peripheral residues reduced transport but did not abolish it completely. It is suggested that this basic ladder provides an electrophoretic path along which the substrate is guided to the restriction pore[271]. Opposite of the constriction pore a binding pocket has been reported for several OprD porin family members which has been associated with substrate specificity. Mutations in this binding pocket are associated with lost and/or changed substrate specificity for OccD1 and OccK2[271].

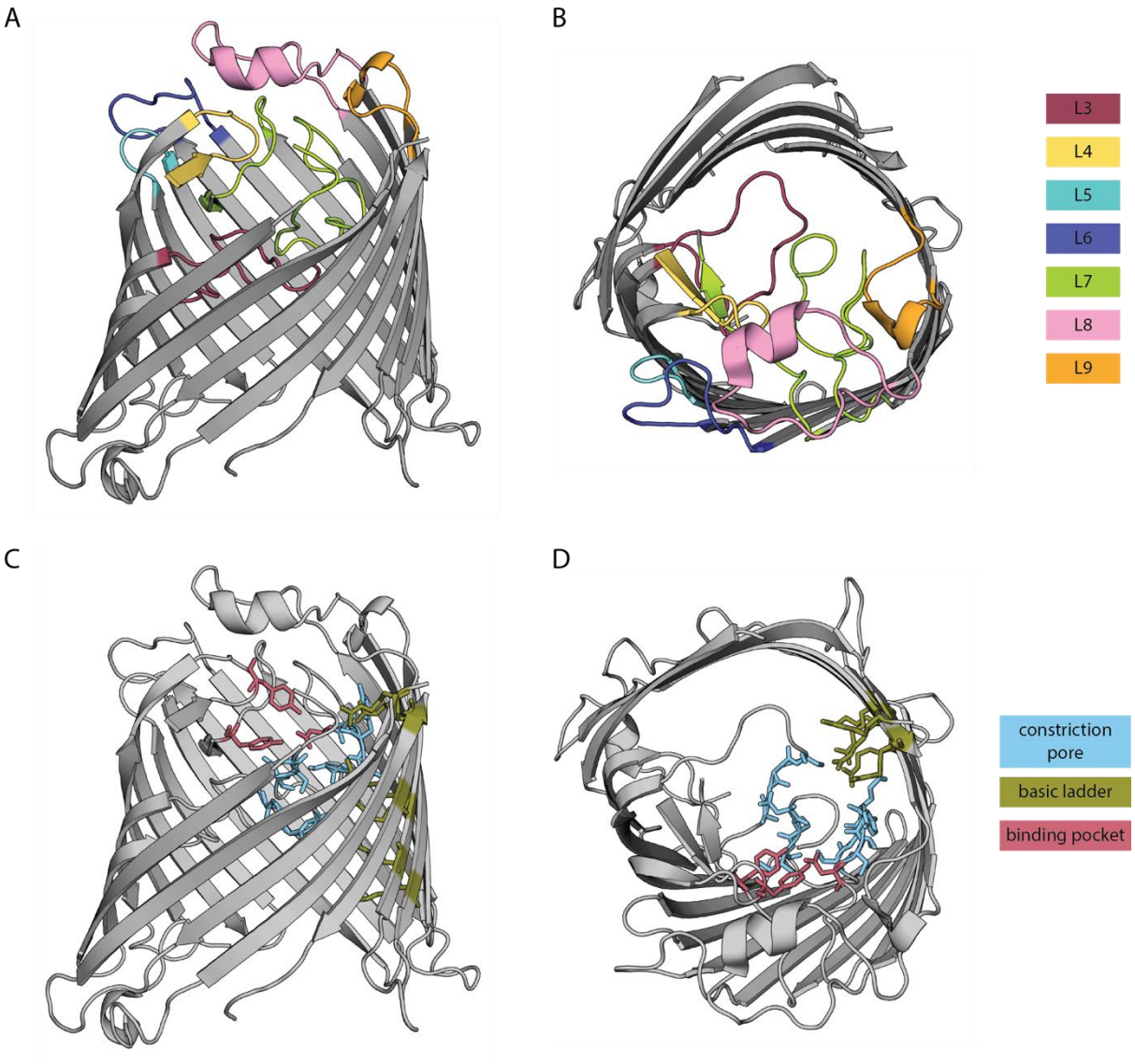

Figure 18: Structure of the porin OprD solved by X-ray crystallography (pdb 3YS7). Side view (A) and top view (B) of the 16 stranded β-barrel with its extracellular loops L3- L9. L3 and L7 build the constriction pore, Loop 1 and 2 are not resolved in the crystal structure. C and D depict residues forming the constriction pore in bright blue (A127 – S130 in L3, D295 – I297 and S302 – D307 in L7, R391 in strand 17 and R410 in strand 18), residues forming the basic ladder in green (R30, R39, K375, R389, R391, R410) and the negatively charged binding pocket in red (Y176, Y282 and D307)[270,271].

A sequence alignment clusters all OprD family members into two distinct sub families, which have been named the OccD and the OccK subfamily, with their members OccD1 - OccD8 and OccK1- OccK11[272]. Both the original and the OccD/OccK nomenclature will be used here for the description of the individual family members. Based on all structures available, it is noteworthy that all structures of OccK members have been crystallized in a conformation

revealing an open pore opposed to structures of OccD members whose crystal structures are characterized by a very small closed pore or no pore at all. This could hint to a distinct transport and binding mechanism; however little experimental information is available.

In order to complement knowledge on the transport and binding mechanism of OprD family porins gained by structure elucidation, their substrate specificity and biophysical properties have been the subject of several in vitro studies[270–274]. The experimental approach focuses on electrophysiology experiments, uptake assays (liposome swelling assays) and MD simulations. Table A2 in the appendix summarizes core results on these characteristics. Measurement of conductance values in single-channel planar lipid bilayers revealed variations in conductance values among the investigated porins. Additionally, a multistate gating behavior could be observed among OprD family members indicating dynamics within the porins. Movements of the extracellular loops are suggested to play are crucial role in pore dynamics. Furthermore, the low-conductance OpdL/OccK4 and OpdQ/OccK6 channels revealed a voltage dependence of their kinetic rate constants and of their free energy difference between the open substates.

Substrate specificities

The first attempts to characterize their substrate specificity were growth experiments on single carbon sources and the investigation of induced expression by addition of single substrates[255,275,276]. These experiments associated members of the OprD family with the uptake of nutritional substances such as basic amino acids and small molecules as glucoronate (OpdF/OccK2), cis-aconitate (OpdH/OccK5), nitrate (OpdQ/OccK7) and pyroglutamate (OpdO/OccK3). To further investigate substrate specificities the transport of several compounds was determined by in vitro assays using membrane vesicles produced by *E. coli* overexpressing single porins[272,273,277]. Overall, these assays established a preference of OccD porins for cations and small positively charged amino acids and of OccK porins for anions. Furthermore, it was observed that OccK porins prefer cyclic substrates. This is in line with previous studies suggesting basic amino acids are main substrates for OprD family members. An overview of the specificities for the tested substrates by growth experiments and liposome swelling assays is given in table 1 in the appendix. Due to the fact that OccD family members have been crystallized in closed conformations and the lack of co-crystal structures of porins bound to a substrate, MD simulations on OprD/OccD1 and

OprE/OccK8 have been used to answer the question how these porins can translocate substrates through a pore that is substantially smaller than the suggested substrates[278,279]. Both porins show a dynamic pore that can widen upon substrate translocation and in both cases extracellular L7 plays a role in establishing these pore dynamics. Substrate specificity is mainly investigated by liposome swelling assays and substrate induced expression patterns, however, no clear insights into definite specificities could be obtained. From these studies it becomes clear that these porins can transport substances such as basic amino acids and small nutritional molecules but a clear differentiation between the porins and an explanation for the existence of so many different porins has not been provided so far. Furthermore, liposome swelling assays are an *in vitro* method lacking the native lipid environment and might give artificial results since it is known that LPS is affecting the translocation behavior of porins[280].

Despite many investigations, a clear picture of the substrate specificity and the translocation mechanism of these porins remains elusive. Although shown for some porins by missing resolution in crystal structures and complemented by MD simulations, a precise experimental description of loop movements and their influence on pore dynamics is still missing.

Transport of antibiotics

OprD/OccD1 is the second most abundant porin in the outer membrane of *P. aeruginosa* and has been found to be involved in the uptake of the antibiotics of the carbapenem group, especially imipenem and meropenem[281,282]. Resistant *P. aeruginosa* strains have revealed mutations resulting in the down regulation of OprD expression or in the expression of a shorter OprD-construct[283–285]. MD simulations could indeed confirm translocation of imipenem by OprD whereas the carbapenem ertapenem was rejected. Here, extracellular loop L2, one of the more dynamic loops, was involved in the rejection of ertapenem[286]. Also OpdC/OccD2 and OpdP/OccD3 have been reported to be involved in carbapenem uptake[287,288]. Ceftazidime, an antibiotic from the group of cephalosporins commonly used during *P. aeruginosa* infections has been shown to be translocated by OprE/OccK8 (liposome swelling assays)[279]. Permeation of the same antibiotic through OpdH/OccK5 has been concluded from reduced minimal inhibitory concentrations (MIC) in a ΔopdH

mutant[276]. MD simulations of this porin demonstrated a pore widening upon ceftazidime passage.

In order to combat the threat *P. aeruginosa* infections represent to human health, it is fundamental to fully understand the resistance mechanisms underlying the success of this bacterium. Getting antibiotics into *P. aeruginosa* is the first step in treating infected patients but it is a huge challenge due to the low outer membrane permeability. Therefore, it is crucial to elucidate the existing entry possibilities for antibiotics into *P. aeruginosa*. Five members of the OprD porin family have been proven to be able to translocate antibiotics into the cell. Knowledge about the remaining family members, their expression profile, substrate specificities and affinity for antibiotics is of highest importance since it opens the door to an intelligent and purposeful design of new antimicrobial substances.

7. Chapter 2 - Aim of the study

One of the unique features of *P. aeruginosa* and key criteria for its high versatility and adaptability is the large set of substrate-specific outer membrane porins. The OprD porin family currently comprises 19 known members, many of which have been shown to translocate small nutritional substrates across the membrane. Furthermore, it has been well established that OprD/OccD1 serves as entry for carbapenems to cross the outer membrane. Several additional OprD porin members have been suggested to play a similar role in antibiotic uptake (OpdC/OccD2, OpdP/OccD3, OpdH/OccK5 and OprE/OccK8). However, a clear picture of their specificity with respect to expression patterns and conditions, substrate affinity and translocation as well as their ability to take up antibiotics is still missing. This is partly due to the fact that many studies have been conducted under *in vitro* or even *in silico* conditions using single substrates. A holistic view of expression patterns and substrate specificities under *in vivo* conditions and in the context of a more realistic nutritional environment would advance our understanding of how *P. aeruginosa* is able to benefit from a tremendously high metabolic versatility while managing to keep the permeability across the outer membrane restricted.

This study aimed to clarify the role of the 40 identified *P. aeruginosa* porins for antibiotic uptake under *in vivo* conditions. Furthermore, expression patterns of porin family members during lung infections in mouse models were determined. These finding will help to better understand the role of individual specific porins under disease conditions. Additionally, an *in vivo* assay was developed to investigate substrate consumption by individual porins from a nutrient mix mimicking nutrient availability in the lung. Using an NMR spectroscopy-based assay, it was possible to determine the simultaneous consumption of a number of different nutritional compounds allowing to define characteristic substrate preferences of individual porins.

Outer membrane permeability: Antimicrobials and diverse nutrients bypass porins in *Pseudomonas aeruginosa*

Johanna Ude[a,1], Vishwachi Tripathi[a,1], Julien M. Buyck[a,1], Sandra Söderholm[a], Olivier Cunrath[a], Joseph Fanous[a], Beatrice Claudi[a], Adrian Egli[b,c], Christian Schleberger[a], Sebastian Hiller[a,2], and Dirk Bumann[a,2]

[a]Biozentrum, University of Basel, CH-4056 Basel, Switzerland; [b]University Hospital, University of Basel, CH-4056 Basel, Switzerland; and [c]Department of Biomedicine, University of Basel, CH-4056 Basel, Switzerland

Edited by Staffan Normark, Karolinska Institutet, Stockholm, Sweden, and approved June 24, 2021 (received for review April 22, 2021)

Gram-negative bacterial pathogens have an outer membrane that restricts entry of molecules into the cell. Water-filled protein channels in the outer membrane, so-called porins, facilitate nutrient uptake and are thought to enable antibiotic entry. Here, we determined the role of porins in a major pathogen, *Pseudomonas aeruginosa*, by constructing a strain lacking all 40 identifiable porins and 15 strains carrying only a single unique type of porin and characterizing these strains with NMR metabolomics and antimicrobial susceptibility assays. In contrast to common assumptions, all porins were dispensable for *Pseudomonas* growth in rich medium and consumption of diverse hydrophilic nutrients. However, preferred nutrients with two or more carboxylate groups such as succinate and citrate permeated poorly in the absence of porins. Porins provided efficient translocation pathways for these nutrients with broad and overlapping substrate selectivity while efficiently excluding all tested antibiotics except carbapenems, which partially entered through OprD. Porin-independent permeation of antibiotics through the outer-membrane lipid bilayer was hampered by carboxylate groups, consistent with our nutrient data. Together, these results challenge common assumptions about the role of porins by demonstrating porin-independent permeation of the outer-membrane lipid bilayer as a major pathway for nutrient and drug entry into the bacterial cell.

membrane transport | bacterial outer membrane | lipid bilayer | diffusion | antimicrobial resistance

Antimicrobial resistance is a major worldwide threat to human health. The World Health Organization has classified Enterobacteriaceae, *Pseudomonas aeruginosa*, and *Acinetobacter baumannii* as the most concerning pathogens ("critical priority") (1). All three pathogens are Gram-negative bacteria with the characteristic inner and outer membranes. The outer membrane is a stringent permeability barrier that restricts the entry of most molecules and therefore presents a major challenge for the development of urgently needed novel antibiotics (2–5).

The outer membrane consists of an asymmetric lipid bilayer with lipopolysaccharide (LPS) in the outer leaflet and phospholipids in the inner leaflet and various outer-membrane proteins that are embedded in, or attached to, the lipid bilayer. LPS contains negatively charged phosphate and carboxylate groups that are cross-linked by divalent Mg^{2+} and Ca^{2+} cations, resulting in stable clusters of LPS molecules that reduce the permeation of small molecules by 10- to 100-fold compared to phospholipid bilayers (6). Some outer membrane proteins form water-filled channels (so-called porins) that facilitate translocation of molecules through the outer membrane (4, 5). Enterobacteriaceae have general "unspecific" porins that permit the entry of molecules with a size of up to 600 Da. By contrast, *P. aeruginosa* and *A. baumannii* have a large set of "specific" porins that permit the entry of only few molecules with sizes below 200 Da. In addition, all three pathogens have porins with mainly structural roles in stabilizing the link between outer membrane and the underlying peptidoglycan layer (OmpA and OprF). It has been proposed that a small fraction of these structural porin molecules form large unspecific pores that permit entry of larger molecules at low rates (7), but this model remains controversial.

Antimicrobials and nutrients can penetrate the outer membrane by two different pathways, through the lipid bilayer or through porins. Hydrophobic molecules might predominantly use the lipid pathway, while hydrophilic molecules might prefer porins. However, the quantitative relevance of each pathway for outer-membrane permeability remains unknown (3, 8, 9). Even slow permeation pathways that mediate concentration-equilibration times in the order of minutes (instead of seconds) can yield relevant intracellular drug concentrations in bacteria with generation times of more than 20 min, unless drug-efflux pumps and/or hydrolases diminish drug levels (2).

Translocation pathways and their selectivity for specific physicochemical properties of molecules are crucial for the rational improvement of drug entry into Gram-negative bacteria. The important contribution of large cation-selective porins such as OmpF and OmpC for outer-membrane translocation into Enterobacteriaceae enabled the establishment of rules for medicinal

Significance

Novel antibiotics are urgently needed to resolve the current antimicrobial resistance crisis. For critical pathogens, drug entry through the cell envelope is one of the major challenges in the development of effective novel antibiotics. Envelope proteins forming water-filled channels, so-called porins, are commonly thought to be essential for entry of hydrophilic molecules, but we show here for the critical pathogen *Pseudomonas aeruginosa* that almost all antibiotics and diverse hydrophilic nutrients bypass porins and instead permeate directly through the outer membrane lipid bilayer. However, carboxylate groups hinder bilayer penetration, and *Pseudomonas* thus needs porins for efficient utilization of carboxylate-containing nutrients such as succinate. The major porin-independent entry route might open opportunities for facilitating drug delivery into bacteria.

Author contributions: J.U., V.T., J.M.B., S.H., and D.B. designed research; J.U., V.T., J.M.B., S.S., O.C., J.F., B.C., A.E., and C.S. performed research; A.E. contributed new reagents/analytic tools; J.U., V.T., J.M.B., S.S., O.C., J.F., B.C., A.E., C.S., S.H., and D.B. analyzed data; and D.B. wrote the paper.

The authors declare no competing interest.

This article is a PNAS Direct Submission.

This open access article is distributed under Creative Commons Attribution-NonCommercial-NoDerivatives License 4.0 (CC BY-NC-ND).

[1]J.U., V.T., and J.M.B. contributed equally to this work.

[2]To whom correspondence may be addressed. Email: sebastian.hiller@unibas.ch or dirk.bumann@unibas.ch.

This article contains supporting information online at https://www.pnas.org/lookup/suppl/doi:10.1073/pnas.2107644118/-/DCSupplemental.

Published July 29, 2021.

chemistry to improve whole-cell activities of antimicrobials against these bacteria (10–12). These porins have been extensively studied, and in particular OmpF has a major impact on susceptibility to various β-lactam antibiotics (13). However, an *Escherichia coli* Δ*ompC* Δ*ompF* double mutant retains substantial susceptibility to diverse other antibiotics (9), suggesting alternative translocation pathways.

For *P. aeruginosa*, physicochemical parameters favoring translocation have been more difficult to identify (10, 14, 15). Both *P. aeruginosa* and *A. baumannii* have lower outer-membrane permeability than Enterobacteriaceae for hydrophilic molecules because they lack unspecific porins (16), making antimicrobial development particularly difficult for these critical pathogens. Specific porins might facilitate antibiotic entry into *P. aeruginosa* (17), but clear evidence for standard assay conditions is only available for penetration of carbapenems through OprD (18). Functional studies of individual porins in *P. aeruginosa* are hampered by the large diversity of specific porins that are thought to each enable uptake of a few nutrients (19). Phenotypes of inactivating one particular porin might be masked by the numerous remaining other porins. To circumvent these issues, individual porins have been purified and reconstituted in artificial membranes, or expressed in *E. coli*, to determine their substrate specificity. However, the results might not reflect porin functions in their native context because their channel properties differ depending on the lipid environment (20, 21).

In this study, we overcame these difficulties using extensive mutagenesis. In contrast to previous assumptions, we show that wild-type *P. aeruginosa* PA14 and a PA14 Δ40 mutant that lacks all identifiable 40 porin genes have indistinguishable susceptibility to diverse antibiotics. Moreover, the Δ40 strain grew normally on rich media, and nutrient consumption assays revealed substantial porin-independent uptake of diverse hydrophilic nutrients. Bringing back individual porins accelerated uptake of some neutral/zwitterionic molecules and was essential for efficient consumption of negatively charged carboxylate-containing compounds. Instead of narrow substrate specificity, porins actually had broad overlapping substrate selectivity. These results demonstrate an unexpected but efficient porin-independent translocation pathway through the outer-membrane lipid bilayer for diverse hydrophilic compounds and all antipseudomonal antibiotics. A detailed understanding of this pathway will facilitate the development of novel antibiotics.

Results

The "General" Porin OprF Has Limited Relevance for Translocation of Antimicrobials. OprF is one of the most abundant proteins in the *P. aeruginosa* outer membrane (4). Based on experiments with OprF reconstituted in liposomes, a minor open-channel conformer of OprF has been proposed to be the major entry pathway for various hydrophilic molecules including many antibiotics (7) (Fig. 1*A*). To test this idea in the native context of intact *P. aeruginosa* cells, we constructed mutants of the virulent clinical isolate *P. aeruginosa* UCBPP-PA14 (22) that lacked *oprF* or expressed chromosomal *oprF* variants with truncated C termini (*oprF* K188* and *oprF* V315*; the amino acid numbers include the 24 amino acids of the signal peptide that are cleaved off during maturation) (23). These mutants would be partially (*oprF* V315*) or completely (*oprF* K188*) incapable of enlarging the N-terminal eight-strand β-barrel by incorporating further β-strands from the usually globular peptidoglycan-binding C-terminal domain (7). The Δ*oprF* mutant would also be unable to form dimers with fused β-barrels (24). All three *P. aeruginosa* mutants had wild-type fitness in rich culture media, as expected (23).

If the large-channel conformer of OprF is indeed the major entry route for antibiotics as proposed, all three mutants should be less susceptible to antimicrobials. However, minimal inhibitory concentrations (MIC) and inhibition zones in disk diffusion tests (antibiograms) for diverse antibiotics (Fig. 1*B*) showed only minor differences between wild type and mutants that were mostly within the accuracy of the respective assays (twofold for MIC values and 2 mm for inhibition zones). Piperacilin showed fourfold higher MIC against *oprF* mutants, but this was inconsistent with unaltered inhibition zones. A minor impact of *oprF* mutations on susceptibility to β-lactam antibiotics has previously been reported (13). Tetracycline had increased activity against *oprF* mutants in both assays, suggesting potential indirect effects of dysfunctional OprF increasing sensitivity to this translational inhibitor, but not to aminoglycosides. The overall limited impact of OprF on antimicrobial susceptibility was not a result of increased outer-membrane permeability compensating for reduced entry through OprF in the mutants, because azithromycin and rifampin, which are sensitive indicators for outer-membrane barrier function in *Pseudomonas* (25, 26), remained poorly active in all three mutants. Together, these data indicate a limited role of OprF in antimicrobial translocation across the outer membrane.

"Substrate-Specific" Porins Have Limited Impact on Antimicrobial Translocation. In addition to OprF, *P. aeruginosa* encodes dozens of "substrate-specific" porins that might mediate antibiotic uptake (19). One of these porins, OprD (also called OccD1), facilitates translocation of carbapenems (18), and OpdP/OccD3 might also contribute to this under special circumstances (27). In addition, OpdH/OccK5 and OprE/OccK8 have been implicated in translocation of the cephalosporin ceftazidime (28, 29), whereas OprO and OprP can transport fosmidomycin in vitro (30). To determine the relevance of these and other porins for the translocation of diverse antimicrobials in intact bacteria, we constructed a series of porin deletion mutants. We generated clean gene deletions to minimize potential polar effects on the expression of downstream genes. Initial characterization showed unaltered susceptibilities (with the exception of the known OprD–carbapenem link) in agreement with previous "resistome" data (27, 31–34). To test the possibility that phenotypes of single porin mutants were buffered by other porins, we mined the PA14 genome and identified a total of 40 porin candidates (*SI Appendix*, Table S1). Several combinations of porin deletions still resulted in unaltered antibiotic susceptibilities.

Eventually, we generated a strain, PA14 Δ40, that lacks all 40 porin genes as verified by whole-genome sequencing. During the construction this strain acquired nine secondary mutations including the loss of a duplicate transfer RNA-Asp gene and two nonsynonymous mutations in protein-encoding genes. None of the affected genes had a known association with outer-membrane permeability or antimicrobial susceptibility (32–34) (*SI Appendix*, *Supplementary Information Text* and Table S2). PA14 Δ40 grew at rates comparable to the wild type in rich culture media and showed wild-type susceptibility to diverse antimicrobials under standard assay conditions (Fig. 1*B*). The only clear change was a moderately reduced susceptibility (i.e., higher MIC values and smaller inhibition zones) to the carbapenems meropenem and imipenem, which could be explained almost entirely by the well-known role of OprD/OccD1.

Together, these data demonstrate that the 40 porins are not the major entry pathway for antibiotics under standard conditions. We cannot exclude that induction of certain porins with low expression levels in standard Mueller–Hinton medium might permit antimicrobial entry under nonstandard conditions (27, 28). However, mass spectrometry–based proteome analysis revealed that *P. aeruginosa* porin abundance in Mueller–Hinton broth closely mimics porin patterns as observed in two different rodent infection models (Fig. 1*C*), suggesting that standard assays comprise all clinically relevant porins.

Diverging Requirements of "Specific" Porins for Nutrient Uptake. The PA14 Δ40 strain grew normally on rich media and on minimal media containing 10 mM acetamide or arginine as the sole carbon/energy

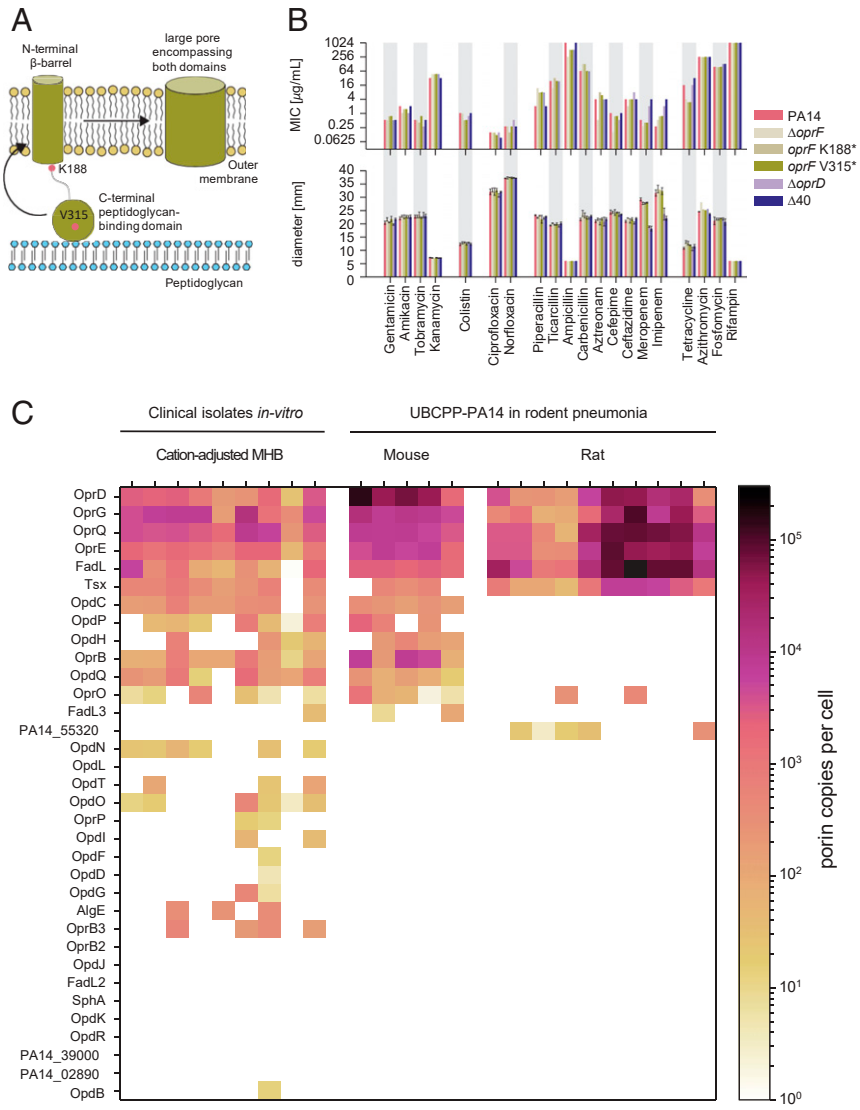

Fig. 1. Porin involvement in *P. aeruginosa* antimicrobial susceptibility. (*A*) Model of OprF with a large majority of two-domain conformer with a narrow outer-membrane β-barrel and a C-terminal domain linking the outer membrane with peptidoglycan and a minority of one-domain conformer with a large pore. (*B*) MIC (*Upper*) and antibiograms (*Lower*) of wild-type *P. aeruginosa* UCBPP-PA14 and various porin mutants. Means and SD of three experiments are shown. (*C*) Porin abundance in clinical *P. aeruginosa* strains in vitro and in UCBPP-PA14 in two rodent pneumonia models as determined by targeted proteomics.

source but poorly on minimal media containing the otherwise preferred carbon/energy sources (35) glutamate or succinate (Fig. 2*A* and *SI Appendix*, Fig. S1*A*), indicating a key role of porins for efficient uptake of some but not all nutrients. To test this idea, we mixed 16 chemically diverse carbon/energy sources (organic acids, amino acids, and glucose) that are known to be utilized by PA14 (36) at concentrations of 100 μM and quantified their consumption by PA14 wild type and PA14 Δ40 using NMR spectroscopy (37) (Fig. 2*B* and *SI Appendix*, Figs. S1*B* and S2). We used comparatively low nutrient concentrations to reduce interference by other potentially rate-limiting steps in nutrient utilization (i.e., transport across the inner membrane and catabolism) (38) and to minimize the contribution of inefficient unspecific translocation pathways (31). To enable consistent growth of PA14 Δ40 (and PA14), we also included 10 mM acetamide, which was readily consumed by both strains (Fig. 2 *A*, *C*, and *D* and *SI Appendix*, Fig. S1*A*). We preadapted the strains to this medium to ensure proper induction of respective utilization pathways and to minimize lag phases that occurred after switching media with different nutrients.

P. aeruginosa wild type consumed all 16 components within a few hours with the typical pseudomonal preference for succinate, glutamine, proline, and asparagine (35) (Fig. 2 *C* and *D*). The porin-free strain PA14 Δ40 consumed small (alanine) and positively charged (histidine and arginine) nutrients at 80 to 100% of the wild-type rates (Fig. 2*E*). Although some porins such as OprD/OccD1 and closely related paralogs can permit translocation of arginine (20), they were obviously not required for wild-type arginine consumption rates (31). By contrast, all nutrients that had two or more carboxylate groups (aconitate, aspartate, citrate, glutamate, and succinate) showed marked porin dependency (PA14 Δ40 had <20% of wild-type consumption rates). Other compounds had intermediate porin dependency (asparagine, glycine, glucose, glutamine, proline, pyruvate, and tyrosine), indicating that the porin-free outer membrane was partially permeable for these compounds, but porins facilitated translocation.

Together, these data showed that the outer membrane of *P. aeruginosa* permitted entry of hydrophilic/amphiphilic compounds with substantial rates, even in the absence of all 40 identifiable

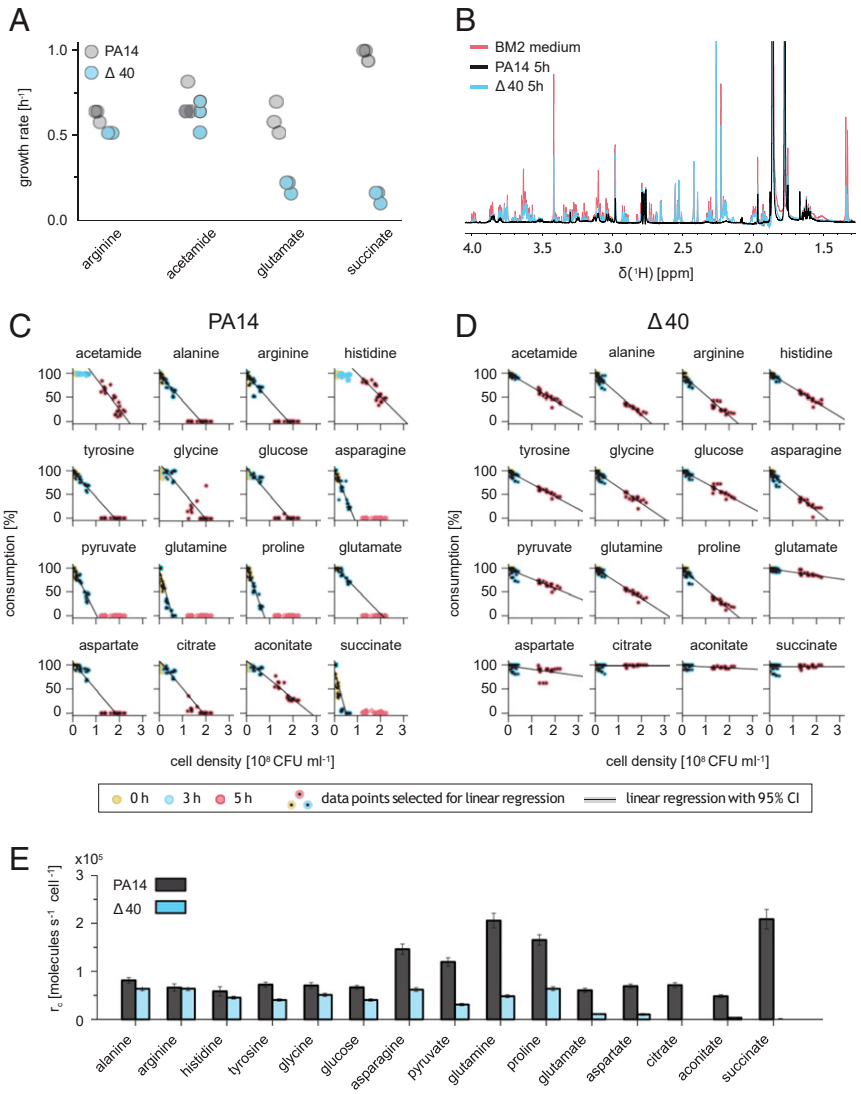

Fig. 2. Porin dependency of *P. aeruginosa* nutrient uptake. (*A*) Growth rates of *P. aeruginosa* PA14 wild-type and porin-free PA14 Δ40 in BM2 minimal media containing a single energy/carbon source. (*B*) One-dimensional ^{1}H-NMR spectrum of modified BM2 medium containing 16 different nutrients before and after 5 h growth of *P. aeruginosa* PA14 wild type or porin-free PA14 Δ40. (*C* and *D*) PA14 nutrient consumption as measured by one-dimensional [^{1}H] NMR spectroscopy. Each dot represents individual data for 1 of 21 independent cultures. (*E*) PA14 Δ40 nutrient consumption as measured by one-dimensional [^{1}H] NMR spectroscopy. Each dot represents individual data for 1 of 21 independent cultures. Uptake rates for individual nutrients based on data shown in *C* and *D*. Means and SDs are shown.

porins. This includes the preferred carbon sources alanine and arginine but also other amino acids and glucose that are accessible for *P. aeruginosa* in millimolar concentrations in the lung of cystic fibrosis (CF) and non-CF patients (39, 40). This compound uptake was not caused by general membrane leakage/permeabilization in the absence of porins because small molecules with two or more carboxylate groups (such as succinate) were effectively excluded.

Complex Substrate Selectivity of Individual Porins. To determine the contribution of individual porins to nutrient uptake, we expressed single porin genes in the porin-free PA14 Δ40 background. For all constructs we used the same P_{oprD} promoter on low-copy plasmids to minimize interference by specific porin-induction patterns (28). This strategy enabled determination of nutrient translocation through a single porin in the native membrane context without interference by other porins. We focused on 13 porins that we detected in various rodent infection models and in diverse clinical isolates grown under standard conditions for clinical microbiology (Mueller–Hinton broth) (Fig. 1*C*). This set included all nine porins detected in the lung of CF patients (41). For comparison, we included also the two porins OpdI/OccD5 and OpdL/OccK4 that were poorly expressed under all these conditions ("cryptic" porins).

FadL and Tsx had no impact on consumption of any of the tested nutrients (Fig. 3 *A* and *B* and *SI Appendix*, Fig. S3), consistent with their proposed selectivity for fatty acids and nucleosides, respectively, which were not included in our nutrient mix. OprG had no detectable impact on nutrient consumption, arguing against an important role for uptake of small amino acids including glycine and alanine (42) under native conditions, consistent with its narrow channel consisting of eight β-strands (19). OprB enabled wild-type consumption rates specifically for glucose, as expected (38). The remaining porins enabled consumption of 3 to 11 different nutrients at near wild-type levels. Importantly, no porin except for OprB enabled consumption of glucose, indicating no general membrane leakage as a result of forced porin expression.

Each of the other porins had a distinct substrate spectrum, while at the same time each nutrient was able to translocate through several different porins. The tricarboxylates, citrate and aconitate,

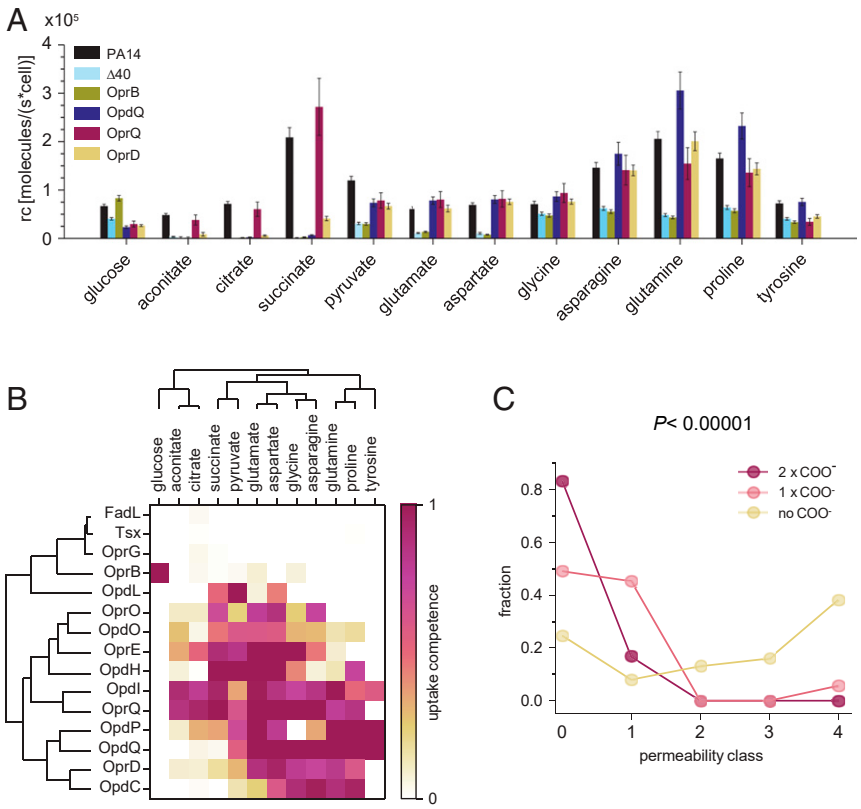

Fig. 3. Nutrient uptake through single porins in absence of other porins. (*A*) Nutrient consumption rates of PA14 Δ40 strains expressing a single porin from a low-copy-number plasmid. Means and averages for three independent cultures (single-porin strains) or 21 cultures (PA14, PA14 Δ40) are shown. (*B*) Substrate selectivity of 15 porins determined in single-porin strains. The capacity of each porin to boost nutrient consumption from baseline levels in PA14 Δ40 to wild-type levels is shown. Porins and nutrients are grouped based on unsupervised clustering. (*C*) Permeability of 472 antimicrobial compounds with detectable antipseudomonal activity (15). Following the published analysis, compounds are grouped in permeability classes according to the MIC values for efflux-deficient *P. aeruginosa* strains with intact (P Δ6) or abolished (P Δ6-pore) outer membrane permeability barrier (class 0, MIC of PA Δ6-pore is less than 20% of PA Δ6; 1, 20 to 40%; 2, 40 to 60%, 3, 60 to 80%; 4 more than 80%). Statistical significance was analyzed with the χ^2 test.

entered almost exclusively through just two porins, OpdI/OccD5 and OprQ/OccD6, but hardly through the previously postulated OpdH/OccK5, consistent with negative electrophysiology data (28). The aromatic amino acid tyrosine translocated mainly through OpdP/OccD3 and OpdQ/OccK6, and partially through OpdI/OccD5. The previously implicated OpdT/OccD4 was not among our set of expressed porins. Glutamate translocated efficiently through several porins of both the OpdK/OccK and OprD/OccD families (OprE/OccK8, OprQ/OccD6, OpdI/OccD5, OpdQ/OccK6, and OpdH/OccK5) and partially through OprD/OccD1 and OprO. Results for OprE/OccK8 were consistent with recent liposome swelling assays (29). Succinate also translocated through members of both porin subfamilies (OpdH/OccK5, OpdI/OccD5, OprE/OccK8, and OprQ/OccD6). The "cryptic" porin OpdI/OccD5 had transport capabilities similar to the abundantly expressed and distantly related subfamily member OprQ/OccD6, which might explain why OpdI/OccD5 was not expressed under standard conditions. The "cryptic" porin OpdL/OccK4 had an unusually narrow substrate spectrum with a preference for pyruvate, suggesting that it might be induced when this nutrient is available. The broad range of substrates of some porins contrasted with efficient exclusion of only narrow sets of nutrients (e.g., glycine–OpdP, succinate–OpdQ, and proline–OprE).

These data do not support the previously proposed distinct substrate spectra of porin subfamilies (OprD/OccD1, positively charged amino acids; OpdK/OccK subfamily, net negative charge). This proposal was based on observations from porins expressed in *E. coli* (20) which might have affected their channel properties. Recent electrophysiology data for OprE/OccK8 also question a simple dichotomy for substrates between the two subfamilies (29). Unsupervised clustering for transport capabilities observed in this study yielded incomplete separation of the two subfamilies and no signature substrates for either subfamily (Fig. 3*B*). Furthermore, the clustering did not conform with overall sequence similarity within each subfamily (19) (e.g., the sequence of OccD1 is closer to OccD3 and OccD6 than to OccD2, which is, however, more similar in terms of substrates).

Finally, chemically similar substrates did cluster together (tricarboxylates citrate/aconitate; small negatively charged acids succinate/pyruvate; negatively charged amino acids glutamate/aspartate) although the zwitterionic amino acids formed two separate clusters tyrosine/glutamine/proline and glycine/asparagine, possibly driven by molecular size. Together, these data show that certain porins share substrate preferences independently of their evolutionary relatedness. This might facilitate identification of relevant structure–function relationships against commonly inherited channel properties in future studies.

Taken together, these data show 1) substantial porin-independent translocation of certain nutrients and 2) broad porin substrate spectra and marked overlap, but also efficient porin-specific nutrient exclusion.

Carboxylate Groups Slow Translocation. Porin-independent translocation was crucial for antibiotic activity (Fig. 1 *B* and *C*). Compound properties that interfere with this pathway should thus be avoided in antimicrobial discovery and development. Our nutrient

consumption data for compounds with masses below 200 Da indicated that two or more carboxylate groups blocked porin-independent translocation (Fig. 2 *C* and *D*; aconitate, citrate, and succinate). To extend these observations, we reanalyzed recent datasets for more than 500 antipseudomonal compounds in the 250- to 700-Da size range (14, 15). In particular, we compared MIC values for efflux-deficient *P. aeruginosa* strains with intact outer membrane barrier (P Δ6, lacking six major efflux systems) or abolished barrier function because of insertion of water-filled pores with ∼2.4-nm diameter (P Δ6-pore). We focused on these efflux-deficient strains to unravel the contribution of the outer membrane translocation with minimal interference by efflux (16). Antimicrobials such as gentamicin do not gain activity in P Δ6-pore compared to P Δ6, suggesting that they can permeate already the wild-type outer membrane efficiently. Large antimicrobials such as azithromycin (758.88 Da) and erythromycin (728.38 Da) are 128-fold more potent against P Δ6-pore compared to P Δ6, indicating that the intact outer membrane provides an efficient barrier for these molecules.

Previous analysis of these data has revealed molecular fragments promoting translocation through the wild-type outer membrane (primary and secondary amine groups, benzene rings, and trifluoromethyl groups) (15). Our reanalysis showed an additional marked negative impact of carboxylate groups on membrane permeation (Fig. 3*C*). Fifty out of 53 molecules (94%) with one carboxylate group and all six compounds with two carboxylates were bad permeators ["class 0," activity gain in P Δ6-pore greater than fivefold; "class 1," gain between 5- and 2.5-fold (15)], while only 135 out of 413 molecules (33%) without carboxylates had such bad permeation capabilities. These results indicate that carboxylate groups slow outer-membrane permeation. This carboxylate penalty supports and extends our findings for porin-independent nutrient uptake (Fig. 2 *C* and *D*).

It is important to note that the antimicrobial ceftazidime has two carboxylate groups and is a "poor permeator" [64-fold activity gain in P Δ6-pore (14)], yet it remains the first choice for treating patients with susceptible *P. aeruginosa* infections (43). Poor permeation is thus compatible with clinical efficacy if other aspects such as target binding and efflux avoidance are favorable (as is the case for ceftazidime). Efficient translocation is, however, crucial for compounds with less-favorable efflux and target-binding properties (4, 16, 44).

Discussion

Porins with water-filled channels are commonly assumed to be essential for efficient translocation of hydrophilic compounds across the outer membrane of Gram-negative bacteria. Our comprehensive deletion of all porin genes in a clinically relevant *P. aeruginosa* isolate and the generation of a series of *P. aeruginosa* strains that carry only one type of porin provided unique opportunities for determining porin function in the native outer-membrane environment.

We observed that the porin-free mutant PA14 Δ40 grew normally on rich media and, unexpectedly, also on minimal media containing a single, hydrophilic carbon/energy source. Quantification of consumption rates using NMR spectroscopy showed porin-independent uptake of diverse water-soluble molecules with rates in the range of 50,000 molecules s^{-1} per cell at an external concentration of 100 μM. However, nutrients with two or more carboxylate groups permeated poorly in the absence of porins. These results indicate a remarkable permeability of the porin-free outer membrane for many but not all hydrophilic molecules.

In addition to porins, the Bam complex (45, 46), secretins (47), and outer-membrane channels of efflux systems (3) are thought to transiently form large, unspecific pores in the outer membrane. However, such large unspecific pores seem to play a limited role for nutrient uptake by *P. aeruginosa* because small molecules such as succinate and citrate permeate only slowly in the absence of porins. Instead, many molecules likely translocate directly through the lipid bilayer (15, 48–52). This translocation pathway is consistent with the preference for amines and effective exclusion of carboxylates: Amines can efficiently compete with Mg^{2+} and Ca^{2+} cations (53) that form salt bridges with phosphate and carboxylate groups of LPS, thereby weakening the gel-like Mg^{2+}/phosphate/LPS core clusters and enhancing translocation [the "self-promoted uptake" concept (48)]. By contrast, carboxylates might displace water molecules of the inner hydration shell of Mg^{2+}, thus forming stable complexes (54) that link the carboxylates to the rigid gel-like Mg^{2+}/phosphate/LPS core clusters without weakening them, thereby slowing permeation.

Although the outer-membrane lipid bilayer enabled substantial porin-independent permeation by many hydrophilic molecules, valuable and preferred nutrients with two or more carboxylate groups such as succinate had low permeation rates in the absence of porins. The large OprD/Occ family of porins may have evolved specifically for uptake of compounds with carboxylate groups (20), thus opening translocation pathways for these poorly permeating but valuable nutrients. Many porins had unexpectedly broad substrate spectra, which challenges the one porin–one nutrient model. On the other hand, each porin excluded effectively individual nutrients with high specificity, although these nutrients are readily transported by closely related porin family members. This combination of promiscuous uptake and highly specific exclusion suggests that porin evolution was mostly shaped by selection against the entry of toxic compounds while specific uptake of only one nutrient was not critical. Most nutrients that could use various porins for entry were covered by a combination of just two porins, OprE/OccK8 and OprQ/OccD6, which are abundant in various *P. aeruginosa* clinical isolates when grown in standard medium, and in PA14 in different rodent models (Fig. 1*C*). Uptake of additional substrates could be covered by substrate-induced expression of other porins (31). This substrate overlap may also explain why clinical isolates often down-regulate or inactivate OprD/OccD1, resulting in diminished susceptibility to carbapenems (55). This loss should not impair *Pseudomonas* nutrition because the abundant porins OprE/OccK8 and OprQ/OccD6 cover the same nutrients as OprD/OccD1 (at least among the nutrients tested in this study). Indeed, OprD loss in clinical isolates has no detectable fitness costs in rodent pneumonia models (in fact, fitness is greatly increased for unknown reasons) (56). Porin redundancy thus facilitates emergence of carbapenem resistance.

Our antimicrobial susceptibility data show that neither the "general" porin OprF nor the "specific" porins were relevant for translocation of diverse antimicrobials under standard conditions, with the sole exception of previously identified partial permeation of carbapenems through OprD. These results provide further support for the relevance of porin-independent permeation of the outer-membrane lipid bilayer. Recent data confirm that *E. coli* lacking both major unspecific porins OmpC and OmpF show decreased susceptibility to several β-lactam antibiotics (9), consistent with the role of the major porins for uptake of these drugs (13). However, some β-lactams and diverse other antibiotics retain most of their activity against this *ompC ompF* mutant (9), suggesting efficient alternative entry pathways. This could suggest a similar porin-independent entry pathway, but other still-remaining porins or disturbed barrier function in the mutant could also be involved.

In conclusion, diverse hydrophilic compounds can penetrate the *P. aeruginosa* outer-membrane bilayer at relevant rates independently of porins. Porins are mostly required for utilization of valuable nutrients containing multiple carboxylate groups, which permeate poorly through the porin-free outer membrane. Porins provide efficient translocation pathways for these nutrients but efficiently exclude antibiotics. Antibiotics thus have to enter the cell by direct penetration of the outer-membrane lipid bilayer, resulting in a penalty for molecules carrying carboxylate groups. Thus, replacement of carboxylate groups (which are present

in many current antibiotics) by isosteres (57) might be considered to accelerate compound translocation across the *P. aeruginosa* outer membrane. Future studies should further characterize this largely neglected translocation pathway, to identify additional molecular properties that determine translocation rates of antimicrobials.

Materials and Methods

Bacterial Strains and Growth Conditions. All *P. aeruginosa* mutants used in this study are derived from the clinical isolate UCBBP-PA14 (22). In addition, we analyzed various *P. aeruginosa* clinical isolates from the University Hospital Basel strain collection. *E. coli* Sm10λ*pir* was used for cloning and to conjugate plasmids into *P. aeruginosa*. All bacteria were cultured at 37 °C in lysogeny broth (LB) except for mating, for which we used *P. aeruginosa* grown overnight at 42 °C. For growth assays, bacteria were grown in overnight in LB and then overnight in basal medium 2 (BM2; http://cmdr.ubc.ca/bobh/method/media-recipes/) minimal medium with 10 mM acetamide as carbon source. After washing, the bacterial were inoculated in BM2 containing the carbon source of choice at an initial optical density at 600 nm (OD_{600}) = 0.05.

Antibiotics and Reagents. Amikacin (disulfate salt; potency 77.60%), aztreonam (potency 92%), azithromycin (potency 92.70%), cefepime (hydrochloride, 83.82%), ciprofloxacin (potency 78.60%), colistin (sulfate salt; potency, 67.50%), gentamicin (sulfate salt, potency 67.70%), imipenem (monohydrate, potency 93.66%), kanamycin (sulfate salt, potency 83.16%), meropenem (trihydrate, potency 87.64%), piperacillin (sodium salt, potency 94.60%), tetracycline (potency 100%), ticarcillin (disodium salt, potency 90.62%), and tobramycin (potency 95.20%) were purchased from Sigma-Aldrich. Ampicillin (disulfate salt, potency 77.60%) and carbenicillin (disodium salt, potency 89.58%) were purchased from Roth. Ceftazidime was purchased from European Pharmacopeia. Unless stated otherwise, all other reagents were of analytical grade and were purchased from Sigma-Aldrich-Fluka.

Gene Deletion and Episomal Porin Expression. Strains and plasmids used in this study are listed in *SI Appendix*, Table S3. Primers are listed in *SI Appendix*, Table S4.

Knockout vectors were constructed as described (58) with the following modifications. Seven hundred-base pair sequences of the flanking regions of the porin gene were PCR-amplified with primers designed with Snapgene software (GSL Biotech LLC). The fragments were gel-purified and inserted into pEXG2 plasmid (59) by Gibson assembly (60). The assembled plasmid was transformed into competent SM10λ*pir* prepared with Mix & Go (Zymo Research Corporation) and plated on LB agar containing 50 μg/mL kanamycin and 15 μg/mL gentamicin. Sequenced-verified clones were mated for 4 h with PA14 strains at 37 °C. Single cross-over events were selected on plates containing 15 μg/mL gentamicin and 20 μg/mL irgasan. Colonies were picked and grown in LB for 4 h and streaked on 5% sucrose plates overnight at 30 °C. *P. aeruginosa* clones were confirmed by sequencing and stored at −80 °C in LB containing 9% dimethyl sulfoxide. Whole-genome sequencing was done as described previously (58). Geneious Prime 2019.0.4 was used to map the reads to the *P. aeruginosa* UCBPP-PA14 reference sequence NC_008463.1 and to identify variations.

A plasmid backbone for expression of individual porins was constructed using Gibson assembly of the TrfA-OriV origin of replication from pAD6 (61), a derivative of the low-copy-number plasmid RK2 (62), the gentamicin resistance cassette and origin of transfer (*oriT*) from pEXG2, rpsl and rrnB terminators, and the P_{oprD} promoter amplified from PA14. A porin gene was inserted downstream of P_{oprD}. For electroporation of porin-expression plasmids, 20-mL PA14 Δ40 overnight cultures in LB were washed thrice with ice-cold 0.3 M sucrose and resuspended in 100 μL cold 0.3 M sucrose. Electroporation was done with 1 μL plasmid solution in 2-mm cuvettes at 25 μF/400 Ohm/2.5 kV. After addition of 1 mL prewarmed LB and incubation for 1 h at 37 °C, cells were plated on LB agar containing 15 μg/mL gentamicin.

Drug Susceptibility Tests. The MIC of drugs was determined by a twofold dilution assay in a 96-well plate according to Clinical and Laboratory Standards Institute guidelines (inoculum of ∼10^6 colony-forming units [CFU]/mL; reading after 20- to 24-h incubation) in cation-adjusted Mueller–Hinton broth (63). Growth of bacteria at 37 °C was examined by visual inspection after 20-h incubation. The MIC was defined as the lowest concentration of an antibiotic that completely prevented visible cell growth. Drug susceptibility was also determined with antibiogram measurements with 20 different antibiotics (Bio-Rad commercial disk). Overnight cultures of *P. aeruginosa* strains were diluted at OD_{600} = 0.1 and were spread on 120- × 120-mm^2 MHB II plates and air-dried in a laminar flow and then discs containing antibiotics were placed on the plates. Plates were incubated at 37 °C for 20 h. The diameter of halos surrounding the discs were measured as an indication of growth inhibition.

Nutrient Consumption Assays. *P. aeruginosa* strains were grown overnight in defined nutrient medium (BM2 containing 10 mM acetamide and 100 μM of 10 amino acids [alanine, arginine, asparagine, aspartate, glutamate, glutamine, glycine, histidine, proline, tyrosine], glucose, *cis*-aconitate, citrate, succinate, and pyruvate). Bacteria were washed and resuspended in prewarmed nutrient medium at OD_{600} = 0.005. Cultures were incubated at 37 °C and 180 rpm and samples were taken after 2, 3, and 5 h of growth. OD_{600} and CFU were determined at each time point. The remaining volumes were filtered through a 0.2-μm pore filter and stored at −80 °C until NMR analysis.

NMR spectra were measured on a 600-MHz Bruker Avance III HD NMR spectrometer equipped with a cryogenic QCI-F probe. One-dimensional [^{1}H] spectra were recorded with a free induction decay size of 32,000 points and 256 transients at 298 K. Water was suppressed by excitation sculpting. Spectra were processed using TopSpin 3.6 by applying an exponential window function with line broadening factor of 0.3 Hz and zero filling to 64,000 points prior to Fourier transformation. For each substance, an isolated signal was chosen for analysis (*SI Appendix*, Fig. S2). Peak intensities were determined by comparison with nutrient medium as reference.

Analysis of Consumption Kinetics. We assumed that during exponential growth, r_C, the average consumption rate per bacterium of nutrient *X* from the medium is constant. The consumption rate of nutrient *X* by the bacterial population is thus proportional to the cell density $n(t)$:

$$\frac{d[X]}{dt} = -r_C \cdot n(t) = -r_C \cdot n_0 \cdot e^{kt},$$

where n_0 is the density of bacteria at $t = 0$ and k the growth rate constant. Integration results in the residual substance concentration at time *T*:

$$[X](T) = \int_0^T \frac{d[X]}{dt}\ dt = [X]_o - \frac{r_C}{k} \cdot n(T)$$

and the total nutrient consumption M_X, which depends linearly on the cell density $n(T)$:

$$M_X(T) = [X]_o - [X](T) = \frac{r_C}{k} \cdot n(T).$$

The cell density relates to the OD_{600} via a proportionality factor $\bar{z}$:

$$n(T) = \frac{N}{V_0} = \bar{z} \cdot \mathrm{OD}_{600},$$

where *N* is the number of CFU determined in a volume V_0 of cell culture. In separate calibration experiments, $\bar{z}$ was determined to be 9.8×10^8 CFU·mL^{-1} and k was determined for each strain by exponential fitting of growth curves. The consumption rates r_C was then obtained from linear fits of data pairs [M_x, $n(T)$].

To account for differential consumption preferences (delayed uptake characterized by 1) a lag-phase, 2) moderate uptake, and 3) fast uptake), different subsets of data points were used for linear regression modeling (as indicated in Fig. 1*C*):

1) Data points at $t = 3$ and 5 h
2) Data points at $t = 0$, 2, 3, and 5 h
3) Data points at $t = 0$, 2 and 3 h.

For calculating the uptake competence of each porin for each nutrient *X*, the consumption rate of the single-porin strain for *X* was normalized to a range defined by the value of the consumption rates of PA14 and Δ40:

$$\text{uptake competence (porin)}_X = \frac{k_{X(porin)} - k_{X(\Delta 40)}}{k_{X(PA14)} - k_{X(\Delta 40)}} \cdot 100.$$

Values below 0 were set to 0 and values above 100 were set to 100.

Proteomics. *P. aeruginosa* porins were detected by targeted proteomics using parallel reaction monitoring on a high-resolution and accurate mass instrument with absolute quantification using heavy-isotope-labeled reference peptides as described previously (29). We analyzed PA14 and various clinical isolates grown to exponential phase in cation-adjusted Mueller–Hinton broth. We also reanalyzed previously obtained blood or lung homogenates from mice and rats (29) that had been obtained at 24 h postinfection by intratracheal instillation of an agar bead containing 10^7 CFU of PA14.

MICROBIOLOGY

Curve Fittings and Statistical Analysis. Curve fitting analyses and calculations of regression parameters were made with GraphPad Prism (version 4.03) software for Windows and statistical analysis with GraphPad Instat version 3.06 for Windows.

Data Availability. All study data are included in the article and/or *SI Appendix*.

ACKNOWLEDGMENTS. The work was supported by the European Union and the European Federation of Pharmaceutical Industries and Associations (IMI, ND4BB-TRANSLOCATION) and Swiss National Science Foundation (310030_156818, 310030_182315, NRP 72-177449, NCCR AntiResist) to D.B. and Biozentrum PhD fellowships to J.U. and V.T. We thank Prof. Dr. Daniel Häussinger for providing access to his NMR spectrometers and fruitful discussions on data analysis.

1. E. Tacconelli *et al*., Discovery, research, and development of new antibiotics: The WHO priority list of antibiotic-resistant bacteria and tuberculosis. *Lancet Infect. Dis.* **18**, 318–327 (2018).
2. R. E. Hancock, The bacterial outer membrane as a drug barrier. *Trends Microbiol.* **5**, 37–42 (1997).
3. H. I. Zgurskaya, C. A. López, S. Gnanakaran, Permeability barrier of Gram-negative cell envelopes and approaches to bypass it. *ACS Infect. Dis.* **1**, 512–522 (2015).
4. H. Nikaido, Molecular basis of bacterial outer membrane permeability revisited. *Microbiol. Mol. Biol. Rev.* **67**, 593–656 (2003).
5. J. Vergalli *et al*., Porins and small-molecule translocation across the outer membrane of Gram-negative bacteria. *Nat. Rev. Microbiol.* **18**, 164–176 (2020).
6. D. S. Snyder, T. J. McIntosh, The lipopolysaccharide barrier: Correlation of antibiotic susceptibility with antibiotic permeability and fluorescent probe binding kinetics. *Biochemistry* **39**, 11777–11787 (2000).
7. E. Sugawara, K. Nagano, H. Nikaido, Alternative folding pathways of the major porin OprF of Pseudomonas aeruginosa. *FEBS J.* **279**, 910–918 (2012).
8. A. H. Delcour, Outer membrane permeability and antibiotic resistance. *Biochim. Biophys. Acta* **1794**, 808–816 (2009).
9. U. Choi, C. R. Lee, Distinct roles of outer membrane porins in antibiotic resistance and membrane integrity in *Escherichia coli*. *Front. Microbiol.* **10**, 953 (2019).
10. M. F. Richter *et al*., Predictive compound accumulation rules yield a broad-spectrum antibiotic. *Nature* **545**, 299–304 (2017).
11. S. Acosta-Gutiérrez *et al*., Getting drugs into Gram-negative bacteria: Rational rules for permeation through general porins. *ACS Infect. Dis.* **4**, 1487–1498 (2018).
12. E. N. Parker *et al*., Implementation of permeation rules leads to a FabI inhibitor with activity against Gram-negative pathogens. *Nat. Microbiol.* **5**, 67–75 (2020).
13. R. E. Hancock, W. A. Woodruff, Roles of porin and beta-lactamase in beta-lactam resistance of Pseudomonas aeruginosa. *Rev. Infect. Dis.* **10**, 770–775 (1988).
14. C. J. Cooper *et al*., Molecular properties that define the activities of antibiotics in Escherichia coli and Pseudomonas aeruginosa. *ACS Infect. Dis.* **4**, 1223–1234 (2018).
15. R. A. Mansbach *et al*., Machine learning algorithm identifies an antibiotic vocabulary for permeating Gram-negative bacteria. *J. Chem. Inf. Model.* **60**, 2838–2847 (2020).
16. H. I. Zgurskaya, V. V. Rybenkov, Permeability barriers of Gram-negative pathogens. *Ann. N. Y. Acad. Sci.* **1459**, 5–18 (2020).
17. R. Tommasi, D. G. Brown, G. K. Walkup, J. I. Manchester, A. A. Miller, ESKAPEing the labyrinth of antibacterial discovery. *Nat. Rev. Drug Discov.* **14**, 529–542 (2015).
18. J. P. Quinn, E. J. Dudek, C. A. DiVincenzo, D. A. Lucks, S. A. Lerner, Emergence of resistance to imipenem during therapy for Pseudomonas aeruginosa infections. *J. Infect. Dis.* **154**, 289–294 (1986).
19. S. Chevalier *et al*., Structure, function and regulation of Pseudomonas aeruginosa porins. *FEMS Microbiol. Rev.* **41**, 698–722 (2017).
20. E. Eren *et al*., Substrate specificity within a family of outer membrane carboxylate channels. *PLoS Biol.* **10**, e1001242 (2012).
21. F. Dogan Guzel *et al*., Towards understanding single-channel characteristics of OccK8 purified from Pseudomonas aeruginosa. *Eur. Biophys. J.* **50**, 87–98 (2021).
22. J. He *et al*., The broad host range pathogen Pseudomonas aeruginosa strain PA14 carries two pathogenicity islands harboring plant and animal virulence genes. *Proc. Natl. Acad. Sci. U.S.A.* **101**, 2530–2535 (2004).
23. E. G. Rawling, F. S. Brinkman, R. E. Hancock, Roles of the carboxy-terminal half of Pseudomonas aeruginosa major outer membrane protein OprF in cell shape, growth in low-osmolarity medium, and peptidoglycan association. *J. Bacteriol.* **180**, 3556–3562 (1998).
24. H. Ishida, A. Garcia-Herrero, H. J. Vogel, The periplasmic domain of Escherichia coli outer membrane protein A can undergo a localized temperature dependent structural transition. *Biochim. Biophys. Acta* **1838**, 3014–3024 (2014).
25. C. J. Balibar, M. Grabowicz, Mutant alleles of lptD increase the permeability of Pseudomonas aeruginosa and define determinants of intrinsic resistance to antibiotics. *Antimicrob. Agents Chemother.* **60**, 845–854 (2015).
26. G. Krishnamoorthy *et al*., Synergy between active efflux and outer membrane diffusion defines rules of antibiotic permeation into Gram-negative bacteria. *MBio* **8**, e01172-17 (2017).
27. V. M. Isabella *et al*., Toward the rational design of carbapenem uptake in Pseudomonas aeruginosa. *Chem. Biol.* **22**, 535–547 (2015).
28. S. Tamber, E. Maier, R. Benz, R. E. Hancock, Characterization of OpdH, a Pseudomonas aeruginosa porin involved in the uptake of tricarboxylates. *J. Bacteriol.* **189**, 929–939 (2007).
29. S. Samanta *et al*., Getting drugs through small pores: Exploiting the porins pathway in Pseudomonas aeruginosa. *ACS Infect. Dis.* **4**, 1519–1528 (2018).
30. C. Piselli, R. Benz, Fosmidomycin transport through the phosphate-specific porins OprO and OprP of Pseudomonas aeruginosa. *Mol. Microbiol.*, 10.1111/mmi.14693 (2021).
31. S. Tamber, M. M. Ochs, R. E. Hancock, Role of the novel OprD family of porins in nutrient uptake in Pseudomonas aeruginosa. *J. Bacteriol.* **188**, 45–54 (2006).
32. E. B. Breidenstein, B. K. Khaira, I. Wiegand, J. Overhage, R. E. Hancock, Complex ciprofloxacin resistome revealed by screening a Pseudomonas aeruginosa mutant library for altered susceptibility. *Antimicrob. Agents Chemother.* **52**, 4486–4491 (2008).
33. A. Dötsch *et al*., Genomewide identification of genetic determinants of antimicrobial drug resistance in Pseudomonas aeruginosa. *Antimicrob. Agents Chemother.* **53**, 2522–2531 (2009).
34. C. Alvarez-Ortega, I. Wiegand, J. Olivares, R. E. Hancock, J. L. Martínez, Genetic determinants involved in the susceptibility of Pseudomonas aeruginosa to beta-lactam antibiotics. *Antimicrob. Agents Chemother.* **54**, 4159–4167 (2010).
35. F. Rojo, Carbon catabolite repression in Pseudomonas: Optimizing metabolic versatility and interactions with the environment. *FEMS Microbiol. Rev.* **34**, 658–684 (2010).
36. J. A. Bartell *et al*., Reconstruction of the metabolic network of Pseudomonas aeruginosa to interrogate virulence factor synthesis. *Nat. Commun.* **8**, 14631 (2017).
37. V. Behrends, H. D. Williams, J. G. Bundy, Metabolic footprinting: Extracellular metabolomic analysis. *Methods Mol. Biol.* **1149**, 281–292 (2014).
38. J. L. Wylie, E. A. Worobec, The OprB porin plays a central role in carbohydrate uptake in Pseudomonas aeruginosa. *J. Bacteriol.* **177**, 3021–3026 (1995).
39. K. L. Palmer, L. M. Aye, M. Whiteley, Nutritional cues control Pseudomonas aeruginosa multicellular behavior in cystic fibrosis sputum. *J. Bacteriol.* **189**, 8079–8087 (2007).
40. R. La Rosa, H. K. Johansen, S. Molin, Adapting to the airways: Metabolic requirements of *Pseudomonas aeruginosa* during the infection of cystic fibrosis patients. *Metabolites* **9**, E234 (2019).
41. X. Wu *et al*., In vivo proteome of Pseudomonas aeruginosa in airways of cystic fibrosis patients. *J. Proteome Res.* **18**, 2601–2612 (2019).
42. I. Kucharska, P. Seelheim, T. Edrington, B. Liang, L. K. Tamm, OprG harnesses the dynamics of its extracellular loops to transport small amino acids across the outer membrane of Pseudomonas aeruginosa. *Structure* **23**, 2234–2245 (2015).
43. T. Babich *et al*., Ceftazidime, carbapenems, or piperacillin-tazobactam as single definitive therapy for Pseudomonas aeruginosa bloodstream infection: A multisite retrospective study. *Clin. Infect. Dis.* **70**, 2270–2280 (2020).
44. W. W. Nichols, "Permeability of bacteria to antibacterial agents" in *Antibiotic Discovery and Development*, T. Dougherty, M. Pucci, Eds. (Springer, 2012), pp. 849–879.
45. V. Robert *et al*., Assembly factor Omp85 recognizes its outer membrane protein substrates by a species-specific C-terminal motif. *PLoS Biol.* **4**, e377 (2006).
46. L. Estrada Mallarino *et al*., TtOmp85, a β-barrel assembly protein, functions by barrel augmentation. *Biochemistry* **54**, 844–852 (2015).
47. E. Disconzi *et al*., Bacterial secretins form constitutively open pores akin to general porins. *J. Bacteriol.* **196**, 121–128 (2014).
48. R. E. Hancock, V. J. Raffle, T. I. Nicas, Involvement of the outer membrane in gentamicin and streptomycin uptake and killing in Pseudomonas aeruginosa. *Antimicrob. Agents Chemother.* **19**, 777–785 (1981).
49. T. Kitahara, H. Yoneyama, T. Nakae, Antibiotic diffusion pathways in the outer membrane of Pseudomonas aeruginosa. *Biochem. Biophys. Res. Commun.* **238**, 457–461 (1997).
50. P. Plesiat, J. R. Aires, C. Godard, T. Köhler, Use of steroids to monitor alterations in the outer membrane of Pseudomonas aeruginosa. *J. Bacteriol.* **179**, 7004–7010 (1997).
51. C. A. López, H. Zgurskaya, S. Gnanakaran, Molecular characterization of the outer membrane of Pseudomonas aeruginosa. *Biochim. Biophys. Acta Biomembr.* **1862**, 183151 (2020).
52. D. S. Patel *et al*., Dynamics and interactions of OmpF and LPS: Influence on pore accessibility and ion permeability. *Biophys. J.* **110**, 930–938 (2016).
53. C. Galanos, O. Lüderitz, Electrodialysis of lipopolysaccharides and their conversion to uniform salt forms. *Eur. J. Biochem.* **54**, 603–610 (1975).
54. T. Dudev, J. Cowan, C. Lim, Competitive binding in magnesium coordination chemistry: Water versus ligands of biological interest. *J. Am. Chem. Soc.* **121**, 7665–7673 (1999).
55. P. D. Lister, D. J. Wolter, N. D. Hanson, Antibacterial-resistant Pseudomonas aeruginosa: Clinical impact and complex regulation of chromosomally encoded resistance mechanisms. *Clin. Microbiol. Rev.* **22**, 582–610 (2009).
56. D. Roux *et al*., Fitness cost of antibiotic susceptibility during bacterial infection. *Sci. Transl. Med.* **7**, 297ra114 (2015).
57. C. Ballatore, D. M. Huryn, A. B. Smith, 3rd, Carboxylic acid (bio)isosteres in drug design. *ChemMedChem* **8**, 385–395 (2013).
58. O. Cunrath *et al*., Quantitative contribution of efflux to multi-drug resistance of clinical Escherichia coli and Pseudomonas aeruginosa strains. *EBioMedicine* **41**, 479–487 (2019).
59. A. Rietsch, I. Vallet-Gely, S. L. Dove, J. J. Mekalanos, ExsE, a secreted regulator of type III secretion genes in Pseudomonas aeruginosa. *Proc. Natl. Acad. Sci. U.S.A.* **102**, 8006–8011 (2005).
60. D. G. Gibson *et al*., Enzymatic assembly of DNA molecules up to several hundred kilobases. *Nat. Methods* **6**, 343–345 (2009).
61. J. G. Malone *et al*., YfiBNR mediates cyclic di-GMP dependent small colony variant formation and persistence in Pseudomonas aeruginosa. *PLoS Pathog.* **6**, e1000804 (2010).
62. M. Jahn, C. Vorpahl, T. Hübschmann, H. Harms, S. Müller, Copy number variability of expression plasmids determined by cell sorting and Droplet Digital PCR. *Microb. Cell Fact.* **15**, 211 (2016).
63. Clinical and Laboratory Standards Institute, "Methods for dilution antimicrobial susceptibility tests for bacteria that grow aerobically" (CLSI document M7-A7, Clinical and Laboratory Standards Institute, Wayne, PA, 2012).

8. Chapter 2 - Discussion and Outlook

With our investigations about the role of specific outer membrane porins of *P. aeruginosa* for antibiotic and nutrient transport we contributed to a better understanding of the membrane permeability of this challenging bacterium. The results can help to progress the rational design of novel antimicrobial substances against *P. aeruginosa* that are urgently needed. *In vivo* conditions revealed that, except of OrpD, none of the other 40 porins represents an entry for antibiotics opposing to earlier *in vitro* studies[275,276,287,288]. In contrast, we find that many substrates can be transported across the outer membrane independently from specific and general porins, a translocation pathway that has been also been found to be important for the permeation of many antibiotics[289]. Molecules with no or one carboxylate groups are favored for this pathway. Therefore, it is important that future research on the development of new antibiotics focuses on improving the membrane permeability of those substances. This makes a great case for the development and application of antimicrobial peptides (AMPs). Members of this group of antimicrobials directly target the bacterial membrane and often contain a high amount of positively charged amino acids like arginine and lysine as well as hydrophobic residues such as valine, tryptophane, isoleucine and phenylalanine[290,291]. Interestingly, substrates for which we observed porin-independent translocation (arginine, alanine, histidine) belong to those amino acid types suggesting similarities regarding the translocation mechanism. The synergistic interaction of AMPs and conventional antibiotics has been shown to be effective against multidrug resistant *P. aeruginosa* strains and may lead to new treatment opportunities[292].

The outer membrane porin OprD is the only porin that could be confirmed as entry point for antibiotics in our study. A better and more detailed knowledge about the interaction of OprD with carbapenems on a structural level could help to improve current antibiotics and discover new possibilities for the treatment of *P. aeruginosa* infections. However, it proved difficult to understand the exceptional affinity of OprD for carbapenems when comparing it with the structures of other OprD family porins. This also applies to the understanding of the substrate profiles we discovered for the individual porins based on their porin structures.

A major challenge here is the lack of knowledge about porin dynamics. As described in the introduction, some of the extracellular loops exhibit a high level of flexibility which might contribute to the substrate selectivity of the porins. The lack of knowledge about substrates for individual porins as well as low affinities to their substrates prevented the elucidation co-crystal structures with bound substrates. Therefore, for many porins the substrate binding site remains elusive. Furthermore, the crystal structures of OprD members of the OccD subclass reveal closed constrictions pores making it difficult to precisely describe substrate translocation through this porin. In order to understand the interaction of OprD family members with their substrates including the preference of OprD for carbapenems solution NMR experiments and biophysical methods would be highly suited because an elucidation of the dynamic behavior of these porins would deepen our knowledge about the transport mechanism. Furthermore our in vivo assay can reveal relative substrate affinities of single nutrients for individual porins and establish substrate preferences leading to possibilities to characterize substrate binding on a structural level.

The discovery of overlapping substrate profiles raises the question about the evolutionary reason of all 40 currently known porins in the genome of *P. aeruginosa*. Since standard laboratory conditions as well as isolates from lung infection showed the expression of a similar and reduced porin subset it still remains elusive under which conditions *P. aeruginosa* requires all other porins. The relevance of this question is emphasized by the observation that a combination of just two porins OprE/OccK8 and OprQ/OccD6, covered uptake of most nutrients. Many studies mainly investigated the induction of porin expression upon growth on beneficial nutritional substrates. However, exclusion patterns within substrate profiles might suggest that a porin's specificity does not reside within its uptake potential but within its ability to exclude specific compounds. We hypothesize that certain porins are expressed under conditions in which the permeation of specific toxic substrates needs to be avoided (Fig 19). Due to overlapping uptake profiles, porin expression can be regulated according to the presence of toxic compounds without or only minimally compromising maximum exhaustion of the nutritional environment. This can readily be seen from the down-regulation of OprD in antibiotic resistant isolates[282]. This idea might explain how the evolution of many porins with promiscuous overlapping substrate selectivities helps *P. aeruginosa* to achieve a strict control over the outer membrane permeability while

maximizing its adaptability to diverse nutritional environments. It therefore is interesting to challenge this idea by testing our single-porin expressing strains for growth of usually toxic substances.

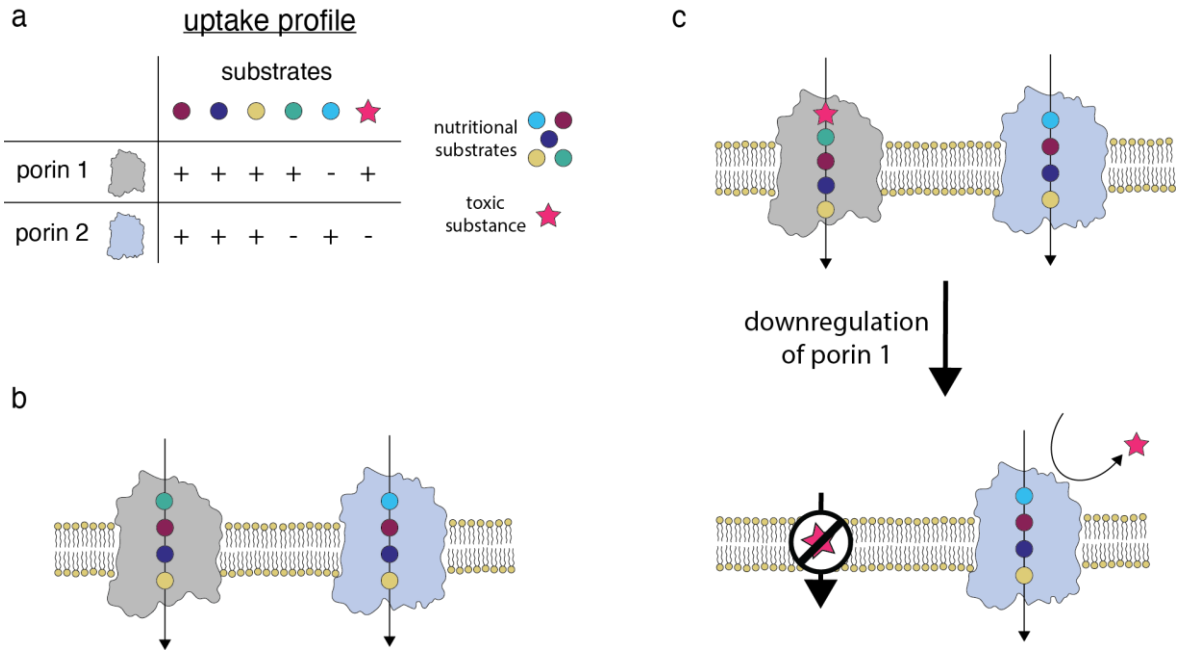

Figure 19: Schematic representation to illustrate the idea how porins with substrate specific exclusion patterns might help to prevent permeation of toxic compounds across the outer membrane of *P. aeruginosa*. a: Uptake profiles of two hypothetical outer membrane porins, nutrients are depicted as coloured circles, a toxic compound is shown as a star. b: During non-toxic conditions both porins are expressed and enable maximum exploitation of the nutritional environment. c: The presence of a toxic compound leads to down-regulation of the porin enabling permeation with only minimal consequences on substrate uptake.

9. Chapter 2 - Appendix

porin name	pdb code of crystal structure	pore diameter (Å) in crystal structure	residues forming the constriction pore	residues involved in substrate binding	residues involved in basic ladder	conductance [pS] and gating states (up to 3 states, O1 – O3)	substrates
OprD/ OccD1	2ODJ (apo)[270]	closed pore [270,272]	A127 – S130, D295 – I297, S302 – D307, R391 R410 [270]	D307, Y176, Y282 [272]	R30, R39, K375, R389, R391, R410 [272]	15, few spikes [272]	arginine D-arginine histidine ornithine arg-arg-dipeptide [272] glutamate alanine [284]
	4FOZ (Y282R/D307H, mutant) [271]					O1: 21 (main state) O2: 889 [277]	
	3SY7 (apo) [271]						
OccD2	3SY9 (apo) [272]	closed pore			R412, R391, H26, N406	15, several spikes [272]	arginine [272]
						na	
OccD3	3SYB (apo) [272]					700pS, infrequent state [272]	arginine [272]

			N172, R173, R449, R205, Y326, E216, D342, S338, Q20, S331		R205, R173, R220, H328, R449	O1: 3 O2: 667 (main) [277]	
OccD4						178, with few downward spikes [272] O1: 3 O2: 159 (main state) [277]	
OccD5						22, with upward spikes [272] O1: 24 (main state) O2: 239 [277]	arginine [272]
OccD6						312 [272] O1: 417 (main state) O2: 1899 [277]	arginine [272]
OccK1	2QTK (apo)[274]		R22, R126, R158, R284, D123, D289 [273]			294 [272]	benzoate glucoronate pyroglutamate

	3SYS (apo) [272] 2Y2X (holo, bound to vanillate, to be published)					O1: 223 O2: 307 (main state) O3: 357 [273]	vanillate 3-nitrobenzoate 4-nitrobenzoate adipate caproate octanoate [272]
OccK2	3SZD (apo) [272] 4FMS (holo, bound to glucoronate) [271]		R26, R129, R161, R280, R327, R387. D126, D292 [273]	D126, R129 (L3) R161 (L4) R280, S285, G286, D292, S297 (L7) [272]		233 pS, noisy [272] O1: 73 O2: 242 (main state) O3: 371 [273]	benzoate glucoronate pyroglutamate 4-nitrobenzoate [272]
OccK3	3SZV (apo) [272]		R123, R317, R358, R374, D121, D276, D287 [273]		R19	145 [272]	benzoate glucoronate pyroglutamate [272]

			R374, T122, N120, D276, F282, Q284, I283 (carbonyl)			O1: 144 (main state) [273]	
OccK4	3T0S (apo) [272]	3.5 [273]	R13, R120, R124, D121, D122 [273]			47 [272] O1: 43 (main) O2: 358 [273]	benzoate glucoronate pyroglutamate [272]
OccK5	3T20 (apo) [272]	4 [273]	R31, R134, K179, R334, R374, R376, R392[273]		R20, R381, R123	340, with downward spikes [272]	benzoate glucoronate pyroglutamate [272]
			R281, R365, Q290, V289 (carbonyl), **F288**, N282, N120, G122			O1: 33 O2: 353 (main state) [273]	

OccK6	3T24 (apo) [272]	4 [273]	R124, R156, R172, R384, D285, E382 [273] R384, Q293, I292 (carbonyl), F291, D285, N121, R156, S123, R124			75, with few upward spikes [272] O1: 71 (main state) O2: 302 [273]	benzoate glucoronate pyroglutamate [272]
OccK7	4FRT (apo) To be published					379 [272] O1: 276 O2: 379 (main state) O3: 463[273]	benzoate pyroglutamate glucoronate [272]
OccK8	4FRX (apo) [279]	Small pore, highly charged [279]	V23 (carbonyl), Q324, R421, R131, N128, T316, S315, R163, K327, I325 (carbonyl), D322		R330, Q329, K327, Q417, R163, R131		

Table A2: Summary of structural and biophysical characteristics and known specificities of porins of the OprD family. If not referenced accordingly, residues involved in constriction pore formation, formation of the basic ladder and substrate specificity were identified from examination of the respective crystal structure.

PNAS
www.pnas.org

Supplementary Information for

Outer membrane permeability: antimicrobials and diverse nutrients bypass porins in *Pseudomonas aeruginosa*

Johanna Ude[1,4], Vishwachi Tripathi[1,4], Julien M. Buyck[1,4], Sandra Söderholm[1], Olivier Cunrath[1], Joseph Fanous[1], Beatrice Claudi[1], Adrian Egli[2,3], Christian Schleberger[1], Sebastian Hiller[1,*], Dirk Bumann[1,*]

[1]Biozentrum, [2]University Hospital, [3]Department Biomedicine, University of Basel, CH-4056 Switzerland; [4]these authors contributed equally.

*Corresponding authors: Sebastian Hiller, Dirk Bumann

Email: sebastian.hiller@unibas.ch, dirk.bumann@unibas.ch

This PDF file includes:

Supplementary Information Text

Secondary mutations in strain PA14 Δ40. Whole-genome sequencing of parental PA14 and PA14 Δ40 confirmed accurate deletion of 40 porin genes and identified nine secondary mutations in PA14 Δ40 (SI, Supplementary Table S2).

Specifically, we identified:

i) loss of a duplicate tRNA-asp gene (PA14_24120, identical copy of the adjacent PA14_24130);

ii) two non-synonymous mutations: PA14_02870 D16N (affecting a non-conserved residue in the HTH domain of a probable transcriptional regulator), PA14_72090 R26H (affecting a residue outside of recognizable domains in a hypothetical protein),

iii) two synonymous mutations in codon 538 of PA14_28710 (encoding the β subunit of phenylalanyl-tRNA synthetase) and in codon 1,172 PA14_33610 (encoding pyochelin synthetase PchF);

iv) four intergenic mutations upstream of PA14_16990 (encoding a hypothetical protein), PA14_55640 (encoding exonuclease SbcD), and PA14_66490 (encoding the transcriptional regulator DhcR).

None of the associated genes show a link to altered antimicrobial susceptibility in comprehensive transposon library screens, with the exception of PA14_33610 *pchF*. Transposon inactivation of *pchF* results in two-fold higher MIC (the smallest detectable change) for ciprofloxacin (1), but the impact of the synonymous mutation in codon 1,172 of *pchF* in PA14 Δ40 is likely small compared to full gene inactivation. LpxC and other genes that might affect barrier function were not mutated.

Together, these data suggest no major impact of the secondary mutations in PA14 Δ40 on phenotypes relevant for this study. This was consistent with the unaltered susceptibility PA14 Δ40 to a large diversity of antimicrobials.

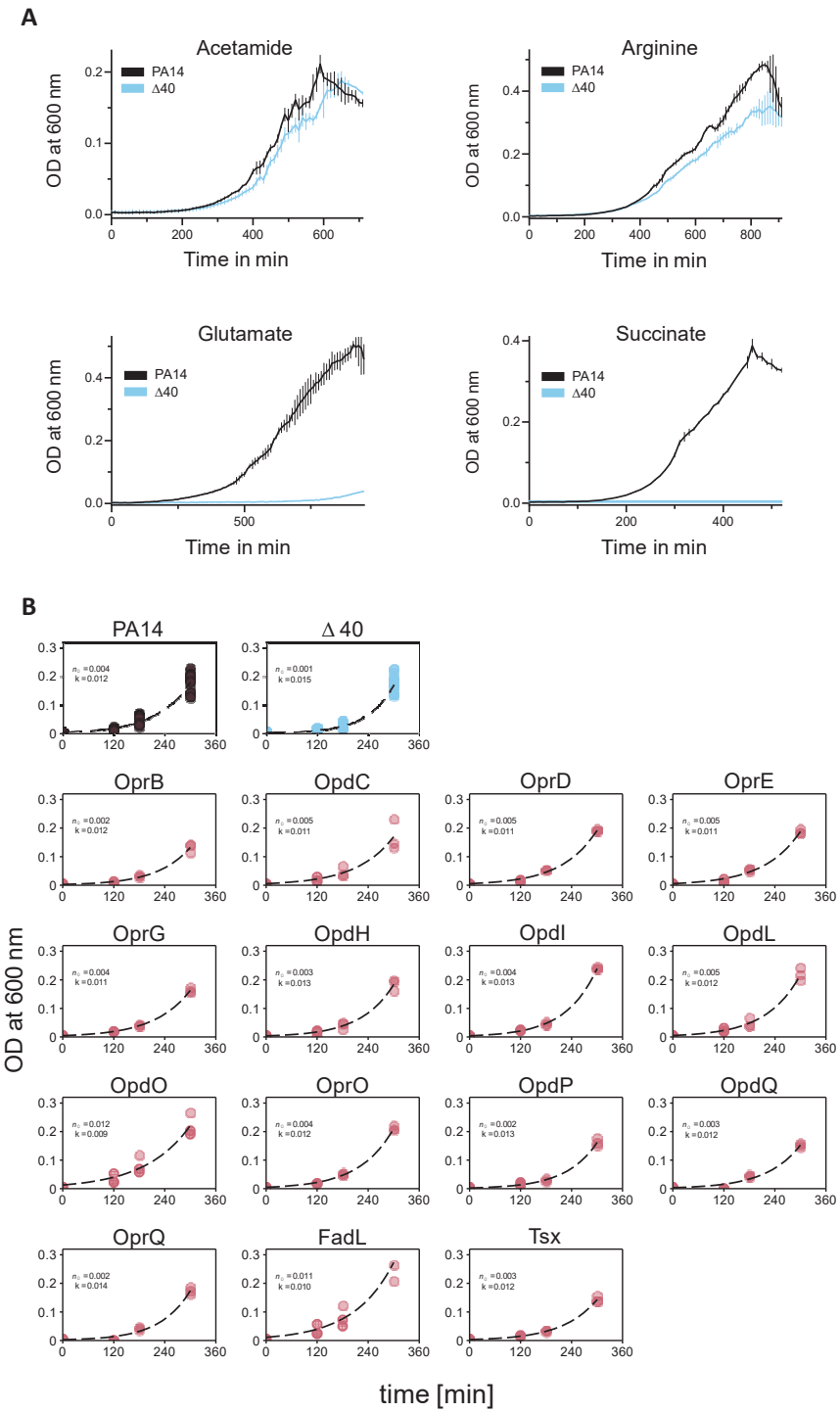

Fig. S1. Growth of porin-free PA14 Δ40 on single carbon/energy sources (A) and growth of PA14, PA14 Δ40, and 15 single-porin strains on medium containing 16 different carbon/energy sources (B).

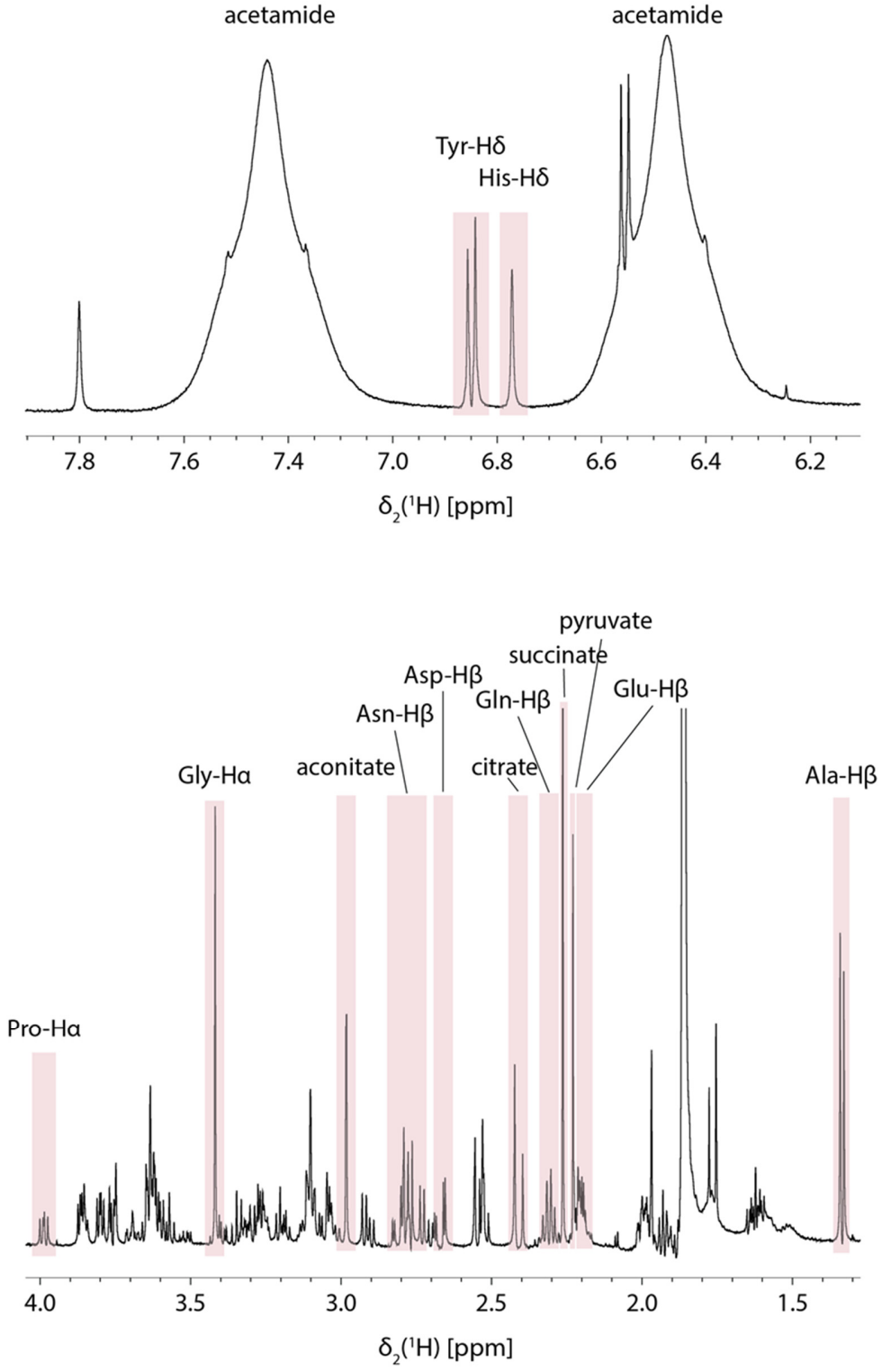

Fig. S2. 1D ^{1}H-NMR spectrum of BM2 medium supplemented with nutrients of interest. Peaks used for substrate quantification are highlighted with red boxes. The acetamide peaks at 7.45 and 6.45 ppm are broadened due to chemical exchange with water.

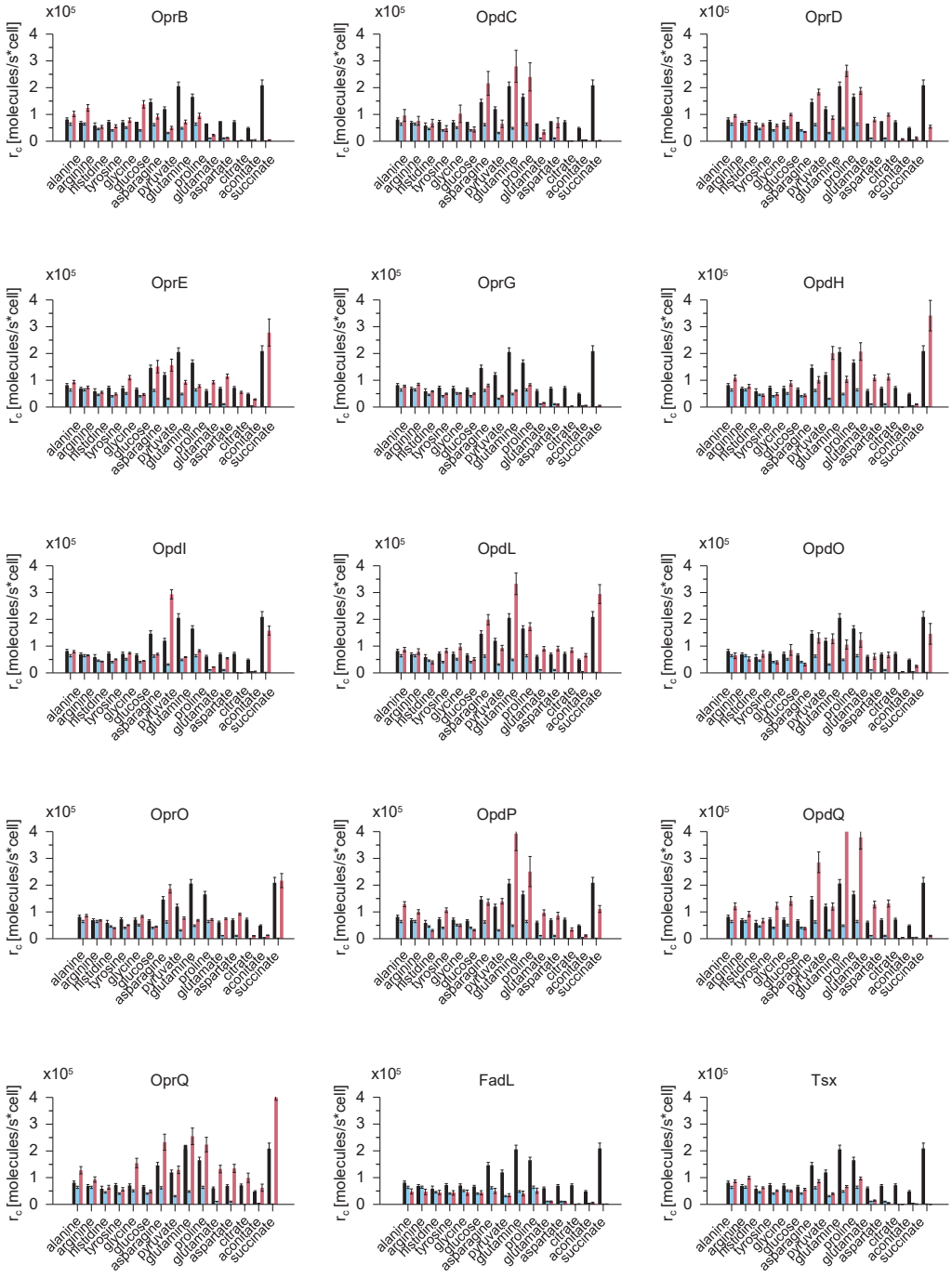

Fig. S3. Consumption rates of 15 single-porin strains for 16 nutrients individual porins (red) compared to PA14 (black) and PA14 Δ40 (blue). Means and standard deviations for three independent cultures are shown.

Table S1. Candidate outer-membrane porins encoded by UCPBPP-PA14.

PA14 locus	PAO1 locus	Gene name	Postulated substrates	PubMedIDs	Comments
PA14_01770	no ortholog			26578582	similar to *tsx*
PA14_02020	PA0162	*opdC, occD2*	arginine, histidine	16352820, 26578582	
PA14_02060	PA0165	*tsx*	nucleosides	26578582	based on similarity to *E. coli tsx*
PA14_02370	PA0189	*opdI, occD5*	arginine	26578582	
PA14_02890	PA0234			26578582	similar to *tsx*
PA14_02980	PA0240	*opdF, occK2*	benzoate, **carbenicillin**, **cefoxitin**, **gentamicin**, glucoronate, 4-nitrobenzoate, pyroglutamate, **temocillin**	16352820, 22272184, 26578582	
PA14_03800	PA0291	*oprE, occK8*	arabinose, ribose, glucose, galactose, mannose, N-acetylglucosamine	2539376	
PA14_09850	PA4179	*opdN, occK10*	5-aminolevulinate, glutamate	16352820, 17470813	
PA14_10440	PA4137	*opdL, occK4*	benzoate, glucuronate, phenylacetate, pyroglutamate	16352820, 17470813, 22272184	
PA14_10870	PA4099	*oprB3*		26578582	similar to *oprB*
PA14_11270	PA4067	*oprG*	alanine, glycine, hydrophobic molecules, iron (II), phtalate, serine, valine	16352820, 17470813, 21124774, 26655471, 26578582	
PA14_15280	PA3772	*qbdB*			similar to *sphA*
PA14_16630	PA3692	*lptF*			no outer membrane beta-barrel protein but OmpA-like peptidoglycan-binding domain
PA14_17890	PA3588	*opdR, occK11*	phenylacetate	16352820, 17470813	
PA14_18510	PA3544	*algE*	alginate (secretion)	23335756	
PA14_21610	PA3280	*oprO*	pyrophosphate	1370289, 26578582	
PA14_21620	PA3279	*oprP*	phosphate	1370289, 26578582	

PA14_23030	PA3186	*oprB*	arabinose, arginine, galactose, glucose, glucuronate, lysine, xylose	FEMS Microbiology Letters 8, 105-9 (1980), 9733092, 23066028	
PA14_24790	PA3038	*opdQ, occK6*	benzoate, glucoronate, nitrate, pyroglutamate	22369314, 22272184, 22824298	
PA14_28400	PA2760	*oprQ, occD6*	arginine, dipterpenoids	16352820, 17470813, 26578582	
PA14_29220	PA2700	*opdB, occD7*	arginine, proline	16352820, 26578582	
PA14_32270	PA2505	*opdT, occD4*	tyrosine	16352820	
PA14_32640	no ortholog			This study	similar to *sphA*
PA14_33380	no ortholog			This study	similar to *sphA*
PA14_33410	PA2420	*opdJ, occD8*	arginine, aromatic amino acids	16352820, 17470813, 26578582	
PA14_34960	PA2291	*opbA, oprB2*	glucose	26578582	similar to *oprB*
PA14_36090	PA2213	*opdG, occK9*		26578582	
PA14_37260	PA2113	*opdO, occK3*	benzoate, **cefotaxime**, glucoronate, pyroglutamate	16352820, 22272184, 26578582	
PA14_39000	PA1974			26578582	
PA14_39270	PA1951	*fapF*	amyloid (secretion)	23504942	
PA14_41570	PA1777	*oprF*	non-specific, ferri-siderophores, nitrate, toluene	12408810, 1322882, 1322952, 8611765, 26578582	structural role in outer membrane and link to peptdioglycan
PA14_41750	PA1764	*fadL2*		26578582	similar to *fadL*
PA14_47540	PA1288	*fadL*	fatty acids	23069386	
PA14_51070	PA1025	*opdD, occK7*	benzoate, glucoronate, **meropenem**, pyroglutamate	26578582	
PA14_51880	PA0958	*oprD, occD1*	arginine, arginine-arginine, gluconate, histidine, **imipenem**, lysine, **meropenem**, ornithine	1906263, 2109575, 2118530, 7639767, 8253668, 22272184	

PA14_54520	PA0755	*opdH, occK5*	benzoate, **ceftazidime**, cis-aconitate, glucoronate, pyroglutamate, tricarboxylates, vanillate	16352820, 17114261, 26578582	
PA14_55320	PA0696			9714719	similar to cyanobacterial porin *somB*
PA14_58410	PA4501	*opdP, occD3*	arginine, **doripenem**, glycine-glutamate, **imipenem**, **meropenem**	16352820, 16790014, 28440622, 25910245, 26578582	
PA14_60730	PA4589	*fadL3*		26578582	similar to *fadL*
PA14_64720	PA4898	*opdK, occK1*	adipate, benzoate, caproate, glucoronate, histidine, 4-nitrobenzoate, octanoate, pyroglutamate, vanillate	16352820, 18611376, 22272184, 26578582	
PA14_70300	PA5325	*sphA*	hydrophobic molecules, sphingosine	24465209, 26149193	

Table S2. Secondary mutations in UCPBPP-PA14 Δ40.

	Coordinates	Change	Locus PA14	PAO1 ortholog	Gene Product	Effect	AST* link	Comment
gene loss	2,092,561..2,092,751	Deletion	PA14_24120	PA3094.2	tRNA-Asp	Gene loss	No	Loss of duplicate tRNA gene, identical to adjacent PA14_24130
non-synonymous	252,705	G -> A	PA14_02870	PA0233	probable transcriptional regulator	D16N	No	Non-conserved residue in HTH domain
	6,425,382	G -> A	PA14_72090	PA5461	hypothetical protein	R26H	No	Outside of identified domains
synonymous	2,473,090	C -> T	PA14_28710	PA2739	phenylalanyl-tRNA synthetase, beta subunit	silent change in codon 538	No	
	2,960,130	G -> C	PA14_33610	PA4225	pyochelin synthetase PchF	silent change in codon 1,172	Yes	A transposon mutant has a two-fold increased MIC for ciprofloxacin (ref. 32)
intergenic	1,455,338	A -> G	PA14_16990	PA3662	hypothetical protein	82 bp upstream	No	No motif identified in pseudomonas.com
	4,957,532	A -> G	PA14_55640	PA4281	exonuclease SbcD	318 bp upstream	No	No motif identified in pseudomonas.com
	4,957,549..4,957,550	GC -> AT	PA14_55640	PA4281	exonuclease SbcD	300 bp upstream	No	No motif identified in pseudomonas.com
	5,931,608	(T)6 -> (T)5	PA14_66490	PA1998	transcriptional regulator DhcR	27 bp upstream	No	The mutated position is part of an inverted repeat in PAO1, but the repeat is not conserved in PA14

* Impact of gene inactivation on antimicrobial susceptibility testing

Table S3. Strains and plasmids used in this study.

Strain	Description	Resistance	Reference
E. coli SM10	Cloning strain	KAN	
P. aeruginosa PA14	UCBBP-PA14 clinical strain	None	14983043
PA14 Δ*occD1*	PA14 lacking *occD1 / oprD*	None	This study
PA14 Δ*oprF*	PA14 lacking *oprF*	None	This study
PA14 *oprF K*188*	PA14 with *oprF* truncated after serine 187	None	This study
PA14 *oprF V*315*	PA14 with *oprF* truncated after arginine 314	None	This study
PA14 Δ40	PA14 lacking 40 porin genes	None	This study
PA14 Δ40 / pJBOC-*occD1*	PA14 Δ40 expressing only *occD1* / *oprD*	GEN	This study
PA14 Δ40 / pJBOC-*occD2*	PA14 Δ40 expressing only *occD2* / *opdC*	GEN	This study
PA14 Δ40 / pJBOC-*occD3*	PA14 Δ40 expressing only *occD3* / *opdP*	GEN	This study
PA14 Δ40 / pJBOC-*occD5*	PA14 Δ40 expressing only *occD5* / *opdI*	GEN	This study
PA14 Δ40 / pJBOC-*occD6*	PA14 Δ40 expressing only *occD6* / *oprQ*	GEN	This study
PA14 Δ40 / pJBOC-*occK4*	PA14 Δ40 expressing only *occK4* / *opdL*	GEN	This study
PA14 Δ40 / pJBOC-*occK5*	PA14 Δ40 expressing only *occK5* / *opdH*	GEN	This study
PA14 Δ40 / pJBOC-*occK6*	PA14 Δ40 expressing only *occK6* / *opdQ*	GEN	This study
PA14 Δ40 / pJBOC-*occK7*	PA14 Δ40 expressing only *occK7* / *opdD*	GEN	This study
PA14 Δ40 / pJBOC-*occK8*	PA14 Δ40 expressing only *occK8* / *oprE*	GEN	This study
PA14 Δ40 / pJBOC-*oprG*	PA14 Δ40 expressing only *oprG*	GEN	This study
PA14 Δ40 / pJBOC-*oprO*	PA14 Δ40 expressing only *oprO*	GEN	This study
PA14 Δ40 / pJBOC-*tsx*	PA14 Δ40 expressing only *tsx*	GEN	This study
PA14 Δ40 / pJBOC-*oprB*	PA14 Δ40 expressing only *oprB*	GEN	This study
PA14 Δ40 / pJBOC-*fadL*	PA14 Δ40 expressing only *fadL*	GEN	This study
Plasmid	**Description**	**Resistance**	**Reference**
pAD6	derivative of low copy-number plasmid PK2	AMP	20300602
pEXG2	suicide vector for gene deletion in *P. aeruginosa*	GEN	15911752
pEXG2 Δ*occD1*	suicide vector for deleting *occD1*	GEN	This study
pEXG2 Δ*occD2*	suicide vector for deleting *occD2*	GEN	This study
pEXG2 Δ*occD3*	suicide vector for deleting *occD3*	GEN	This study

pEXG2 Δ*occD4*	suicide vector for deleting *occD4*	GEN	This study
pEXG2 Δ*occD5*	suicide vector for deleting *occD5*	GEN	This study
pEXG2 Δ*occD6*	suicide vector for deleting *occD6*	GEN	This study
pEXG2 Δ*occD7*	suicide vector for deleting *occD7*	GEN	This study
pEXG2 Δ*occD8*	suicide vector for deleting *occD8*	GEN	This study
pEXG2 Δ*occK1*	suicide vector for deleting *occK1*	GEN	This study
pEXG2 Δ*occK2*	suicide vector for deleting *occK2*	GEN	This study
pEXG2 Δ*occK3*	suicide vector for deleting *occK3*	GEN	This study
pEXG2 Δ*occK4*	suicide vector for deleting *occK4*	GEN	This study
pEXG2 Δ*occK5*	suicide vector for deleting *occK5*	GEN	This study
pEXG2 Δ*occK6*	suicide vector for deleting *occK6*	GEN	This study
pEXG2 Δ*occK7*	suicide vector for deleting *occK7*	GEN	This study
pEXG2 Δ*occK8*	suicide vector for deleting *occK8*	GEN	This study
pEXG2 Δ*occK9*	suicide vector for deleting *occK9*	GEN	This study
pEXG2 Δ*occK10*	suicide vector for deleting *occK10*	GEN	This study
pEXG2 Δ*occK11*	suicide vector for deleting *occK11*	GEN	This study
pEXG2 Δ*oprG*	suicide vector for deleting *oprG*	GEN	This study
pEXG2 Δ*oprO*	suicide vector for deleting *oprO*	GEN	This study
pEXG2 Δ*oprP*	suicide vector for deleting *oprP*	GEN	This study
pEXG2 Δ*algE*	suicide vector for deleting *algE*	GEN	This study
pEXG2 Δ*tsx*	suicide vector for deleting *tsx*	GEN	This study
pEXG2 Δ*oprB*	suicide vector for deleting *oprB*	GEN	This study
pEXG2 Δ*oprB2*	suicide vector for deleting *oprB2*	GEN	This study
pEXG2 Δ*oprB3*	suicide vector for deleting *oprB3*	GEN	This study
pEXG2 Δ*fadL*	suicide vector for deleting *fadL*	GEN	This study
pEXG2 Δ*fadL2*	suicide vector for deleting *fadL2*	GEN	This study
pEXG2 Δ*fadL3*	suicide vector for deleting *fadL3*	GEN	This study
pEXG2 Δ*sphA*	suicide vector for deleting *sphA*	GEN	This study
pEXG2 ΔPA14_01770	suicide vector for deleting PA14_01770	GEN	This study
pEXG2 ΔPA14_02890	suicide vector for deleting PA14_02890	GEN	This study
pEXG2 ΔPA14_15280	suicide vector for deleting PA14_15280	GEN	This study
pEXG2 Δ*lptF*	suicide vector for deleting *lptF*	GEN	This study
pEXG2 ΔPA14_32640	suicide vector for deleting PA14_32640	GEN	This study
pEXG2 ΔPA14_33380	suicide vector for deleting PA14_33380	GEN	This study
pEXG2 ΔPA14_39000	suicide vector for deleting PA14_39000	GEN	This study
pEXG2 ΔPA14_39270	suicide vector for deleting PA14_39270	GEN	This study
pEXG2 ΔPA14_55320	suicide vector for deleting PA14_55320	GEN	This study
pEXG2 Δ*oprF*	suicide vector for deleting *oprF*	GEN	This study
pEXG2 Δ*oprF* K188*	suicide vector for truncating *oprF* after codon 187	GEN	This study
pEXG2 Δ*oprF* V314*	suicide vector for truncating *oprF* after codon 314	GEN	This study
pJBOC	very low copy-number plasmid carrying the P_{oprD} promoter	GEN	This study

pJBOC P_{oprD}-*occD1*	*occD1*-expression plasmid	GEN	This study
pJBOC P_{oprD}-*occD2*	*occD2*-expression plasmid	GEN	This study
pJBOC P_{oprD}-*occD3*	*occD3*-expression plasmid	GEN	This study
pJBOC P_{oprD}-*occD5*	*occD5*-expression plasmid	GEN	This study
pJBOC P_{oprD}-*occD6*	*occD6*-expression plasmid	GEN	This study
pJBOC P_{oprD}-*occK4*	*occK4*-expression plasmid	GEN	This study
pJBOC P_{oprD}-*occK5*	*occK5*-expression plasmid	GEN	This study
pJBOC P_{oprD}-*occK6*	*occK6*-expression plasmid	GEN	This study
pJBOC P_{oprD}-*occK7*	*occK7*-expression plasmid	GEN	This study
pJBOC P_{oprD}-*occK8*	*occK8*-expression plasmid	GEN	This study
pJBOC P_{oprD}-*oprG*	*oprG*-expression plasmid	GEN	This study
pJBOC P_{oprD}-*oprO*	*oprO*-expression plasmid	GEN	This study
pJBOC P_{oprD}-*tsx*	*tsx*-expression plasmid	GEN	This study
pJBOC P_{oprD}-*oprB*	*oprB*-expression plasmid	GEN	This study
pJBOC P_{oprD}-*fadL*	*fadL*-expression plasmid	GEN	This study

Table S4. Primers used in this study.

Plasmid	Oligo	template	Sequence of relevant primers (5'-3')
pEXG2	JB-021 pEXG2 fw	pEXG2	ATAGTGAACGGCAGGTAAGC
	JB-022 pEXG2 rv	pEXG2	TCAACGACAGGAGCACGATC
pEXG2 ΔoccD1	JB OprD R1 f	PA14	CCAGTGCCAAGCTTACCGTCATTCATGGACAGC
	JB OprD R1 Rv	PA14	TTTCGTTGCCTGTCGGTCGATGTGATTGCTCCTTTGGTTTTG
	JB OprD R3 f	PA14	AAACCAAAGGAGCAATCACATCGACCGACAGGCAACG
	JB OprD R3 Rv	PA14	GTACCCGGGGATCCGTGTAGAGACCCGAGGCCAG
	JB-005 OprD R1 Fw	PA14	AAGTCGCCGAGCAACAGGGTG
	JB-006 OprD R3 Rv	PA14	CCGGCAGCGTTCATTTCCTCG
pEXG2 ΔoccD2	JB-023 OccD2 R1 f	PA14	tgtaaagcaagcttGAAGAGTCCTCGCTGATGACCAA
	JB-024 OccD2 R1 Rv	PA14	AAGGGCCCAGCGCGCGGGGCTGCGGTTGCTCCTTCTTACA
	JB-025 OccD2 R3 f	PA14	TGTAAGAAGGAGCAACCGCAGCCCCGCGCGCTGGGCCCTT
	JB-026 OccD2 R3 Rv	PA14	gagcccggggatccGCCTGGGTGCAGCTTTCCTACGC
	JB-047 OccD2 R1 check	PA14	CCAGATCCTTGCTGCCGCCATAC
	JB-048 OccD2 R3 check	PA14	ACCGCCCGATTCCCACCCTC
pEXG2 ΔoccD3	JB-027 OccD3 R1 f	PA14	tgtaaagcaagcttCGATGCCGGTGCAGCGTC
	JB-028 OccD3 R1 Rv	PA14	GGCCGCCGGTTGTCGCAGGTCTGATTGCTCCCTTTATTGTTGTCATGGC
	JB-029 OccD3 R3 f	PA14	ACAATAAAGGGAGCAATCAGACCTGCGACAACCGGCGG
	JB-030 OccD3 R3 Rv	PA14	gagcccggggatccCTTGGCGTAGCGCTTGAAGACG
	JB-049 OccD3 R1 check	PA14	TGACGAAACCATCAAGGACG
	JB-050 OccD3 R3 check	PA14	ATGGCGAACACCAGATTGTC
pEXG2 ΔoccD4	JB-031 OccD4 R1 f	PA14	tgtaaagcaagcttTGCCGCCTTCTTCCGCCAGG
	JB-032 OccD4 R1 Rv	PA14	GATGGGGCGGCGGCGCGCCTGGCGATTGCTCCAGATCGGTTCATGTCTG
	JB-033 OccD4 R3 f	PA14	ACCGATCTGGAGCAATCGCCAGGCGCGCCGCCGCCCCATC
	JB-034 OccD4 R3 Rv	PA14	gagcccggggatccTCGCCGGCCATCAGCCGCCAGC
	JB-051 OccD4 R1 check	PA14	GGGCATTGCAGGAGTAAGGTGG
	JB-052 OccD4 R3 check	PA14	CTGTCGTCGGCGTTCAGCAC
pEXG2 ΔoccD5	JB-035 OccD5 R1 f	PA14	tgtaaagcaagcttTATCTCGGCGTGCAGCCGGGCTC
	JB-036 OccD5 R1 Rv	PA14	CAGGTGGGAGAAAACAATAACGCCCCGGGCCGCGGCTC
	JB-037 OccD5 R3 f	PA14	CCGAGCCGCGGCCCGGGGCGTTATTGTTTTCTCCCACCTGAGTGCCAGG
	JB-038 OccD5 R3 Rv	PA14	gagcccggggatccGGACTCCCCCTCCGGCGGCG
	JB-053 OccD5 R1 check	PA14	GCGATCATCGGCAAGTCC
	JB-054 OccD5 R3 check	PA14	GGCCTTGAAGTAGCTGTCCATG
pEXG2 ΔoccD6	JB OprQ R1 f	PA14	AGGTCGACTCTAGACTGCATCATCACCCCGGAAGGC
	JB OprQ R1 Rv	PA14	CAACAACCAGGAACAATAAGTCAAACCTGCGAGCGCGACG
	JB OprQ R3 f	PA14	CGTCGCGCTCGCAGGTTTGACTTATTGTTCCTGGTTGTTGGC
	JB OprQ R3 Rv	PA14	GTACCCGGGGATCCCTCTTCCCTCTTCCTCGCG
	JB-013 OprQ R1 Fw	PA14	GGCAAGTGGGAGGTGAACTACG
	JB-014 OprQ R3 Rv	PA14	ATCGTTCTGCGGCCATCCTC
pEXG2 ΔoccD7	JB-039 OccD7 R1 f	PA14	tgtaaagcaagcttACCGCGCGCACCAACACCGA
	JB-040 OccD7 R1 Rv	PA14	CCTCGCCCGGAGTTTTCCCGCCATGACCGCACCCGCCGCC
	JB-041 OccD7 R3 f	PA14	GGCGGCGGGTGCGGTCATGGCGGGAAAACTCCGGGCGAGGCG
	JB-042 OccD7 R3 Rv	PA14	gagcccggggatccCCGCATGGCCTTCCAGGGCG
	JB-055 OccD7 R1 check	PA14	TTCGCCGCGCACGATCAGG
	JB-056 OccD7 R3 check	PA14	GCGCAACATCGAGCGGGTG
pEXG2 ΔoccD8	JB-043 OccD8 R1 f	PA14	tgtaaagcaagcttTCGCGTGCAGCGCCTG
	JB-044 OccD8 R1 Rv	PA14	AACGACTACGGACCGGACCCACCCACGGAACCAGAAAAAAGAGA
	JB-045 OccD8 R3 f	PA14	TTTTTTCTGGTTCCGTGGGTGGGTCCGGTCCGTAGTCGTT
	JB-046 OccD8 R3 Rv	PA14	gagcccggggatccGTTGCTGATCGACCACCAGAGC
	JB-057 OccD8 R1 check	PA14	GCGCTGATCTGTTTCAACTGG
	JB-058 OccD8 R3 check	PA14	GCCAACTTCAACGGCCAG
pEXG2 ΔoccK1	JB OpdK R1 f	PA14	CCAGTGCCAAGCTTGATGACCTTCAGCAACACCGACAG
	JB OpdK R1 Rv	PA14	AAAAACGGAGCACAATAACACGGACGCTGTCTCGCCGCTC
	JB OpdK R3 f	PA14	GAGCGGCGAGACAGCGTCCGTGTTATTGTGCTCCGTTTTT
	JB OpdK R3 Rv	PA14	GTACCCGGGGATCCCGATCAACCGTATCATCGTC
	JB-103 OccK1 R1	PA14	GCTGGCCTACTTCAACAACAC
	JB-104 OccK1 R3	PA14	CTGGAGCAGGCGGTGAATG
pEXG2 ΔoccK2	JB-059 OccK2 R1 f	PA14	ttccacacattatacgagccggaagcataaatgtaaagcaCTCGCGGTGATCCGCAC
	JB-060 OccK2 R1 Rv	PA14	AAGAACGAAGGGACACTCCCAGCCTACGCGCCGAC
	JB-061 OccK2 R3 f	PA14	ACGGGGTCGGCGCGTAGGCTGGGAGTGTCCCTTCGTTCTTGTTCTCTAGG
	JB-062 OccK2 R3 rv	PA14	ggaaattaattaaggtaccgaattcgagctcgagcccgggAGGAGCCGCCCGC
	JB-105 OccK2 R1	PA14	CCAAGTTCCTTTCCGGTTTC
	JB-106 OccK2 R3	PA14	GTGGCGCAACTACTACAACC

pEXG2 ΔoccK3	JB-063 OccK3 R1 f	PA14	ttccacacattatacgagccggaagcataaatgtaaagcaGGTGGTGCGTCGGCT
	JB-064 OccK3 R1 Rv	PA14	AGGTCATTGCTCGCCGGACCGCTGGGGTTTCCTCGGT
	JB-065 OccK3 R3 f	PA14	TCGACCGAGGAAACCCCAGCGGTCCGGCGAGCAATGAC
	JB-066 OccK3 R3 rv	PA14	ggaaattaattaaggtaccgaattcgagctcgagcccgggGTCTGCGCCTCCAGCG
	JB-107 OccK3 R1	PA14	CCGCCATCCTCTACTCGCTG
	JB-108 OccK3 R3	PA14	GTTGGCTCATGCCGCCTC
pEXG2 ΔoccK4	JB-067 OccK4 R1 f	PA14	ttccacacattatacgagccggaagcataaatgtaaagcaGGCTGCACCCTGCAAC
	JB-068 OccK4 R1 Rv	PA14	AACAACCAAGGGAAGAATCGAGCGCGGCCCCT
	JB-069 OccK4 R3 f	PA14	CGGCCCCAAGGGGCCGCGCTCGATTCTTCCCTTGGTTGTTGTTCTTGTAGG
	JB-070 OccK4 R3 rv	PA14	ggaaattaattaaggtaccgaattcgagctcgagcccgggCACCCTCAGCAGGACCAG
	JB-109 OccK4 R1	PA14	GTTCGGCTACACCCTGCTGC
	JB-110 OccK4 R3	PA14	AACGGATAGAGGTCGCGCAC
pEXG2 ΔoccK5	JB-071 OccK5 R1 f	PA14	ttccacacattatacgagccggaagcataaatgtaaagcaGGGCGATCATCGCTTCCAG
	JB-072 OccK5 R1 Rv	PA14	TGTGGAGTTCTTGTTCTGGCGCAGTGGTCTCCGATTCTTGTT
	JB-073 OccK5 R3 f	PA14	CAAGAATCGGAGACCACTGCGCCAGAACAAGAACTCCACAGG
	JB-074 OccK5 R3 rv	PA14	ggaaattaattaaggtaccgaattcgagctcgagcccgggAGGCGCATGTCGCC
	JB-111 OccK5 R1	PA14	GATCTCGATGGCGTCGGCGCTGG
	JB-112 OccK5 R3	PA14	ACCCGCGAACTACCGGCCAGAC
pEXG2 ΔoccK6	JB-075 OccK6 R1 f	PA14	tatacgagccggaagcataaatgtaaagcaGGGGTCAGCGGGCTG
	JB-076 OccK6 R1 Rv	PA14	GAGGAGACAATAACACGGCAGGCCCCG
	JB-077 OccK6 R3 f	PA14	CGCGGGGCCTGCCGTGTTATTGTCTCCTCGAGCGCTTGGG
	JB-078 OccK6 R3 rv	PA14	taaggtaccgaattcgagctcgagcccgggCGATCGCATCCTGCTGTCC
	JB-015 OpdQ R1 Fw	PA14	CGTCGAGCATCCCGTTCCTG
	JB-016 OpdQ R3 Rv	PA14	TCGCTTACCAGAAAGTCGTCC
pEXG2 ΔoccK7	JB-079 OccK7 R1 f	PA14	ttccacacattatacgagccggaagcataaatgtaaagcaTACCTGGCCGCCGG
	JB-080 OccK7 R1 Rv	PA14	ACGACGAAGAGACAACAACAAGCGGACTTGAGTTTCCCG
	JB-081 OccK7 R3 f	PA14	TCGGGAAACTCAAGTCCGCTTGTTGTTGTCTCTTCGTCGTCAGTGGATAGACAC
	JB-082 OccK7 R3 rv	PA14	ggaaattaattaaggtaccgaattcgagctcgagcccgggCCACAAGTGCACCGCC
	JB-113 OccK7 R1	PA14	GAAGAGAACGTCGCCGAGAAC
	JB-114 OccK7 R3	PA14	CGTGCAGCCATCATCGAGG
pEXG2 ΔoccK8	JB OprE R1 f	PA14	CCAGTGCCAAGCTTGAGGGGCTCGGTGCCCTCTAC
	JB OprE R1 Rv	PA14	TTCCATGCCTGGCCGGCGCCTGGTCTTTTCCCCATTGGTATTGC
	JB OprE R3 f	PA14	TACCAATGGGGAAAAGACCAGGCGCCGGCCAGGCATGGAAAAG
	JB OprE R3 Rv	PA14	GTACCCGGGGATCCATCACCACCGAGGAATGCCTGCTC
	JB-007 OprE R1 Fw	PA14	TTCCAGGAGGGCGAACAAAG
	JB-008 OprE R3 Rv	PA14	GCTACCGCACCGACGACTTC
pEXG2 ΔoccK9	JB-083 OccK9 R1 f	PA14	ttccacacattatacgagccggaagcataaatgtaaagcaTGGAACTCCAGCAGCCAG
	JB-084 OccK9 R1 Rv	PA14	TGGGAAAAGGAAAAACAACAGCGCAGGGCCGT
	JB-085 OccK9 R3 f	PA14	CAGCGAGAACGGCCCTGCGCTGTTGTTTTTCCTTTTCCCAGGCCGAAGC
	JB-086 OccK9 R3 rv	PA14	ggaaattaattaaggtaccgaattcgagctcgagcccgggGACGACCTCTGGACCTCGCG
	JB-115 OccK9 R1	PA14	AGGCCCTCGGTGACGAACAG
	JB-116 OccK9 R3	PA14	GTTGCACTGGTTCGCCGAGC
pEXG2 ΔoccK10	JB-087 OccK10 R1 f	PA14	ttccacacattatacgagccggaagcataaatgtaaagcaCTGGGACTTCACCCGCC
	JB-088 OccK10 R1 Rv	PA14	CCGCTGTCGAGAGTCACCGCGCCGTCGCGCCGGAACG
	JB-089 OccK10 R3 f	PA14	GTGCGTTCCGGCGCGACGGCGCGGTGACTCTCGACAGCGGG
	JB-090 OccK10 R3 rv	PA14	ggaaattaattaaggtaccgaattcgagctcgagcccgggCTTCCAGGTGGACGAGCC
	JB-117 OccK10 R1	PA14	GCGACATCGCCAACGCCATC
	JB-118 OccK10 R3	PA14	ATGCTCGACCTCGCCCGAC
pEXG2 ΔoccK11	JB-091 OccK11 R1 f	PA14	ttccacacattatacgagccggaagcataaatgtaaagcaTCCCAGGCGCGCTAC
	JB-092 OccK11 R1 Rv	PA14	GCCGCCAAGGGCTGAGCGGCACGCACTCCGAACGGG
	JB-093 OccK11 R3 f	PA14	GGCGCCCGTTCGGAGTGCGTGCCGCTCAGCCCTTGG
	JB-094 OccK11 R3 rv	PA14	ggaaattaattaaggtaccgaattcgagctcgagcccgggTGCGCACCGCCGAGC
	JB-119 OccK11 R1	PA14	GAGACCGGCGACAACGTGG
	JB-120 OccK11 R3	PA14	AGCCGGTACGCTTCACCAG
pEXG2 ΔoprG	JB OprG R1 f	PA14	CCAGTGCCAAGCTTATTTCCTGGTCCAGGCGCTG
	JB OprG R1 Rv	PA14	TACAAGGAATGGAGCTCATCGTCGTAGACTGTCGCGGGGC
	JB OprG R3 f	PA14	GCCCCGCGACAGTCTACGACGATGAGCTCCATTCCTTGTATTAG
	JB OprG R3 Rv	PA14	GTACCCGGGGATCCTGTCGATCCGCCTATGAC
	JB-011 OprG R1 Fw	PA14	AGACCCGCGACTTCATCTAC
	JB-012 OprG R3 Rv	PA14	CTATGAGTGGAGCCTGCTCG
pEXG2 ΔoprO	JB-298 OprO R1 F	PA14	ttccacacattatacgagccggaagcataaatgtaaagcaAGCTTGGCCACCATCGA
	JB-299 OprO R1 R	PA14	gagcagatcgttgtcgcttccgaagatttccc
	JB-300 OprO R3 F	PA14	ccattaaggggaaatcttcggaagcgacaacg
	JB-301 OprO R3 R	PA14	ggaaattaattaaggtaccgaattcgagctcgagcccggggatccGTATTGCCGTTG
	JB-306 OprO F	PA14	gcgcctgtacctggcgccgg
	JB-307 OprO R	PA14	agtcacggtagacggtgccgcc
pEXG2 ΔoprP	JB-302 OprP R1 F	PA14	ttccacacattatacgagccggaagcataaatgtaaagcaAGCTTTCTACCCATATC

	JB-303 OprP R1 R	PA14	ccggacggggcccgagcgcccaggtaagtccc
	JB-304 OprP R3 F	PA14	ccgaacaggggacttacctgggcgctcgggcc
	JB-305 OprP R3 R	PA14	ggaaattaattaaggtaccgaattcgagctcgagcccggggatccTTCGTTGACGTC
	JB-308 OprP F	PA14	cggcgccggcaagtggctt
	JB-309 OprP R	PA14	acgctgggtgaagccatcgccac
pEXG2 ΔalgE	JB-292 AlgE R1 F	PA14	ttccacacattatacgagccggaagcataaatgtaaagcaAGCTTCAGGCCGGCTCC
	JB-293 AlgE R1 R	PA14	gaagaagagccagaaagcctgccccgcgagga
	JB-294 AlgE R3 F	PA14	gtccggtttcctcgcggggcaggctttctggc
	JB-295 AlgE R3 R	PA14	ggaaattaattaaggtaccgaattcgagctcgagcccggggatccGGGTCGACTCGG
	JB-296 AlgE F	PA14	tacacctcggcgccgcccca
	JB-297 AlgE R	PA14	agaaggccctgctcgaacag
pEXG2 Δtsx	JB-127 TsX R1 F	PA14	ttccacacattatacgagccggaagcataaatgtaaagcaGCACCGATTCGCAGATCG
	JB-128 TsX R1 Rv	PA14	GGCAGCCCCGCGCGACGGACTGAAACGCTCCTGGAGTGAATAGCTTTTTTTCTAGTGG
	JB-129 TsX R3 F	PA14	TTCACTCCAGGAGCGTTTCAGTCCGTCGCGCGG
	JB-130 TsX R3 Rv	PA14	ggaaattaattaaggtaccgaattcgagctcgagcccgggGACGATGCCGGTGACCAG
	JB-131 TsX R1	PA14	CGGCCAGATCGTCCTGC
	JB-132 TsX R3	PA14	GCCGAGGTCGGTGATGC
pEXG2 ΔoprB	JB-172 OprB R1 f	PA14	ttccacacattatacgagccggaagcataaatgtaaagcaagcttAAGCTGCGGGTGGAAATGCG
	JB OprB R1 Rv	PA14	CGGAGCAGGCAACGCGACGGTTCCAGCGTCCTCGTGGTTG
	JB OprB R3 f	PA14	CAACCACGAGGACGCTGGAACCGTCGCGTTGCCTGCTCCG
	JB-173 OprB R3 Rv	PA14	ggaaattaattaaggtaccgaattcgagctcgagcccggggatccGGGCTGCAGGGCGAAGCTG
	JB-095 OprB R1	PA14	GCGGCCCAAGGTCTACCTG
	JB-096 OprB R3	PA14	CTCCAGCTCCATGCCGTGC
pEXG2 ΔoprB2	JB-174 OprB2 R1 f	PA14	ttccacacattatacgagccggaagcataaatgtaaagcaagcttGCGGGTCGCCGAAGGCGAC
	JB OprB2 R1 Rv	PA14	CGGTTGTCCGAAGCAACAGCGCGAACGCTTCCTCGTTGCGAATGG
	JB OprB2 R3 f	PA14	CGCAACGAGGAAGCGTTCGCGCTGTTGCTTCGGACAACCGC
	JB-175 OprB2 R3 Rv	PA14	ggaaattaattaaggtaccgaattcgagctcgagcccggggatccAGTAGCGGTCGCCGAACTCGGTG
	JB-097 OprB2 R1	PA14	GCCATCCCATCGGCAACCTG
	JB-098 OprB2 R3	PA14	GTACGGATGCGCCAGGCTTC
pEXG2 ΔoprB3	JB-166 OprB3 R1 f	PA14	ggaagcataaatgtaaagcaagcttGAAGTCGGCGTTGTACGGC
	JB-167 OprB3 R1 Rv	PA14	GCCTTGCCCGCGCCACCTGGCA
	JB-168 OprB3 R3 f	PA14	TGGCGCGGGCAAGGCACTCGTCTTG
	JB-169 OprB3 R3 Rv	PA14	gagctcgagcccggggatccCGTCGCCCTCGGCC
	JB-099 OprB3 R1	PA14	GTTCGCCGTTGACCTGGGTG
	JB-100 OprB3 R3	PA14	AGCAGGTGCTGGTCACTGG
pEXG2 ΔfadL	JB FadL R1 f	PA14	CCAGTGCCAAGCTTTTGCGCGAGGCCGTCATG
	JB FadL R1 Rv	PA14	TTTTTCGTTGGCGCGTGCGATGTTGGAGCAACTCCTGTGTATAACGG
	JB FadL R3 f	PA14	ACACAGGAGTTGCTCCAACATCGCACGCGCCAACGAAAAAG
	JB FadL R3 Rv	PA14	GTACCCGGGGATCCGCTGCTGGAACTGGGCATGG
	JB-017 FadL R1 Fw	PA14	GGGCCATCGGAATAGAAGCTGC
	JB-018 FadL R3 Rv	PA14	CTGCTGGGACTCGCCTGGTG
pEXG2 ΔfadL2	JB-121 FadL2 R1 F	PA14	ttccacacattatacgagccggaagcataaatgtaaagcaTTGCAGGTCCTGGTAGAGATCG
	JB-122 FadL2 R1 Rv	PA14	ACCCGCGAGCGAGGCCTGTTGGGCTGGAGCATGATGCG
	JB-123 FadL2 R3 F	PA14	CGCGCATCATGCTCCAGCCCAACAGGCCTCGCTCGCGG
	JB-124 FadL2 R3 Rv	PA14	ggaaattaattaaggtaccgaattcgagctcgagcccgggTTCGACTACGGGATCTGGGACAAC
	JB-125 FadL2 R1	PA14	TCGGCATCCAGTTCGGTGAAATC
	JB-126 FadL2 R3	PA14	AAGACCAGCGGCGGCAC
pEXG2 ΔfadL3	JB FadL3 R1 f	PA14	CCAGTGCCAAGCTTGCCCTTCGGATCGAAGTCGGAG
	JB FadL3 R1 Rv	PA14	GCCTGTTTGCCAGAAAACCAACCCGGCCGTAGGCAGAGAAAG
	JB FadL3 R3 f	PA14	TTCTCTGCCTACGGCCGGGTTGGTTTTCTGGCAAACAGGC
	JB FadL3 R3 Rv	PA14	GTACCCGGGGATCCCTGAGCGTTTCGTCCATGGC
	JB-101 FadL3 R1	PA14	CGGTACAGCTCGCTCATG
	JB-102 FadL3 R3	PA14	GCCAACTCACTGGAAGGATAC
pEXG2 ΔsphA	JB-330 PA14_70300 R1 Fw	PA14	ttccacacattatacgagccggaagcataaatgtaaagcaagcttacaccagcaggctggcgaagaactcctcga
	JB-331 PA14_70300 R1 Rv	PA14	tgccgcttcgttccgatgccgggcgggctcttattattgtttgg
	JB-332 PA14_70300 R3 Fw	PA14	acaataataagagcccgcccggcatcggaacgaagcgg
	JB-333 PA14_70300 R3 Rv	PA14	ggaaattaattaaggtaccgaattcgagctcgagcccggggatccatgggctacgacccct
	JB-334 PA14_70300 R1 check	PA14	agcggcatggatgagttcgatg
	JB-335 PA14_70300 R3 check	PA14	ctgggtgaattgctggcgct
pEXG2 ΔPA14_01770	JB-492 PA14_01770 R1F	PA14	ttccacacattatacgagccggaagcataaatgtaaagcaagcttGCCGCTGGCCGAAGGCAAC
	JB-493 PA14_01770 R1R	PA14	TTCCCATGCGCAAAGCCCTGGGCTACGCGTTCTGAGCG
	JB-494 PA14_01770 R3F	PA14	CGCGCTCAGAACGCGTAGCCCAGGGCTTTGCGCATGGGAAGTCCT

	JB-495 PA14_01770 R3R	PA14	ggaaattaattaaggtaccgaattcgagctcgagcccggggatccCCGGCATCCTGGGGGGA
	JB-496 PA14_01770 R1 check	PA14	CCGCCGACGTACACGGCA
	JB-497 PA14_01770 R3 check	PA14	CCTGGCATGTCGCTTGCTG
pEXG2 ΔPA14_02890	JB-318 PA14_02890 R1 Fw	PA14	ttccacacattatacgagccggaagcataaatgtaaagcaagcttggcgcggtcgacct
	JB-319 PA14_02890 R1 Rv	PA14	tagggcggcggcgcatcgccgctgtgtgtcct
	JB-320 PA14_02890 R3 Fw	PA14	caaccagcaggacacacagcggcgatgcgccgc
	JB-321 PA14_02890 R3 Rv	PA14	ggaaattaattaaggtaccgaattcgagctcgagcccggggatcccgccggcaccctgct
	JB-322 PA14_02890 R1 check	PA14	cggacatcaccgtcggcgtcacc
	JB-323 PA14_02890 R3 check	PA14	agcagacggtgcaggcccgc
pEXG2 ΔPA14_15280	JB-498 PA14_15280 R1F	PA14	ttccacacattatacgagccggaagcataaatgtaaagcaagcttTGATATAGAAGGTGAGCACGGCGAGG
	JB-499 PA14_15280 R1R	PA14	GTCACATGACCCACCGCACCGTCCATGTGTTCTGAGGAGGCG
	JB-500 PA14_15280 R3F	PA14	CCTCCTCAGAACACATGGACGGTGCGGTGGGTCA
	JB-501 PA14_15280 R3R	PA14	ggaaattaattaaggtaccgaattcgagctcgagcccggggatccTCGCCCTCTATCGCACGC
	JB-502 PA14_15280 R1 check	PA14	ACCGATCCCCGCGCC
	JB-503 PA14_15280 R3 check	PA14	GACATCGGTGAGCTGCTCTGC
pEXG2 ΔPA14_16630	JB-360 PA14_16630 R1 Fw	PA14	ttccacacattatacgagccggaagcataaatgtaaagcaagctttggtgctgttcgacaccgagcagaaggg
	JB-361 PA14_16630 R1 Rv	PA14	cgtgattaaggatgacccctaagccctacggaagcccaaaag
	JB-362 PA14_16330 R3 Fw	PA14	ttgggcttccgtagggcttaaggggtcatccttaatcacgaat
	JB-363 PA14_16630 R3 Rv	PA14	ggaaattaattaaggtaccgaattcgagctcgagcccggggatccacggcgttccgcgaccacgccgg
	JB-364 PA14_16630 R1 check	PA14	gtgaagctgtccctggagcc
	JB-365 PA14_16630 R3 check	PA14	ccgtggttgcccgcttca
pEXG2 ΔPA14_32640	JB-504 PA14_32640 R1F	PA14	ttccacacattatacgagccggaagcataaatgtaaagcaagcttCCGGGCAGATCAACCGC
	JB-505 PA14_32640 R1R	PA14	CGCCCATGACCACCCGCATCCGCTACTCGCAGGTCTTCTG
	JB-506 PA14_32640 R3F	PA14	CAGAAGACCTGCGAGTAGCGGATGCGGGTGGTCAT
	JB-507 PA14_32640 R3R	PA14	ggaaattaattaaggtaccgaattcgagctcgagcccggggatccTGCAGCTCTACAGCTTCTTCAACAG
	JB-508 PA14_32640 R1 check	PA14	GCAACTGCTGCCCTGGGG
	JB-509 PA14_32640 R3 check	PA14	CCGGGCCAGGCCTTCTT
pEXG2 ΔPA14_33380	JB-510 PA14_33380 R1F	PA14	ttccacacattatacgagccggaagcataaatgtaaagcaagcttCTGGTTTGTGGTTAGCGGGT
	JB-511 PA14_33380 R1R	PA14	CCCTCATGCGTGCAGCCCTGCTGCTGGCGTTCTGAATCGG
	JB-512 PA14_33380 R3F	PA14	CCGATTCAGAACGCCAGCAGCAGGGCTGCACG
	JB-513 PA14_33380 R3R	PA14	ggaaattaattaaggtaccgaattcgagctcgagcccggggatccGCCGATGACCGAACTGCG
	JB-514 PA14_33380 R1 check	PA14	GACGATTCTGTTACCTCGGGGTTGGA
	JB-515 PA14_33380 R3 check	PA14	ACGCCGCCATGTTGCTGATC
pEXG2 ΔPA14_39000	JB-324 PA14_39000 R1 Fw	PA14	ttccacacattatacgagccggaagcataaatgtaaagcaagcttccagccaggtgttgaccag
	JB-325 PA14_39000 R1 Rv	PA14	ttcacctcgcggagtgcgcctaccgctactttcgaaggaccccg
	JB-326 PA14_39000 R3 Fw	PA14	gtccttcgaaagtagcggtaggcgcactccgcg
	JB-327 PA14_39000 R3 Rv	PA14	ggaaattaattaaggtaccgaattcgagctcgagcccggggatccgcctgcacgaaccgg
	JB-328 PA14_39000 R1 Check	PA14	gcgggtcaccaccaacttttcg
	JB-329 PA14_39000 R3 check	PA14	tgttctgtccgctgccctcg
pEXG2 ΔPA14_39270	JB-516 PA14_39270 R1F	PA14	ttccacacattatacgagccggaagcataaatgtaaagcaagcttGTTGCGCGGGCGCTAC
	JB-517 PA14_39270 R1R	PA14	GCCCCTCAGAAGTAGTAGGGGAGTGTCTGGGTCATGTTTGCC
	JB-518 PA14_39270 R3F	PA14	CAAACATGACCCAGACACTCCCCTACTACTTCTGAGGGGC
	JB-519 PA14_39270 R1F	PA14	ggaaattaattaaggtaccgaattcgagctcgagcccggggatccCACGAACACTTGCTGGAGC
	JB-520 PA14_39270 R1 check	PA14	CCGCCAGCGACCTCTTCG
	JB-521 PA14_39270 R3 check	PA14	ACGCCATCGTCATCGTCGC

pEXG2 ΔPA14_55320	JB-366 PA14_55320 R1 Fw	PA14	ttccacacattatacgagccggaagcataaatgtaaagcaagcttatttcactgggcgagcgc
	JB-367 PA14_55320 R1 Rv	PA14	accttaggagccgtacacaggcgctcctcgaggcag
	JB-368 PA14_55320 R3 Fw	PA14	tggtctgcctcgaggagcgcctgtgtacggctcctaaggtcct
	JB-369 PA14_55320 R3 Rv	PA14	ggaaattaattaaggtaccgaattcgagctcgagcccggggatccgcgctgctgctcgccggc
	JB-370 PA14_55320 R1 check	PA14	gacggaaaggtgttcgatcaggg
	JB-371 PA14_55320 R3 check	PA14	ctgtccatcgacggccaccc
pEXG2 ΔoprF	JB OprF R1 f	PA14	CCAGTGCCAAGCTTATTTGGTCAACCCGAGCATACTGG
	JB OprF R1 Rv	PA14	TCAAGATGGGGATTTAACGGTCGGCTGAGCCTCTAAGGAAAAAC
	JB OprF R3 f	PA14	TTCCTTAGAGGCTCAGCCGACCGTTAAATCCCCATCTTGATGG
	JB OprF R3 Rv	PA14	GTACCCGGGGATCCCTTGAATAAGCCTCACCCCCTG
	JB-009 OprF R1 Fw	PA14	TTGACCCTGAAGGCAGTTCG
	JB-010 OprF R3 Rv	PA14	TAATGGACGTGGCTGCTCTG
pEXG2 oprF187t	JB-282a OprF 187t F	PA14	ggaaattaattaaggtaccgaattcgagctcgagcccggggatccCGAAAAGTTTTCAGATGCGA
	JB-283 OprF 187t R	PA14	AGCCGGGTTTTTCCTTAGAGGCTCAGCCGATTACGAACCACCGAAGTTGAAGCC
pEXG2 oprF314t	JB-284a OprF 314t F	PA14	ggaaattaattaaggtaccgaattcgagctcgagcccggggatccCGAAACCGGCAACAAGAAGG
	JB-285 OprF 314t R	PA14	CCTGAGCCGGGTTTTTCCTTAGAGGCTCAGCCGATTAGCGACCACCTTCTACACCGTAC
pJBOC	oJBOC-001	pOPC	cgccgttggatacaccaaggggttctgcttcggca
	oJBOC-002	pOPC	cccctcaagtgtcaatgaaagtttccaacgcgagccattcTCAGTGAAGCATCAAGACTAACAAATCGTATAATCC
	oJBOC-003	pEXG2	ttgtctgccgaagcagaaccccttggtgtatccaacggc
	oJBOC-004	pEXG2	ATTGCAAACGCTAGGGCCTTGTGTCGAGGTCCCAATACGCgctagcttattacgcgtaattctcgaattg
	oJBOC-005	pAD6	gaatggctcgcgttggaaactt
	oJBOC-006	pAD6	GCGTATTGGGACCTCGACACA
	JB-462 Stop pOprD	PA14	TTCTTAAATCTAGAGGATCctcatgcggaaaccgccagtgca
	oJBOC-036	PA14	gagccattcTCAGTGAAGCATCAAGACTAACAAATCctacgccccataagatgccggt
	oJBOC-045	pJBOC	tgaaagtttccaacgcgagccattcTCAGT
	oJBOC-046	pJBOC	GCGCTACTGCCGCCAGGC
	oJBOC-038	pJBOC	GAATTAGCTTGGCTGTTTTGGCGG
	oJBOC-057	pJBOC	ATGTATATCTCCTTCTTAAATCTAGAGGATCctca
pPoprD-occD1	JB-464 OccD1 Fw	PA14	ccgcatgagGATCCTCTAGATTTAAGAAGGAGATATACATAATGAAAGTGATGAAGTGGAGCGC
	JB-465 OccD1 Rv	PA14	GAAAATCTTCTCTCATCCGCCAAAACAGCCAAGCTAATTCTTACAGGATCGACAGCGGATAGTCG
pPoprD-occD2	JB-176 OccD2 f	PA14	tttccgcagGATCCTCTAGATTTAAGAAGGAGATATACATatgaggaatctgttcgccttgacgccg
	JB-177 OccD2 Rv	PA14	GAAAATCTTCTCTCATCCGCCAAAACAGCCAAGCTAATTCtcagaacacgtcgatgggg
pPoprD-occD3	JB-178 OccD3 f	PA14	tttccgcagGATCCTCTAGATTTAAGAAGGAGATATACATtcaggtgatgagataccaacgagtgacc
	JB-179 OccD3 Rv	PA14	GAAAATCTTCTCTCATCCGCCAAAACAGCCAAGCTAATTCgtttacagcaggttgaaggggaag
pPoprD-occD5	JB-182 OccD5 f	PA14	GAAAATCTTCTCTCATCCGCCAAAACAGCCAAGCTAATTCtcaccagatcgagcgggagt
	JB-183 OccD5 Rv	PA14	tttccgcagGATCCTCTAGATTTAAGAAGGAGATATACATatgcaaaatctcagacgcgc
pPoprD-occD6	JB-466 OccD6 fw	PA14	GAAAATCTTCTCTCATCCGCCAAAACAGCCAAGCTAATTCTCAGAACACGCTGAACGGGTACT
	JB-467 OccD6 Rv	PA14	ccgcatgagGATCCTCTAGATTTAAGAAGGAGATATACATATGTTGAAGAAAAGGATTTGCCTGCT
pPoprD-occK4	JB-196 OccK4 f	PA14	GAAAATCTTCTCTCATCCGCCAAAACAGCCAAGCTAATTCtcaccagagctttagcgtgtaattgacgatgaag
	JB-197 OccK4 Rv	PA14	tttccgcagGATCCTCTAGATTTAAGAAGGAGATATACATatgatcacggcatgcccc
pPoprD-occK5	JB-198 OccK5 f	PA14	tttccgcagGATCCTCTAGATTTAAGAAGGAGATATACATatgtcgacttccctgccgc
	JB-199 OccK5 Rv	PA14	GAAAATCTTCTCTCATCCGCCAAAACAGCCAAGCTAATTCttaccagatcggcagggtatagct
pPoprD-occK6	JB-478 OccK6 Fw	PA14	ccgcatgagGATCCTCTAGATTTAAGAAGGAGATATACATATGAGCATGACCCCGATCG
	JB-479 OccK6 Rv	PA14	GAAAATCTTCTCTCATCCGCCAAAACAGCCAAGCTAATTCTTACCAGAGCGGCAGCGTGTA
pPoprD-occK7	JB-202 OccK7 f	PA14	GAAAATCTTCTCTCATCCGCCAAAACAGCCAAGCTAATTCtcaccacagcggcaacgc
	JB-203 OccK7 Rv	PA14	tttccgcagGATCCTCTAGATTTAAGAAGGAGATATACATatgaaaattcttcccgttccgatgc
pPoprD-occK8	JB-474 OccK8 Fw	PA14	ccgcatgagGATCCTCTAGATTTAAGAAGGAGATATACATATGAAGAGTCGCAAGATCAACAAGTC
	JB-475 OccK8 Rv	PA14	GAAAATCTTCTCTCATCCGCCAAAACAGCCAAGCTAATTCTTACAGCAGCGGCAGGG
pPoprD-oprG	JB-470 OprG Fw	PA14	ccgcatgagGATCCTCTAGATTTAAGAAGGAGATATACATATGCGTAAGTCCTGGCTTACC
	JB-471 OprG Rv	PA14	GAAAATCTTCTCTCATCCGCCAAAACAGCCAAGCTAATTCTCAGAACTTGTAGCCGAAACCGA
pPoprD-oprO	JB-220 OprO f	PA14	tttccgcagGATCCTCTAGATTTAAGAAGGAGATATACATatgatccgtaagcactcgct
	JB-221 OprO Rv	PA14	GAAAATCTTCTCTCATCCGCCAAAACAGCCAAGCTAATTCttagaacacgtactgcaaacggg
pPoprD-tsx	JB-468 Tsx Fw	PA14	ccgcatgagGATCCTCTAGATTTAAGAAGGAGATATACATATGAGCCGCACACTCGC
	JB-469 Tsx Rv	PA14	GAAAATCTTCTCTCATCCGCCAAAACAGCCAAGCTAATTCTCAGAAGTGGTACTTGACCAGGAAG
pPoprD-oprB	JB-224 OprB f	PA14	tttccgcagGATCCTCTAGATTTAAGAAGGAGATATACATatgtacaagaacaagaaaaccagaccg
	JB-225 OprB Rv	PA14	GAAAATCTTCTCTCATCCGCCAAAACAGCCAAGCTAATTCtcagaacaccgtctggatcttgatcc
pPoprD-fadL	JB-476 FadL Fw	PA14	ccgcatgagGATCCTCTAGATTTAAGAAGGAGATATACATATGAAAACAATATGGTTTAAAACCTCTCTCG
	JB-477 FadL Rv	PA14	GAAAATCTTCTCTCATCCGCCAAAACAGCCAAGCTAATTCTCAGAAGCGATAGGTGACCTGGG

SI References

1. Breidenstein EB, Khaira BK, Wiegand I, Overhage J, & Hancock RE (2008) Complex ciprofloxacin resistome revealed by screening a *Pseudomonas aeruginosa* mutant library for altered susceptibility. *Antimicrob Agents Chemother* 52(12):4486-4491.

Acknowledgements

I am very grateful for the opportunity to accomplish my PhD under the supervision of Prof. Dr. Sebastian Hiller. I consider myself as very lucky being able to work on such an interesting and challenging project with the coolest method ever! I appreciate the confidence and trust you had in me by giving me so much freedom in my research projects and by offering all those numerous possibilities I got to deepen my knowledge and skills. I grew tremendously as a researcher but also as a human being, and I wouldn't want to miss these experiences.

I want to thank Prof. Dr. Anne Spang for the kindness of reading and evaluating my thesis, as well as for taking actively part in my PhD committee with very valuable contributions.

I dearly appreciate the close collaboration with Guillaume who taught me the insights of good science. Your patient and kind guidance allowed me to progress with my project, your ideas complemented mine.

During my second project I had the pleasure to work with Prof. Dr. Dirk Bumann on a very exciting topic. It was a very fruitful experience and I will miss the welcoming and enriching time I spent working together with Vish and Sandra.

I would like to express my special thanks to Prof. Dr. Daniel Häussinger for providing his NMR equipment, but moreover for his kind and very helpful support with spectra analysis.

My sincere thanks also go to Dr. Timothy Sharpe whose experience with biophysical experiments was indispensable for the success of my experiments.

Many thanks go to all members of the Hiller group. I enjoyed my time with you and I will never forget the support you gave me in hard times and the laughter in fun times.

My special thanks go to Bastian, who always had an open ear for my questions and even better, most of the times a very good answer. I am dearly grateful for having shared so much

lab time with you, Chris. You showed me the many parallel universes around us and brought back faith into mine. Hundeep, you were a great lab companion, perfect for both, scientific discussions as well as the bestest chocolate breaks. You always motivated me to do better and. Joka, it was great having you as my PhD companion, I hope you never lose this strength I admire you for. Thomas was the best python teacher one could imagine, I would have lost patience with myself, but you made everything fun and easy for me. Your NMR spectroscopic experience helped me several times to tame stormy spectra and jelly samples and you are a great office neighbor!

My parents and my sister are the best family one could wish for. I am so grateful for everything you made possible in my life. Without you I never would be where I am now. I am so happy that your door was always open to offer me a sweet home whenever I needed it. After all, not for nothing, I named the cryoprobe of our 700 MHz magnet after my sister Stella.

Without my sweet, kind, great and wonderful friends all this work would never have been possible. I am the happiest person on earth to have you, Katerina, Cora, Maryam, Hundeep and Daniel and I will always appreciate your encouragement to believe in myself.
Thank you, Elisabeth and Rosalie for being such fantastic flat mates. It was and still is a pleasure living with you and sharing the work happiness and suffering with you. Who could understand better the ups and downs of a PhD?

My life without skiing and the mountains is unthinkable, therefore I want to express my deep happiness about having shared so many trips to the mountains with Andi and Johannes. These experiences shaped me as the human being I am and not infrequently, the discussion we had on a skitour contributed to the scientific progress of my projects.

Last but not least I want to thank Leopold for all the delicious food he prepared without any complaint ever.

References

1. Moser E, Laistler E, Schmitt F, Kontaxis G. Ultra-high field NMR and MRI-the role of magnet technology to increase sensitivity and specificity. *Front Phys*. 2017;5(AUG):1-15. doi:10.3389/fphy.2017.00033

2. Flynn PF, Mattiello DL, Hill HDW, Wand AJ. Optimal use of cryogenic probe technology in NMR studies of proteins. *J Am Chem Soc*. 2000;122(19):4823-4824. doi:10.1021/ja993743x

3. Liu M, Mao XA, Ye C, Huang H, Nicholson JK, Lindon JC. Improved Watergate Pulse Sequences for Solvent Suppression in NMR Spectroscopy. *J Magn Reson*. 1998;132(1):125-129. doi:10.1006/jmre.1998.1405

4. Roumestand C, Canet D. Extending the Excitation Sculpting Concept for Selective Excitation. *J Magn Reson*. 2000;147(2):331-339. doi:10.1006/jmre.2000.2206

5. Wider G. Technical aspects of NMR Spectroscopy with biological macromolecules and studies of hydration in solution. *Prog Nucl Magn Reson Spectrosc*. 1998;32(3):193-275. doi:10.1016/S0079-6565(98)00014-4

6. Mori S. Improved Sensitivity of HSQC Spectra of Exchanging Protons at Short Interscan Delays Using a New Fast HSQC (FHSQC) Detection Scheme That Avoids Water Saturation. *Jorunal Magn Reson*. 1995;108(1):94-98.

7. O'Connell MR, Gamsjaeger R, Mackay JP. The structural analysis of protein-protein interactions by NMR spectroscopy. *Proteomics*. 2009;9(23):5224-5232. doi:10.1002/pmic.200900303

8. Williamson MP. Using chemical shift perturbation to characterise ligand binding. *Prog Nucl Magn Reson Spectrosc*. 2013;73:1-16. doi:10.1016/j.pnmrs.2013.02.001

9. Clore GM, Gronenborn AM. Two-, three-, and four-dimensional NMR methods for obtaining larger and more precise three-dimensional structures of proteins in solution. *Annu Rev Biophys Biophys Chem*. 1991;20:29-63. doi:10.1146/annurev.bb.20.060191.000333

10. Weisemann R, Rüterjans H, Bermel W. 3D Triple-resonance NMR techniques for the

sequential assignment of NH and 15N resonances in 15N- and 13C-labelled proteins. *J Biomol NMR*. 1993;3(1):113-120. doi:10.1007/BF00242479

11. Mielke SP, Krishnan V V. Characterization of protein secondary structure from NMR chemical shifts. *Prog Nucl Magn Reson Spectrosc*. 2009;54(3-4):141-165. doi:10.1016/j.pnmrs.2008.06.002

12. Schwarzinger S, Kroon GJA, Foss TR, Chung J, Wright PE, Dyson HJ. Sequence-dependent correction of random coil NMR chemical shifts. *J Am Chem Soc*. 2001;123(13):2970-2978. doi:10.1021/ja003760i

13. Neuhaus D, Van Mierlo CPM. Measurement of Heteronuclear NOE Enhancements in Biological Macromolecules. *J Magn Reson*. 1992;100:221-228.

14. Kumar A, Ernst RR, Wüthrich K. A two-dimensional nuclear Overhauser enhancement (2D NOE) experiment for the elucidation of complete proton-proton cross-relaxation networks in biological macromolecules. *Biochem Biophys Res Commun*. 1980;95(1):1-6.

15. Marion D, Driscoll PC, Kay LE, et al. Overcoming the Overlap Problem in the Assignment of 1H NMR Spectra of Larger Proteins by Use of Three-Dimensional Heteronuclear 1H-15N Hartmann-Hahn-Multiple Quantum Coherence and Nuclear Overhauser-Multiple Quantum Coherence Spectroscopy: Application to Interleukin 1β. *Biochemistry*. 1989;28(15):6150-6156. doi:10.1021/bi00441a004

16. Nilges M. Calculation of protein structures with ambiguous distance restraints. Automated assignment of ambiguous NOE crosspeaks and disulphide connectivities. *J Mol Biol*. 1995;245(5):645-660. doi:10.1006/jmbi.1994.0053

17. Güntert P, Buchner L. Combined automated NOE assignment and structure calculation with CYANA. *J Biomol NMR*. 2015;62(4):453-471. doi:10.1007/s10858-015-9924-9

18. Dobson CM. Protein folding and misfolding. *Nature*. 2003;426(December):1-4.

19. Stefani M, Dobson CM. Protein aggregation and aggregate toxicity: New insights into protein folding, misfolding diseases and biological evolution. *J Mol Med*. 2003;81(11):678-699. doi:10.1007/s00109-003-0464-5

20. Aguzzi A, O'Connor T. Protein aggregation diseases: Pathogenicity and therapeutic perspectives. *Nat Rev Drug Discov*. 2010;9(3):237-248. doi:10.1038/nrd3050

21. Frydman J, Nimmesgern E, Ohtsuka K, Hartl FU. Folding of nascent polypeptide chains in a high molecular mass assembly with molecular chaperones. *Nature*. 1994;370(6485):111-117. doi:10.1038/370111a0

22. Pfanner N. Protein folding: Who chaperones nascent chains in bacteria? *Curr Biol*. 1999;9(19):720-724. doi:10.1016/S0960-9822(99)80467-9

23. Priya S, Sharma SK, Goloubinoff P. Molecular chaperones as enzymes that catalytically unfold misfolded polypeptides. *FEBS Lett*. 2013;587(13):1981-1987. doi:10.1016/j.febslet.2013.05.014

24. Ben-Zvi AP, Goloubinoff P. Review: Mechanisms of disaggregation and refolding of stable protein aggregates by molecular chaperones. *J Struct Biol*. 2001;135(2):84-93. doi:10.1006/jsbi.2001.4352

25. Sharma SK, Christen P, Goloubinoff P. Disaggregating chaperones: an unfolding story. *Curr Protein Pept Sci*. 2009;10(5):432-446. doi:10.2174/138920309789351930

26. Ellis RJ. Assembly chaperones: A perspective. *Philos Trans R Soc B Biol Sci*. 2013;368(1617):3-7. doi:10.1098/rstb.2011.0398

27. De Koning L, Corpet A, Haber JE, Almouzni G. Histone chaperones: An escort network regulating histone traffic. *Nat Struct Mol Biol*. 2007;14(11):997-1007. doi:10.1038/nsmb1318

28. Dierks T, Klappa P, Wiech H, Zimmerman R. The role of molecular chaperones in protein transport into the endoplasmic reticulum. *Mol Chaperones*. 1993:79-85. doi:10.1007/978-94-011-2108-8_10

29. Craig EA. Hsp70 at the membrane: Driving protein translocation. *BMC Biol*. 2018;16(1):1-11. doi:10.1186/s12915-017-0474-3

30. Jung J, Kim J, Roh SH, et al. The HSP70 co-chaperone DNAJC14 targets misfolded pendrin for unconventional protein secretion. *Nat Commun*. 2016;7(May 2015):1-15. doi:10.1038/ncomms11386

31. Shiber A, Ravid T. Chaperoning proteins for destruction: Diverse roles of Hsp70 chaperones and their co-chaperones in targeting misfolded proteins to the proteasome. *Biomolecules*. 2014;4(3):704-724. doi:10.3390/biom4030704

32. Esser C, Alberti S, Höhfeld J. Cooperation of molecular chaperones with the ubiquitin/proteasome system. *Biochim Biophys Acta - Mol Cell Res*. 2004;1695(1-3):171-188. doi:10.1016/j.bbamcr.2004.09.020

33. Arndt V, Rogon C, Höhfeld J. To be, or not to be - Molecular chaperones in protein degradation. *Cell Mol Life Sci*. 2007;64(19-20):2525-2541. doi:10.1007/s00018-007-7188-6

34. Suss O, Reichmann D. Protein plasticity underlines activation and function of ATP-independent chaperones. *Front Mol Biosci*. 2015;2(JUL):1-10. doi:10.3389/fmolb.2015.00043

35. Castanié-Cornet MP, Bruel N, Genevaux P. Chaperone networking facilitates protein targeting to the bacterial cytoplasmic membrane. *Biochim Biophys Acta - Mol Cell Res*. 2014;1843(8):1442-1456. doi:10.1016/j.bbamcr.2013.11.007

36. Goloubinoff P, Sassi AS, Fauvet B, Barducci A, De Los Rios P. Chaperones convert the energy from ATP into the nonequilibrium stabilization of native proteins article. *Nat Chem Biol*. 2018;14(4):388-395. doi:10.1038/s41589-018-0013-8

37. Rüdiger S, Germeroth L, Schneider-Mergener J, Bukau B. Substrate specificity of the DnaK chaperone determined by screening cellulose-bound peptide libraries respect to the bound folding conformer are only partly. *EMBO J*. 1997;16(7):1501-1507. https://www.ncbi.nlm.nih.gov/pmc/articles/PMC1169754/pdf/001501.pdf.

38. Hartl FU, Bracher A, Hayer-Hartl M. Molecular chaperones in protein folding and proteostasis. *Nature*. 2011;475(7356):324-332. doi:10.1038/nature10317

39. Balchin D, Hayer-Hartl M, Hartl FU. In vivo aspects of protein folding and quality control. *Science (80-)*. 2016. doi:10.1126/science.aac4354

40. Buchner J, Grallert H, Jakob U. Molecular Chaperones. *Methods Enzymol*. 1998;290(4):323-338. doi:10.1016/S0076-6879(98)90029-5

41. Kim YE, Hipp MS, Bracher A, Hayer-Hartl M, Ulrich Hartl F. *Molecular Chaperone Functions in Protein Folding and Proteostasis*. Vol 82.; 2013. doi:10.1146/annurev-biochem-060208-092442

42. Rospert S, Chacinska A. Distinct yet linked: Chaperone networks in the eukaryotic cytosol. *Genome Biol*. 2006;7(3):7-9. doi:10.1186/gb-2006-7-3-208

43. Zhao R, Davey M, Hsu YC, et al. Navigating the chaperone network: An integrative map of physical and genetic interactions mediated by the hsp90 chaperone. *Cell*. 2005;120(5):715-727. doi:10.1016/j.cell.2004.12.024

44. Voisine C, Pedersen JS, Morimoto RI. Chaperone networks: Tipping the balance in protein folding diseases. *Neurobiol Dis*. 2010;40(1):12-20. doi:10.1016/j.nbd.2010.05.007

45. Winkler J, Tyedmers J, Bukau B, Mogk A. Chaperone networks in protein disaggregation and prion propagation. *J Struct Biol*. 2012;179(2):152-160. doi:10.1016/j.jsb.2012.05.002

46. Calloni G, Chen T, Schermann SM, et al. DnaK Functions as a Central Hub in the E. coli Chaperone Network. *Cell Rep*. 2012;1(3):251-264. doi:10.1016/j.celrep.2011.12.007

47. Hunt C, Morimoto RI. Conserved features of eukaryotic hsp7O genes revealed by comparison with the nucleotide sequence of human hsp7O (gene structure/heat shock/evolution). *Proc Nati Acad Sci USA*. 1985;82(October):6455-6459. https://www.ncbi.nlm.nih.gov/pmc/articles/PMC390735/pdf/pnas00359-0097.pdf.

48. Rosenzweig R, Nillegoda NB, Mayer MP, Bukau B. The Hsp70 chaperone network. *Nat Rev Mol Cell Biol*. doi:10.1038/s41580-019-0133-3

49. Kityk R, Kopp J, Sinning I, Mayer MP. Structure and Dynamics of the ATP-Bound Open Conformation of Hsp70 Chaperones. *Mol Cell*. 2012;48(6):863-874. doi:10.1016/j.molcel.2012.09.023

50. Schmid D, Baici A, Gehring H, Christen P. Kinetics of molecular chaperone action. *Science (80-)*. 1994;263(5149):971-973. doi:10.1126/science.8310296

51. Bertelsena EB, Chang L, Gestwicki JE, Zuiderweg ERP. Solution conformation of wild-type E. coli Hsp70 (DnaK) chaperone complexed with ADP and substrate. *Proc Natl Acad Sci U S A*. 2009;106(21):8471-8476. doi:10.1073/pnas.0903503106

52. Mayer MP, Schröder H, Rüdiger S, Paal K, Laufen T, Bukau B. Multistep mechanism of substrate binding determines chaperone activity of Hsp70. *Nat Struct Biol*. 2000;7(7):586-593. doi:10.1038/76819

53. Kityk R, Kopp J, Mayer MP. Molecular Mechanism of J-Domain-Triggered ATP Hydrolysis by Hsp70 Chaperones. *Mol Cell*. 2017:1-11. doi:10.1016/j.molcel.2017.12.003

54. Kityk R, Vogel M, Schlecht R, Bukau B, Mayer MP. Pathways of allosteric regulation in Hsp70 chaperones. *Nat Commun*. 2015;6. doi:10.1038/ncomms9308

55. Karzai AW, McMacken R. A bipartite signaling mechanism involved in DnaJ-mediated activation of the Escherichia coli DnaK protein. *J Biol Chem*. 1996;271(19):11236-11246. doi:10.1074/jbc.271.19.11236

56. Laufen T, Mayer MP, Beisel C, et al. Mechanism of regulation of Hsp70 chaperones by DnaJ cochaperones. *Proc Natl Acad Sci U S A*. 1999;96(10):5452-5457. doi:10.1073/pnas.96.10.5452

57. Van Durme J, Maurer-Stroh S, Gallardo R, Wilkinson H, Rousseau F, Schymkowitz J. Accurate prediction of DnaK-peptide binding via homology modelling and experimental data. *PLoS Comput Biol*. 2009;5(8). doi:10.1371/journal.pcbi.1000475

58. Blond-Elguindi S, Cwirla SE, Dower WJ, et al. Affinity panning of a library of peptides displayed on bacteriophages reveals the binding specificity of BiP. *Cell*. 1993;75(4):717-728. doi:10.1016/0092-8674(93)90492-9

59. Schneider M, Rosam M, Glaser M, et al. BiPPred: Combined sequence- and structure-based prediction of peptide binding to the Hsp70 chaperone BiP. *Proteins Struct Funct Bioinforma*. 2016;84(10):1390-1407. doi:10.1002/prot.25084

60. Sekhar A, Velyvis A, Zoltsman G, Rosenzweig R, Bouvignies G, Kay LE. Conserved conformational selection mechanism of Hsp70 chaperone-substrate interactions. *Elife*. 2018;7:e32764. doi:10.7554/eLife.32764

61. Sekhar A, Rosenzweig R, Bouvignies G, Kay LE. Mapping the conformation of a client protein through the Hsp70 functional cycle. *Proc Natl Acad Sci U S A*. 2015;112(33):10395-10400. doi:10.1073/pnas.1508504112

62. Kellner R, Hofmann H, Barducci A, Wunderlich B, Nettels D, Schuler B. Single-molecule spectroscopy reveals chaperone-mediated expansion of substrate protein. *Proc Natl Acad Sci U S A*. 2014;111(37):13355-13360. doi:10.1073/pnas.1407086111

63. Sharma SK, De Los Rios P, Christen P, Lustig A, Goloubinoff P. The kinetic parameters and energy cost of the Hsp70 chaperone as a polypeptide unfoldase. *Nat Chem Biol*. 2010;6(12):914-920. doi:10.1038/nchembio.455

64. French JB, Zhao H, An S, et al. Hsp70/Hsp90 chaperone machinery is involved in the assembly of the purinosome. *Proc Natl Acad Sci U S A*. 2013;110(7):2528-2533.

doi:10.1073/pnas.1300173110

65. Murphy PJM, Morishima Y, Chen H, et al. Visualization and mechanism of assembly of a glucocorticoid receptor·Hsp70 complex that is primed for subsequent Hsp90-dependent opening of the steroid binding cleft. *J Biol Chem*. 2003;278(37):34764-34773. doi:10.1074/jbc.M304469200

66. Nillegoda NB, Kirstein J, Szlachcic A, et al. Crucial HSP70 co-chaperone complex unlocks metazoan protein disaggregation. *Nature*. 2015;524(7564):247-251. doi:10.1038/nature14884

67. Gao X, Carroni M, Nussbaum-Krammer C, et al. Human Hsp70 Disaggregase Reverses Parkinson's-Linked α-Synuclein Amyloid Fibrils. *Mol Cell*. 2015;59(5):781-793. doi:10.1016/j.molcel.2015.07.012

68. Shorter J. The mammalian disaggregase machinery: Hsp110 synergizes with Hsp70 and Hsp40 to catalyze protein disaggregation and reactivation in a cell-free system. *PLoS One*. 2011;6(10). doi:10.1371/journal.pone.0026319

69. Nillegoda NB, Wentink AS, Bukau B. Protein Disaggregation in Multicellular Organisms. *Trends Biochem Sci*. 2018;43(4):285-300. doi:10.1016/j.tibs.2018.02.003

70. Wentink AS, Nillegoda NB, Feufel J, et al. Molecular dissection of amyloid disaggregation by human HSP70. *Nature*. 2020;587(7834):483-488. doi:10.1038/s41586-020-2904-6

71. Nillegoda NB, Bukau B. Metazoan Hsp70-based protein disaggregases: emergence and mechanisms. *Front Mol Biosci*. 2015;2(October):1-12. doi:10.3389/fmolb.2015.00057

72. Goldfarb SB, Kashlan OB, Watkins JN, et al. Differential effects of Hsc70 and Hsp70 on the intracellular trafficking and functional expression of epithelial sodium channels. *Proc Natl Acad Sci U S A*. 2006;103(15):5817-5822. doi:10.1073/pnas.0507903103

73. Craig EA, Marszalek J. How Do J-Proteins Get Hsp70 to Do So Many Different Things? *Trends Biochem Sci*. 2017;42(5):355-368. doi:10.1016/j.tibs.2017.02.007

74. Rosenzweig R, Nillegoda NB, Mayer MP, Bukau B. The Hsp70 chaperone network. *Nat Rev Mol Cell Biol*. 2019;20(11):665-680. doi:10.1038/s41580-019-0133-3

75. Kampinga HH, Andreasson C, Barducci A, Cheetham ME, Cyr D. Function, evolution, and structure of J-domain proteins. 2019:7-15.

76. Kampinga HH, Craig EA. The HSP70 chaperone machinery: J proteins as drivers of functional specificity. *Nat Rev Mol Cell Biol*. 2010;11(8):579-592. doi:10.1038/nrm2941

77. Han W, Christen P. Mechanism of the Targeting Action of DnaJ in the DnaK Molecular Chaperone System *. 2003;278(21):19038-19043. doi:10.1074/jbc.M300756200

78. Guo F, Snapp EL. ERdj3 regulates BiP occupancy in living cells. *J Cell Sci*. 2013;126(6):1429-1439. doi:10.1242/jcs.118182

79. Johnson JL, Craig EA. An essential role for the substrate-binding region of Hsp40s in Saccharomyces cerevisiae. *J Cell Biol*. 2001;152(4):851-856. doi:10.1083/jcb.152.4.851

80. Sha B, Lee S, Cyr DM. The crystal structure of the peptide-binding fragment from the yeast Hsp40 protein Sis1. *Structure*. 2000;8(8):799-807. doi:10.1016/S0969-2126(00)00170-2

81. Lu Z, Cyr DM. The conserved carboxyl terminus and zinc finger-like domain of the co-chaperone Ydj1 assist Hsp70 in protein folding. *J Biol Chem*. 1998;273(10):5970-5978. doi:10.1074/jbc.273.10.5970

82. Jin Y, Awad W, Petrova K, Hendershot L. Regulated release of ERdj3 from unfolded proteins by BiP. *EMBO J*. 2008;27(21):2873-2882. doi:10.1038/emboj.2008.207

83. Baaklini I, Wong MJH, Hantouche C, Patel Y, Shrier A, Young JC. The DNAJA2 substrate release mechanism is essential for chaperone-mediated folding. *J Biol Chem*. 2012;287(50):41939-41954. doi:10.1074/jbc.M112.413278

84. Sha B, Lee S, Cyr DM. The crystal structure of the peptide-binding fragment from the yeast Hsp40 protein Sis1. *Structure*. 2000;8(8):799-807. doi:10.1016/S0969-2126(00)00170-2

85. Li J, Qian X, Sha B. The Crystal Structure of the Yeast Hsp40 Ydj1 Complexed with Its Peptide Substrate. *Structure*. 2003;11(12):1475-1483. doi:10.1016/j.str.2003.10.012

86. Suzuki H, Noguchi S, Arakawa H, Tokida T, Hashimoto M, Satow Y. Peptide-binding

sites as revealed by the crystal structures of the human Hsp40 Hdj1 c-terminal domain in complex with the octapeptide from human Hsp70. *Biochemistry*. 2010;49(39):8577-8584. doi:10.1021/bi100876n

87. Karamanos TK, Tugarinov V, Clore GM. Unraveling the structure and dynamics of the human DNAJB6b chaperone by NMR reveals insights into Hsp40-mediated proteostasis. *Proc Natl Acad Sci U S A*. 2019;116(43):21529-21538. doi:10.1073/pnas.1914999116

88. Cheetham ME, Caplan AJ. Structure, function and evolution of DnaJ: Conservation and adaptation of chaperone function. *Cell Stress Chaperones*. 1998;3(1):28-36. doi:10.1379/1466-1268(1998)003<0028:SFAEOD>2.3.CO;2

89. Hoshino T, Nakaya T, Araki W, Suzuki K, Suzuki T, Mizushima T. Endoplasmic reticulum chaperones inhibit the production of amyloid- β peptides. 2007;589:581-589. doi:10.1042/BJ20061318

90. Qiu XB, Shao YM, Miao S, Wang L. The diversity of the DnaJ/Hsp40 family, the crucial partners for Hsp70 chaperones. *Cell Mol Life Sci*. 2006;63(22):2560-2570. doi:10.1007/s00018-006-6192-6

91. Nakatsukasa K, Huyer G, Michaelis S, Brodsky JL. Dissecting the ER-Associated Degradation of a Misfolded Polytopic Membrane Protein. *Cell*. 2008;132(1):101-112. doi:10.1016/j.cell.2007.11.023

92. Mokranjac D, Berg A, Adam A, Neupert W, Hell K. Association of the Tim14·Tim16 subcomplex with the TIM23 translocase is crucial for function of the mitochondrial protein import motor. *J Biol Chem*. 2007;282(25):18037-18045. doi:10.1074/jbc.M701895200

93. Jiang Y, Rossi P, Kalodimos CG. Structural basis for client recognition and activity of Hsp40 chaperones. *Science (80-)*. 2019;365(6459):1313-1319. doi:10.1126/science.aax1280

94. Rodríguez-González C, Lin S, Arkan S, Hansen C. Co-chaperones DNAJA1 and DNAJB6 are critical for regulation of polyglutamine aggregation. *Sci Rep*. 2020;10(1):1-9. doi:10.1038/s41598-020-65046-5

95. Shen Y, Hendershots LM. ERdj3, a Stress-inducible Endoplasmic Reticulum DnaJHomologue, Serves as a CoFactor for BiP's Interactions with Unfolded Substrates. *Mol Biol Cell*. 2005;16(40 –50):5318-5328. doi:10.1091/mbc.E04

96. Parrales A, Ranjan A, Iyer S V., et al. DNAJA1 controls the fate of misfolded mutant p53 through the mevalonate pathway. *Nat Cell Biol*. 2016;18(11):1233-1243. doi:10.1038/ncb3427

97. Hageman J, Rujano MA, van Waarde MAWH, et al. A DNAJB Chaperone Subfamily with HDAC-Dependent Activities Suppresses Toxic Protein Aggregation. *Mol Cell*. 2010;37(3):355-369. doi:10.1016/j.molcel.2010.01.001

98. Månsson C, Kakkar V, Monsellier E, et al. DNAJB6 is a peptide-binding chaperone which can suppress amyloid fibrillation of polyglutamine peptides at substoichiometric molar ratios. *Cell Stress Chaperones*. 2014;19(2):227-239. doi:10.1007/s12192-013-0448-5

99. Gillis J, Schipper-Krom S, Juenemann K, et al. The DNAJB6 and DNAJB8 protein chaperones prevent intracellular aggregation of polyglutamine peptides. *J Biol Chem*. 2013;288(24):17225-17237. doi:10.1074/jbc.M112.421685

100. Scheele U, Kalthoff C, Ungewickell E. Multiple Interactions of Auxilin 1 with Clathrin and the AP-2 Adaptor Complex. *J Biol Chem*. 2001;276(39):36131-36138. doi:10.1074/jbc.M106511200

101. Voisine C, Cheng YC, Ohlson M, et al. Jac1, a mitochondrial J-type chaperone, is involved in the biogenesis of Fe/S clusters in Saccharomyces cerevisiae. *Proc Natl Acad Sci U S A*. 2001;98(4):1483-1488. doi:10.1073/pnas.98.4.1483

102. Mogk A, Bukau B, Kampinga HH. Cellular Handling of Protein Aggregates by Disaggregation Machines. *Mol Cell*. 2018;69(2):214-226. doi:10.1016/j.molcel.2018.01.004

103. Chapple JP, Van Der Spuy J, Poopalasundaram S, Cheetham ME. Neuronal DnaJ proteins HSJ1a and HSJ1b: A role in linking the Hsp70 chaperone machine to the ubiquitin-proteasome system? *Biochem Soc Trans*. 2004;32(4):640-642. doi:10.1042/BST0320640

104. Chiaw PK, Hantouche C, Wong MJH, et al. Hsp70 and DNAJA2 limit CFTR levels through degradation. *PLoS One*. 2019;14(8):1-27. doi:10.1371/journal.pone.0220984

105. Davey KM, Parboosingh JS, McLeod DR, et al. Mutation of DNAJC19, a human homologue of yeast inner mitochondrial membrane co-chaperones, causes DCMA syndrome, a novel autosomal recessive Barth syndrome-like condition. *J Med Genet*. 2006;43(5):385-393. doi:10.1136/jmg.2005.036657

106. Blumen SC, Astord S, Robin V, et al. A rare recessive distal hereditary motor neuropathy with HSJ1 chaperone mutation. *Ann Neurol*. 2012;71(4):509-519. doi:10.1002/ana.22684

107. Edvardson S, Cinnamon Y, Ta-Shma A, et al. A deleterious mutation in DNAJC6 encoding the neuronal-specific clathrin-uncoating Co-chaperone auxilin, is associated with juvenile parkinsonism. *PLoS One*. 2012;7(5):4-8. doi:10.1371/journal.pone.0036458

108. Vilariño-Güell C, Rajput A, Milnerwood AJ, et al. DNAJC13 mutations in Parkinson disease. *Hum Mol Genet*. 2014;23(7):1794-1801. doi:10.1093/hmg/ddt570

109. Harms MB, Sommerville RB, Allred P, et al. Exome sequencing reveals DNAJB6 mutations in dominantly-inherited myopathy. *Ann Neurol*. 2012;71(3):407-416. doi:10.1002/ana.22683

110. Koutras C, Braun JEA. J protein mutations and resulting proteostasis collapse. *Front Cell Neurosci*. 2014;8(JULY):1-7. doi:10.3389/fncel.2014.00191

111. Huang K, Flanagan JM, Prestegard JH. The influence of C-terminal extension on the structure of the "J-domain" in E. coli DnaJ. *Protein Sci*. 2008;8(1):203-214. doi:10.1110/ps.8.1.203

112. Stark JL, Mehla K, Chaika N, et al. Structure and function of human DnaJ homologue subfamily A member 1 (DNAJA1) and its relationship to pancreatic cancer. *Biochemistry*. 2014;53(8):1360-1372. doi:10.1021/bi401329a

113. Schilke BA, Ciesielski SJ, Ziegelhoffer T, et al. Broadening the functionality of a J-protein/Hsp70 molecular chaperone system. *PLoS Genet*. 2017;13(10):1-29. doi:10.1371/journal.pgen.1007084

114. Nillegoda NB, Stank A, Malinverni D, et al. Evolution of an intricate J-protein network driving protein disaggregation in eukaryotes. *Elife*. 2017;6:1-28. doi:10.7554/eLife.24560

115. Barends TRM, Brosi RWW, Steinmetz A, et al. Combining crystallography and EPR: Crystal and solution structures of the multidomain cochaperone DnaJ. *Acta Crystallogr Sect D Biol Crystallogr*. 2013;69(8):1540-1552. doi:10.1107/S0907444913010640

116. Hagiwara M, Maegawa K ichi, Suzuki M, et al. Structural Basis of an ERAD Pathway

Mediated by the ER-Resident Protein Disulfide Reductase ERdj5. *Mol Cell*. 2011;41(4):432-444. doi:10.1016/j.molcel.2011.01.021

117. Svärd M, Biterova EI, Bourhis JM, Guy JE. The crystal structure of the human co-chaperone P58 IPK. Gasset M, ed. *PLoS One*. 2011;6(7):e22337. doi:10.1371/journal.pone.0022337

118. Maegawa K-I, Watanabe S, Noi K, et al. The Highly Dynamic Nature of ERdj5 Is Key to Efficient Elimination of Aberrant Protein Oligomers through ER-Associated Degradation. *Structure*. 2017;25(6):846-857.e4. doi:10.1016/j.str.2017.04.001

119. Chen T, Yang M, Yu Z, et al. Small GTPase RBJ mediates nuclear entrapment of MEK1/MEK2 in tumor progression. *Cancer Cell*. 2014;25(5):682-696. doi:10.1016/j.ccr.2014.03.009

120. Wall D, Zylicz M, Georgopoulos C. The conserved G/F motif of the DnaJ chaperone is necessary for the activation of the substrate binding properties of the DnaK chaperone. *J Biol Chem*. 1995;270(5):2139-2144. doi:10.1074/jbc.270.5.2139

121. Cajo GC, Horne BE, Kelley WL, Schwager F, Georgopoulos C, Genevaux P. The role of the DIF motif of the DnaJ (Hsp40) co-chaperone in the regulation of the DnaK (Hsp70) chaperone cycle. *J Biol Chem*. 2006;281(18):12436-12444. doi:10.1074/jbc.M511192200

122. Perales-Calvo J, Muga A, Moro F. Role of DnaJ G/F-rich domain in conformational recognition and binding of protein substrates. *J Biol Chem*. 2010;285(44):34231-34239. doi:10.1074/jbc.M110.144642

123. Sondheimer N, Lopez N, Craig EA, Lindquist S. The role of Sis1 in the maintenance of the [RNQ+] prion. *EMBO J*. 2001;20(10):2435-2442. doi:10.1093/emboj/20.10.2435

124. Yan W, Craig EA. The Glycine-Phenylalanine-Rich Region Determines the Specificity of the Yeast Hsp40 Sis1. *Mol Cell Biol*. 1999;19(11):7751-7758. doi:10.1128/mcb.19.11.7751

125. Ruggieri A, Brancati F, Zanotti S, et al. Complete loss of the DNAJB6 G/F domain and novel missense mutations cause distal-onset DNAJB6 myopathy. *Acta Neuropathol Commun*. 2015;3:44. doi:10.1186/s40478-015-0224-0

126. Faust O, Abayev-Avraham M, Wentink AS, et al. HSP40 proteins use class-specific regulation to drive HSP70 functional diversity. *Nature*. 2020;587(7834):489-494.

doi:10.1038/s41586-020-2906-4

127. Gu J, Liu Z, Zhang S, et al. Hsp40 proteins phase separate to chaperone the assembly and maintenance of membraneless organelles. *Proc Natl Acad Sci U S A*. 2020;117(49):31123-31133. doi:10.1073/pnas.2002437117

128. McCaffrey K, Braakman I. Protein quality control at the endoplasmic reticulum. *Essays Biochem*. 2016;60(2):227-235. doi:10.1042/EBC20160003

129. Barlowe CK, Miller EA. Secretory protein biogenesis and traffic in the early secretory pathway. *Genetics*. 2013;193(2):383-410. doi:10.1534/genetics.112.142810

130. Phillips MJ, Voeltz GK. Structure and function of ER membrane contact sites with other organelles. *Nat Rev Mol Cell Biol*. 2016;17(2):69-82. doi:10.1038/nrm.2015.8

131. Tannous A, Pisoni GB, Hebert DN, Molinari M. N-linked sugar-regulated protein folding and quality control in the ER. *Semin Cell Dev Biol*. 2015;41:79-89. doi:10.1016/j.semcdb.2014.12.001

132. Oka OB V, Bulleid NJ. Forming disulfides in the endoplasmic reticulum. *Biochim Biophys Acta - Mol Cell Res*. 2013;1833(11):2425-2429. doi:10.1016/j.bbamcr.2013.02.007

133. Nyathi Y, Wilkinson BM, Pool MR. Co-translational targeting and translocation of proteins to the endoplasmic reticulum. *Biochim Biophys Acta - Mol Cell Res*. 2013;1833(11):2392-2402. doi:10.1016/j.bbamcr.2013.02.021

134. Williams DB. Beyond lectins: The calnexin/calreticulin chaperone system of the endoplasmic reticulum. *J Cell Sci*. 2006;119(4):615-623. doi:10.1242/jcs.02856

135. Trombetta ES, Helenius A. Lectins as chaperones in glycoprotein folding. *Curr Opin Struct Biol*. 1998;8(5):587-592. doi:10.1016/S0959-440X(98)80148-6

136. Gruber CW, Čemažar M, Heras B, Martin JL, Craik DJ. Protein disulfide isomerase: the structure of oxidative folding. *Trends Biochem Sci*. 2006;31(8):455-464. doi:10.1016/j.tibs.2006.06.001

137. Khan HA, Mutus B. Protein disulfide isomerase a multifunctional protein with multiple physiological roles. *Front Chem*. 2014;2(AUG):1-9. doi:10.3389/fchem.2014.00070

138. Göthel SF, Marahiel MA. Peptidyl-prolyl cis-trams isomerases, a superfamily of ubiquitous folding catalysts. *Cell Mol Life Sci*. 1999;55(3):423-436. doi:10.1007/s000180050299

139. Jansen G, Määttänen P, Denisov AY, et al. An interaction map of endoplasmic reticulum chaperones and foldases. *Mol Cell Proteomics*. 2012;11(9):710-723. doi:10.1074/mcp.M111.016550

140. Gidalevitz T, Stevens F, Argon Y. Orchestration of secretory protein folding by ER chaperones. *Biochim Biophys Acta - Mol Cell Res*. 2013;1833(11):2410-2424. doi:10.1016/j.bbamcr.2013.03.007

141. Araki K, Nagata K. Protein folding and quality control in the ER. *Cold Spring Harb Perspect Biol*. 2012;4(8):1-26. doi:10.1101/cshperspect.a015438

142. Tabara K, Iwata Y, Koizumi N. The unfolded protein response. In: *Methods in Molecular Biology*. Vol 1691. ; 2018:223-230. doi:10.1007/978-1-4939-7389-7_17

143. Ma Y, Hendershot LM. The unfolding tale of the unfolded protein response. *Cell*. 2001;107(7):827-830. doi:10.1016/S0092-8674(01)00623-7

144. Hetz C. The unfolded protein response: Controlling cell fate decisions under ER stress and beyond. *Nat Rev Mol Cell Biol*. 2012;13(2):89-102. doi:10.1038/nrm3270

145. Hetz C, Zhang K, Kaufman RJ. Mechanisms, regulation and functions of the unfolded protein response. *Nat Rev Mol Cell Biol*. 2020;21(8):421-438. doi:10.1038/s41580-020-0250-z

146. Hamman BD, Hendershot LM, Johnson AE. BiP maintains the permeability barrier of the ER membrane by sealing the lumenal end of the translocon pore before and early in translocation. *Cell*. 1998;92(6):747-758. doi:10.1016/S0092-8674(00)81403-8

147. Okuda-Shimizu Y, Hendershot LM. Characterization of an ERAD Pathway for Nonglycosylated BiP Substrates, which Require Herp. *Mol Cell*. 2007;28(4):544-554. doi:10.1016/j.molcel.2007.09.012

148. Cesaratto F, Sasset L, Burrone OR. BiP/GRP78 Mediates ERAD Targeting of Proteins Produced by Membrane-Bound Ribosomes Stalled at the STOP-Codon. *J Mol Biol*. 2019;2(431):123-141. doi:10.1016/j.athoracsur.2020.04.003

149. Lamb HK, Mee C, Xu W, et al. The affinity of a major Ca2+ binding site on GRP78 is differentially enhanced by ADP and ATP. *J Biol Chem*. 2006;281(13):8796-8805. doi:10.1074/jbc.M503964200

150. Preissler S, Rato C, Yan Y, Perera LA, Czako A, Ron D. Calcium depletion challenges endoplasmic reticulum proteostasis by destabilising bip-substrate complexes. *Elife*. 2020;9:1-36. doi:10.7554/ELIFE.62601

151. Wang J, Pareja KA, Kaiser CA, Sevier CS. Redox signaling via the molecular chaperone BiP protects cells against endoplasmic reticulum-derived oxidative stress. *Elife*. 2014;3:e03496. doi:10.7554/eLife.03496

152. Bravo R, Parra V, Gatica D, et al. *Endoplasmic Reticulum and the Unfolded Protein Response : Dynamics and Metabolic Integration*. Vol 301.; 2013. doi:10.1016/B978-0-12-407704-1.00005-1

153. Behnke J, Mann MJ, Scruggs FL, Feige MJ, Hendershot LM. Members of the Hsp70 Family Recognize Distinct Types of Sequences to Execute ER Quality Control. *Mol Cell*. 2016;63(5):739-752. doi:10.1016/j.molcel.2016.07.012

154. Otero JH, Lizák B, Hendershot LM. Life and death of a BiP substrate. *Semin Cell Dev Biol*. 2010;21(5):472-478. doi:10.1016/j.semcdb.2009.12.008

155. Yang J, Nune M, Zong Y, Zhou L, Liu Q. Close and Allosteric Opening of the Polypeptide-Binding Site in a Human Hsp70 Chaperone BiP. *Structure*. 2015;23(12):2191-2203. doi:10.1016/j.str.2015.10.012

156. Pobre KFR, Poet GJ, Hendershot LM. The endoplasmic reticulum (ER) chaperone BiP is a master regulator of ER functions: Getting by with a little help from ERdj friends. *J Biol Chem*. 2019;294(6):2098-2108. doi:10.1074/jbc.REV118.002804

157. Dudek J, Greiner M, Müller A, et al. ERj1p has a basic role in protein biogenesis at the endoplasmic reticulum. *Nat Struct Mol Biol*. 2005;12(11):1008-1014. doi:10.1038/nsmb1007

158. Blau M, Mullapudi S, Becker T, et al. ERj1p uses a universal ribosomal adaptor site to coordinate the 80S ribosome at the membrane. *Nat Struct Mol Biol*. 2005;12(11):1015-1016. doi:10.1038/nsmb998

159. Brodsky JL, Schekman R. A Sec63p-BiP complex from yeast is required for protein translocation in a reconstituted proteoliposome. *J Cell Biol*. 1993;123(6 I):1355-1363.

doi:10.1083/jcb.123.6.1355

160. Wittke S, Dunnwald M, Johnsson N. Sec62p, a component of the endoplasmic reticulum protein translocation machinery, contains multiple binding sites for the Sec-complex. *Mol Biol Cell*. 2000;11(11):3859-3871. doi:10.1091/mbc.11.11.3859

161. Yamamoto YH, Kasai A, Omori H, et al. ERdj8 governs the size of autophagosomes during the formation process. *J Cell Biol*. 2020;219(8). doi:10.1083/jcb.201903127

162. Zahedi RP, Völzing C, Schmitt A, et al. Analysis of the membrane proteome of canine pancreatic rough microsomes identifies a novel Hsp40, termed ERj7. *Proteomics*. 2009;9(13):3463-3473. doi:10.1002/pmic.200800722

163. Hosoda A, Kimata Y, Tsuru A, Kohno K. JPDI, a novel endoplasmic reticulum-resident protein containing both a BiP-interacting J-domain and thioredoxin-like motifs. *J Biol Chem*. 2003;278(4):2669-2676. doi:10.1074/jbc.M208346200

164. Tao J, Petrova K, Ron D, Sha B. Crystal structure of P58(IPK) TPR fragment reveals the mechanism for its molecular chaperone activity in UPR. *J Mol Biol*. 2010;397(5):1307-1315. doi:10.1016/j.jmb.2010.02.028

165. Tao J, Sha B. *Structural Insight into the Protective Role of P58(IPK) during Unfolded Protein Response*. Vol 490. 1st ed. Elsevier Inc.; 2011. doi:10.1016/B978-0-12-385114-7.00015-5

166. Pobre KFR, Poet GJ, Hendershot LM. The endoplasmic reticulum (ER) chaperone BiP is a master regulator of ER functions: Getting by with a little help from ERdj friends. *J Biol Chem*. 2019;294(6):2098-2108. doi:10.1074/jbc.REV118.002804

167. Marcus NY, Marcus RA, Schmidt BZ, Haslam DB. Contribution of the HEDJ/ERdj3 cysteine-rich domain to substrate interactions. *Arch Biochem Biophys*. 2007;468(2):147-158. doi:10.1016/j.abb.2007.10.001

168. Nakanishi K, Kamiguchi K, Torigoe T, et al. Localization and function in endoplasmic reticulum stress tolerance of ERdj3, a new member of Hsp40 family protein. *Cell Stress Chaperones*. 2004;9(3):253-264. doi:10.1379/CSC-52.1

169. Chen K, Qu S, Chowdhury S, et al. The endoplasmic reticulum HSP 40 co-chaperone ER dj3/ DNAJB 11 assembles and functions as a tetramer. *EMBO J*. 2017;36(15):2296-2309. doi:10.15252/embj.201695616

170. Massey S, Burress H, Taylor M, et al. Structural and functional interactions between the cholera toxin A1 subunit and ERdj3/HEDJ, a chaperone of the endoplasmic reticulum. *Infect Immun*. 2011;79(11):4739-4747. doi:10.1128/IAI.05503-11

171. Yu M, Haslam RHA, Haslam DB. HEDJ, an Hsp40 co-chaperone localized to the endoplasmic reticulum of human cells. *J Biol Chem*. 2000;275(32):24984-24992. doi:10.1074/jbc.M000739200

172. Khodayari N, Marek G, Lu Y, Krotova K, Wang RL, Brantly M. Erdj3 Has an Essential Role for Z Variant Alpha-1-Antitrypsin Degradation. *J Cell Biochem*. 2017;118(10):3090-3101. doi:10.1002/jcb.26069

173. Genereux JC, Qu S, Zhou M, et al. Unfolded protein response-induced ERdj3 secretion links ER stress to extracellular proteostasis. *EMBO J*. 2015.

174. Buck TM, Brodsky JL. Escaping the endoplasmic reticulum: why does a molecular chaperone leave home for greener pastures? *EMBO J*. 2015;34(1):1-3. doi:10.15252/embj.201490462

175. Weitzmann A, Baldes C, Dudek J, Zimmermann R. The heat shock protein 70 molecular chaperone network in the pancreatic endoplasmic reticulum - A quantitative approach. *FEBS J*. 2007;274(19):5175-5187. doi:10.1111/j.1742-4658.2007.06039.x

176. Van Galen P, Kreso A, Mbong N, et al. The unfolded protein response governs integrity of the haematopoietic stem-cell pool during stress. *Nature*. 2014;510(7504):268-272. doi:10.1038/nature13228

177. Pröls F, Mayer MP, Renner O, et al. Upregulation of the cochaperone Mdg1 in endothelial cells is induced by stress and during in vitro angiogenesis. *Exp Cell Res*. 2001;269(1):42-53. doi:10.1006/excr.2001.5294

178. Berger BJ, Müller TS, Buschmann IR, et al. High levels of the molecular chaperone Mdg1/ERdj4 reflect the activation state of endothelial cells. *Exp Cell Res*. 2003;290(1):82-92. doi:10.1016/S0014-4827(03)00316-1

179. Lai CW, Oteros JH, Hendershots LM, Snapp E. ERdj4 protein is a soluble endoplasmic reticulum (ER) DnaJ family protein that interacts with ER-associated degradation machinery. *J Biol Chem*. 2012;287(11):7969-7978. doi:10.1074/jbc.M111.311290

180. Amin-Wetzel N, Saunders RA, Kamphuis MJ, et al. A J-Protein Co-chaperone Recruits

BiP to Monomerize IRE1 and Repress the Unfolded Protein Response. *Cell*. 2017:1625-1637. doi:10.1016/j.cell.2017.10.040

181. Amin-Wetzel N, Neidhardt L, Yan Y, Mayer MP, Ron D. Unstructured regions in IRE1α specify BiP-mediated destabilisation of the luminal domain dimer and repression of the UPR. *Elife*. 2019;8:1-35. doi:10.7554/eLife.50793

182. Kumar S, Stecher G, Li M, Knyaz C, Tamura K. MEGA X: Molecular evolutionary genetics analysis across computing platforms. *Mol Biol Evol*. 2018;35(6):1547-1549. doi:10.1093/molbev/msy096

183. Thompson JD, Higgins DG, Gibson TJ. CLUSTAL W: Improving the sensitivity of progressive multiple sequence alignment through sequence weighting, position-specific gap penalties and weight matrix choice. *Nucleic Acids Res*. 1994;22(22):4673-4680. doi:10.1093/nar/22.22.4673

184. Delaglio F, Grzesiek S, Vuister GW, Zhu G, Pfeifer J, Bax A. NMRPipe: A multidimensional spectral processing system based on UNIX pipes. *J Biomol NMR*. 1995;6(3):277-293. doi:10.1007/BF00197809

185. Orekhov VY, Ibraghimov I V., Billeter M. MUNIN: A new approach to multi-dimensional NMR spectra interpretation. *J Biomol NMR*. 2001;20(1):49-60. doi:10.1023/A:1011234126930

186. Vranken WF, Boucher W, Stevens TJ, et al. The CCPN data model for NMR spectroscopy: Development of a software pipeline. *Proteins Struct Funct Genet*. 2005;59(4):687-696. doi:10.1002/prot.20449

187. Schwieters CD, Kuszewski JJ, Marius Clore G. Using Xplor-NIH for NMR molecular structure determination. *Prog Nucl Magn Reson Spectrosc*. 2006;48(1):47-62. doi:10.1016/j.pnmrs.2005.10.001

188. Michels AA, Kanon B, Bensaude O, Kampinga HH. Heat shock protein (Hsp) 40 mutants inhibit Hsp70 in mammalian cells. *J Biol Chem*. 1999;274(51):36757-36763. doi:10.1074/jbc.274.51.36757

189. Jarymowycz VA, Stone MJ. Fast time scale dynamics of protein backbones: NMR relaxation methods, applications, and functional consequences. *Chem Rev*. 2006;106(5):1624-1671. doi:10.1021/cr040421p

190. Karamanos TK, Tugarinov V, Clore GM. Unraveling the structure and dynamics of the

human DNAJB6b chaperone by NMR reveals insights into Hsp40-mediated proteostasis. *Proc Natl Acad Sci U S A*. 2019;116(43):21529-21538. doi:10.1073/pnas.1914999116

191. Bertoni M, Kiefer F, Biasini M, Bordoli L, Schwede T. Modeling protein quaternary structure of homo- and hetero-oligomers beyond binary interactions by homology. *Sci Rep*. 2017;7(1):1-15. doi:10.1038/s41598-017-09654-8

192. Vembar SS, Jonikas MC, Hendershot LM, Weissman JS, Brodsky JL. J domain co-chaperone specificity defines the role of BiP during protein translocation. *J Biol Chem*. 2010;285(29):22484-22494. doi:10.1074/jbc.M110.102186

193. Yu HY, Ziegelhoffer T, Osipiuk J, et al. Roles of intramolecular and intermolecular interactions in functional regulation of the Hsp70 J-protein co-chaperone Sis1. *J Mol Biol*. 2015;427(7):1632-1643. doi:10.1016/j.jmb.2015.02.007

194. Yu HY, Ziegelhoffer T, Craig EA. Functionality of Class A and Class B J-protein co-chaperones with Hsp70. *FEBS Lett*. 2015;589(19):2825-2830. doi:10.1016/j.febslet.2015.07.040

195. Behnke J, Mann MJ, Scruggs FL, Feige MJ, Hendershot LM. Members of the Hsp70 Family Recognize Distinct Types of Sequences to Execute ER Quality Control. *Mol Cell*. 2016;63(5):739-752. doi:10.1016/j.molcel.2016.07.012

196. Dejgaard K, Theberge JF, Heath-Engel H, Chevet E, Tremblay ML, Thomas DY. Organization of the Sec61 translocon, studied by high resolution native electrophoresis. *J Proteome Res*. 2010;9(4):1763-1771. doi:10.1021/pr900900x

197. Margittai É, Enyedi B, Csala M, Geiszt M, Bánhegyi G. Composition of the redox environment of the endoplasmic reticulum and sources of hydrogen peroxide. *Free Radic Biol Med*. 2015;83:331-340. doi:10.1016/j.freeradbiomed.2015.01.032

198. Amin-Wetzel N, Saunders RA, Kamphuis MJ, et al. A J-Protein Co-chaperone Recruits BiP to Monomerize IRE1 and Repress the Unfolded Protein Response. *Cell*. 2017:1-13. doi:10.1016/j.cell.2017.10.040

199. Hwang J, Qi L. Quality Control in the Endoplasmic Reticulum: Crosstalk between ERAD and UPR pathways. *Trends Biochem Sci*. 2018;43(8):593-605. doi:10.1016/j.tibs.2018.06.005

200. Gomila M, Peña A, Mulet M, Lalucat J, García-Valdés E. Phylogenomics and

systematics in Pseudomonas. *Front Microbiol*. 2015;6(MAR):1-13. doi:10.3389/fmicb.2015.00214

201. Nikolaidis M, Mossialos D, Oliver SG, Amoutzias GD. Comparative analysis of the core proteomes among the Pseudomonas major evolutionary groups reveals species-specific adaptations for Pseudomonas aeruginosa and Pseudomonas chlororaphis. *Diversity*. 2020;12(8). doi:10.3390/D12080289

202. Passera A, Compant S, Casati P, et al. Not just a pathogen? Description of a plant-beneficial Pseudomonas syringae strain. *Front Microbiol*. 2019;10(JUN). doi:10.3389/fmicb.2019.01409

203. Silby MW, Winstanley C, Godfrey SAC, Levy SB, Jackson RW. Pseudomonas genomes: Diverse and adaptable. *FEMS Microbiol Rev*. 2011;35(4):652-680. doi:10.1111/j.1574-6976.2011.00269.x

204. Remold SK, Brown CK, Farris JE, Hundley TC, Perpich JA, Purdy ME. Differential Habitat Use and Niche Partitioning by Pseudomonas Species in Human Homes. *Microb Ecol*. 2011;62(3):505-517. doi:10.1007/s00248-011-9844-5

205. Crone S, Vives-Flórez M, Kvich L, et al. The environmental occurrence of Pseudomonas aeruginosa. *Apmis*. 2020;128(3):220-231. doi:10.1111/apm.13010

206. Cross A, Allen JR, Burke J, et al. Nosocomial infections due to Pseudomonas aeruginosa: review of recent trends. *Rev Infect Dis*. 1983;5 Suppl 5(December). doi:10.1093/clinids/5.supplement_5.s837

207. Kerr KG, Snelling AM. Pseudomonas aeruginosa: a formidable and ever-present adversary. *J Hosp Infect*. 2009;73(4):338-344. doi:10.1016/j.jhin.2009.04.020

208. Breidenstein EBM, de la Fuente-Núñez C, Hancock REW. Pseudomonas aeruginosa: All roads lead to resistance. *Trends Microbiol*. 2011;19(8):419-426. doi:10.1016/j.tim.2011.04.005

209. Hancock REW, Speert DP. Antibiotic resistance in Pseudomonas aeruginosa: Mechanisms and impact on treatment. *Drug Resist Updat*. 2000;3(4):247-255. doi:10.1054/drup.2000.0152

210. Aloush V, Navon-Venezia S, Seigman-Igra Y, Cabili S, Carmeli Y. Multidrug-resistant Pseudomonas aeruginosa: Risk factors and clinical impact. *Antimicrob Agents Chemother*. 2006;50(1):43-48. doi:10.1128/AAC.50.1.43-48.2006

211. Lister PD, Wolter DJ, Hanson ND. Antibacterial-resistant Pseudomonas aeruginosa: Clinical impact and complex regulation of chromosomally encoded resistance mechanisms. *Clin Microbiol Rev*. 2009;22(4):582-610. doi:10.1128/CMR.00040-09

212. Tam VH, Rogers CA, Chang KT, Weston JS, Caeiro JP, Garey KW. Impact of multidrug-resistant Pseudomonas aeruginosa bacteremia on patient outcomes. *Antimicrob Agents Chemother*. 2010;54(9):3717-3722. doi:10.1128/AAC.00207-10

213. Ferrer M, Valencia M, Torres A. Management of Ventilator-associated Pneumonia. *Intensive Care Med*. 2008:353-364. doi:10.1007/978-0-387-77383-4_33

214. Marschall J. Current strategies for the prevention and management of central line-associated bloodstream infections. *Infect Drug Resist*. 2010:147. doi:10.2147/idr.s10105

215. Cole SJ, Records AR, Orr MW, Linden SB, Lee VT. Catheter-associated urinary tract infection by Pseudomonas aeruginosa is mediated by exopolysaccharide-independent biofilms. *Infect Immun*. 2014;82(5):2048-2058. doi:10.1128/IAI.01652-14

216. Gellatly SL, Hancock REW. Pseudomonas aeruginosa: New insights into pathogenesis and host defenses. *Pathog Dis*. 2013;67(3):159-173. doi:10.1111/2049-632X.12033

217. Bassetti M, Vena A, Croxatto A, Righi E, Guery B. How to manage Pseudomonas aeruginosa infections. *Drugs Context*. 2018;7:1-18. doi:10.7573/dic.212527

218. Nordmann P, Poirel L. Epidemiology and Diagnostics of Carbapenem Resistance in Gram-negative Bacteria. *Clin Infect Dis*. 2019;69(Suppl 7):S521-S528. doi:10.1093/cid/ciz824

219. Mulani MS, Kamble EE, Kumkar SN, Tawre MS, Pardesi KR. Emerging strategies to combat ESKAPE pathogens in the era of antimicrobial resistance: A review. *Front Microbiol*. 2019;10(APR). doi:10.3389/fmicb.2019.00539

220. Mensa J, Barberán J, Soriano A, et al. Antibiotic selection in the treatment of acute invasive infections by pseudomonas aeruginosa: Guidelines by the Spanish society of chemotherapy. *Rev Esp Quimioter*. 2018;31(1):78-100.

221. Doi Y. Treatment Options for Carbapenem-resistant Gram-negative Bacterial Infections. *Clin Infect Dis*. 2019;69(Suppl 7):S565-S575. doi:10.1093/cid/ciz830

222. Hurley MN, Cámara M, Smyth AR. Novel approaches to the treatment of Pseudomonas aeruginosa infections in cystic fibrosis. *Eur Respir J*. 2012;40(4):1014-1023. doi:10.1183/09031936.00042012

223. Tümmler B. Emerging therapies against infections with pseudomonas aeruginosa [version 1; peer review: 2 approved]. *F1000Research*. 2019;8:1-14. doi:10.12688/f1000research.19509.1

224. Cigana C, Bernardini F, Facchini M, et al. Efficacy of the novel antibiotic POL7001 in preclinical models of Pseudomonas aeruginosa pneumonia. *Antimicrob Agents Chemother*. 2016;60(8):4991-5000. doi:10.1128/AAC.00390-16

225. McKenna M. The antibiotic paradox: why companies can't afford to create life-saving drugs. *Nature*. 2020;584(7821):338-341. doi:10.1038/d41586-020-02418-x

226. Stover CK, Pham XQ, Erwin AL, et al. Complete genome sequence of Pseudomonas aeruginosa PAO1, an opportunistic pathogen. *Nature*. 2000;406(6799):959-964. doi:10.1038/35023079

227. Blair JMA, Webber MA, Baylay AJ, Ogbolu DO, Piddock LJV. Molecular mechanisms of antibiotic resistance. *Nat Rev Microbiol*. 2015;13(1):42-51. doi:10.1038/nrmicro3380

228. Davies J. Origins and evolution of antibiotic resistance. *Microbiologia*. 1996;12(1):9-16. doi:10.1128/mmbr.00016-10

229. Zgurskaya HI, López CA, Gnanakaran S. Permeability Barrier of Gram-Negative Cell Envelopes and Approaches to Bypass It. *ACS Infect Dis*. 2016;1(11):512-522. doi:10.1021/acsinfecdis.5b00097

230. Zgurskaya HI, Rybenkov V V. Permeability barriers of Gram-negative pathogens. *Ann N Y Acad Sci*. 2019;1459(Table 1):5-18. doi:10.1111/nyas.14134

231. Hancock REW, Brinkman FSL. Function of Pseudomonas porins in uptake and efflux. *Annu Rev Microbiol*. 2002;56:17-38. doi:10.1146/annurev.micro.56.012302.160310

232. Nikaido H, Yoshimura F. Permeability of Pseudomonas aeruginosa Outer Membrane to Hydrophilic Solutes. *J Bacteriol*. 1982;152(2):636-642.

233. Choi U, Lee CR. Distinct Roles of Outer Membrane Porins in Antibiotic Resistance and Membrane Integrity in Escherichia coli. *Front Microbiol*. 2019;10(APR):1-9.

doi:10.3389/fmicb.2019.00953

234. Mahendran KR, Kreir M, Weingart H, Fertig N, Winterhalter M. Permeation of antibiotics through Escherichia coli OmpF and OmpC porins: Screening for influx on a single-molecule level. *J Biomol Screen*. 2010;15(3):302-307. doi:10.1177/1087057109357791

235. Nestorovich EM, Sugawara E, Nikaido H, Bezrukov SM. Pseudomonas aeruginosa porin OprF. Properties of the channel. *J Biol Chem*. 2006;281(24):16230-16237. doi:10.1074/jbc.M600650200

236. Nikaido H, Nikaido K, Harayama S. Identification and characterization of porins in Pseudomonas aeruginosa. *J Biol Chem*. 1991;266(2):770-779.

237. Takase H, Nitanai H, Hoshino K, Otani T. Requirement of the Pseudomonas aeruginosa tonB gene for high-affinity iron acquisition and infection. *Infect Immun*. 2000;68(8):4498-4504. doi:10.1128/IAI.68.8.4498-4504.2000

238. Adams H, Zeder-Lutz G, Schalk I, Pattus F, Celia H. Interaction of TonB with the outer membrane receptor FpvA of Pseudomonas aeruginosa. *J Bacteriol*. 2006;188(16):5752-5761. doi:10.1128/JB.00435-06

239. Bitter W, Marugg JD, de Weger LA, Tommassen J, Weisbeek PJ. The ferric-pseudobactin receptor PupA of Pseudomonas putida WCS358: homology to TonB-dependent Escherichia coli receptors and specificity of the protein. *Mol Microbiol*. 1991;5(3):647-655. doi:10.1111/j.1365-2958.1991.tb00736.x

240. Koster M, van de Vossenberg J, Leong J, Weisbeek PJ. Identification and characterization of the pupB gene encoding an inducible ferric-pseudobactin receptor of Pseudomonas putida WCS358. *Mol Microbiol*. 1993;8(3):591-601. doi:https://doi.org/10.1111/j.1365-2958.1993.tb01603.x

241. Ankenbauer RG, Quan HN. FptA, the Fe(III)-pyochelin receptor of Pseudomonas aeruginosa: A phenolate siderophore receptor homologous to hydroxamate siderophore receptors. *J Bacteriol*. 1994;176(2):307-319. doi:10.1128/jb.176.2.307-319.1994

242. Noinaj N, Guillier M, Barnard TJ, Buchanan SK. TonB-dependent transporters: Regulation, structure, and function. *Annu Rev Microbiol*. 2010;64:43-60. doi:10.1146/annurev.micro.112408.134247

243. Tsutsumi K, Yonehara R, Ishizaka-Ikeda E, et al. Structures of the wild-type MexAB–OprM tripartite pump reveal its complex formation and drug efflux mechanism. *Nat Commun*. 2019;10(1):1-10. doi:10.1038/s41467-019-09463-9

244. Fraud S, Campigotto AJ, Chen Z, Poole K. MexCD-OprJ multidrug efflux system of Pseudomonas aeruginosa: Involvement in chlorhexidine resistance and induction by membrane-damaging agents dependent upon the AlgU stress response sigma factor. *Antimicrob Agents Chemother*. 2008;52(12):4478-4482. doi:10.1128/AAC.01072-08

245. Fetar H, Gilmour C, Klinoski R, Daigle DM, Dean CR, Poole K. mexEF-oprN multidrug efflux operon of Pseudomonas aeruginosa: Regulation by the MexT activator in response to nitrosative stress and chloramphenicol. *Antimicrob Agents Chemother*. 2011;55(2):508-514. doi:10.1128/AAC.00830-10

246. Morita Y, Tomida J, Kawamura Y. Mexxy multidrug efflux system of Pseudomonas aeruginosa. *Front Microbiol*. 2012;3(NOV):1-13. doi:10.3389/fmicb.2012.00408

247. Hirakata Y, Srikumar R, Poole K, et al. Multidrug efflux systems play an important role in the invasiveness of Pseudomonas aeruginosa. *J Exp Med*. 2002;196(1):109-118. doi:10.1084/jem.20020005

248. Nikaido H. Molecular Basis of Bacterial Outer Membrane Permeability Revisited. *Microbiol Mol Biol Rev*. 2003;67(4):593-656. doi:10.1128/mmbr.67.4.593-656.2003

249. Sugawara E, Nagano K, Nikaido H. Factors affecting the folding of Pseudomonas aeruginosa OprF porin into the one-domain open conformer. *MBio*. 2010;1(4):1-9. doi:10.1128/mBio.00228-10.

250. Sugawara E, Nagano K, Hiroshi N. Alternative Folding Pathways of the Major Porin OprF ofPseudomonas aeruginosa. *FEBS J*. 2012;279(6):910–918. doi:10.1111/j.1742-4658.2012.08481.x.Alternative

251. Gotoh N, Wakebe H, Yoshihara E, Nakae T, Nishino T. Role of protein F in maintaining structural integrity of the Pseudomonas aeruginosa outer membrane. *J Bacteriol*. 1989;171(2):983-990. doi:10.1128/jb.171.2.983-990.1989

252. Cassin EK, Tseng BS. Pushing beyond the envelope: The potential roles of oprf in pseudomonas aeruginosa biofilm formation and pathogenicity. *J Bacteriol*. 2019;201(18):1-12. doi:10.1128/JB.00050-19

253. Funken H, Bartels KM, Wilhelm S, et al. Specific Association of Lectin LecB with the

Surface of Pseudomonas aeruginosa: Role of Outer Membrane Protein OprF. *PLoS One*. 2012;7(10):1-8. doi:10.1371/journal.pone.0046857

254. Bauman SJ, Kuehn MJ. Purification of outer membrane vesicles from Pseudomonas aeruginosa and their activation of an IL-8 response. *Microbes Infect*. 2006;8(9-10):2400-2408. doi:10.1016/j.micinf.2006.05.001

255. Chevalier S, Bouffartigues E, Bodilis J, et al. Structure, function and regulation of Pseudomonas aeruginosa porins. *FEMS Microbiol Rev*. 2017;41(5):698-722. doi:10.1093/femsre/fux020

256. Hantke K. Phage T6 - colicin K receptor and nucleoside transport in Escherichia coli. *FEBS Lett*. 1976;70(1-2):109-112. doi:10.1016/0014-5793(76)80737-5

257. Nikaido H. Porins and specific channels of bacterial outer membranes. *Mol Microbiol*. 1992;6(4):435-442. doi:10.1111/j.1365-2958.1992.tb01487.x

258. Chevalier S, Bouffartigues E, Bodilis J, et al. Structure, function and regulation of Pseudomonas aeruginosa porins. *FEMS Microbiol Rev*. 2017;41(5):698-722. doi:10.1093/femsre/fux020

259. Pseudomonas Genome DB. https://pseudomonas.com/.

260. LaBauve AE, Wargo MJ. Detection of Host-Derived Sphingosine by Pseudomonas aeruginosa Is Important for Survival in the Murine Lung. *PLoS Pathog*. 2014;10(1). doi:10.1371/journal.ppat.1003889

261. Brinkman FSL, Hancock REW, Stover CK. Sequencing solution : use volunteer annotators organized via Internet. *Nature*. 2000;406:2000.

262. Bateman A. UniProt: A worldwide hub of protein knowledge. *Nucleic Acids Res*. 2019;47(D1):D506-D515. doi:10.1093/nar/gky1049

263. O'Leary NA, Wright MW, Brister JR, et al. Reference sequence (RefSeq) database at NCBI: Current status, taxonomic expansion, and functional annotation. *Nucleic Acids Res*. 2016;44(D1):D733-D745. doi:10.1093/nar/gkv1189

264. Van Den Berg B. Structural basis for outer membrane sugar uptake in pseudomonads. *J Biol Chem*. 2012;287(49):41044-41052. doi:10.1074/jbc.M112.408518

265. Modi N, Ganguly S, Bárcena-Uribarri I, Benz R, Van Den Berg B, Kleinekathöfer U. Structure, dynamics, and substrate specificity of the OprO porin from Pseudomonas aeruginosa. *Biophys J*. 2015;109(7):1429-1438. doi:10.1016/j.bpj.2015.07.035

266. Ganguly S, Kesireddy A, Bárcena-Uribarri I, Kleinekathöfer U, Benz R. Conversion of OprO into an OprP-like Channel by Exchanging Key Residues in the Channel Constriction. *Biophys J*. 2017;113(4):829-834. doi:10.1016/j.bpj.2017.07.004

267. Ye J, Berg B Van Den. Crystal structure of the bacterial nucleoside transporter Tsx. 2004;23(16):3187-3195. doi:10.1038/sj.emboj.7600330

268. Van Den Berg B, Black PN, Clemons WM, Rapoport TA. Crystal structure of the long-chain fatty acid transporter FadL. *Science (80-)*. 2004;304(5676):1506-1509. doi:10.1126/science.1097524

269. Hearn EM, Patel DR, Lepore BW, Indic M, Berg B Van Den. Transmembrane passage of hydrophobic compounds through a protein channel wall. *Nature*. 2009;458(7236):367-370. doi:10.1038/nature07678

270. Biswas S, Mohammad MM, Patel DR, Movileanu L, Van Den Berg B. Structural insight into OprD substrate specificity. *Nat Struct Mol Biol*. 2007;14(11):1108-1109. doi:10.1038/nsmb1304

271. Eren E, Parkin J, Adelanwa A, et al. Toward understanding the outer membrane uptake of small molecules by Pseudomonas aeruginosa. *J Biol Chem*. 2013;288(17):12042-12053. doi:10.1074/jbc.M113.463570

272. Eren E, Vijayaraghavan J, Liu J, et al. Substrate Specificity within a Family of Outer Membrane Carboxylate Channels. 2012;10(1). doi:10.1371/journal.pbio.1001242

273. Liu J, Movileanu L. OccK Channels from Pseudomonas aeruginosa Exhibit Diverse Single- Channel Electrical Signatures but Conserved Anion Selectivity. *Biochemistry*. 2012;51:2319−2330.

274. Biswas S, Mohammad MM, Movileanu L, van den Berg B. Crystal Structure of the Outer Membrane Protein OpdK from Pseudomonas aeruginosa. *Structure*. 2008;16(7):1027-1035. doi:10.1016/j.str.2008.04.009

275. Tamber S, Ochs MM, Hancock REW. Role of the novel OprD family of porins in nutrient uptake in Pseudomonas aeruginosa. *J Bacteriol*. 2006;188(1):45-54. doi:10.1128/JB.188.1.45-54.2006

276. Tamber S, Maier E, Benz R, Hancock REW. Characterization of OpdH, a Pseudomonas aeruginosa porin involved in the uptake of tricarboxylates. *J Bacteriol*. 2007;189(3):929-939. doi:10.1128/JB.01296-06

277. Liu J, Wolfe AJ, Eren E, et al. Cation selectivity is a conserved feature in the OccD subfamily of Pseudomonas aeruginosa. *Biochim Biophys Acta - Biomembr*. 2012;1818(11):2908-2916. doi:10.1016/j.bbamem.2012.07.009

278. Parkin J, Khalid S. Atomistic molecular-dynamics simulations enable prediction of the arginine permeation pathway through occd1/oprd from pseudomonas aeruginosa. *Biophys J*. 2014;107(8):1853-1861. doi:10.1016/j.bpj.2014.08.035

279. Samanta S, Bodrenko I, Acosta-Gutiérrez S, et al. Getting Drugs through Small Pores: Exploiting the Porins Pathway in Pseudomonas aeruginosa. *ACS Infect Dis*. 2018;4(10):1519-1528. doi:10.1021/acsinfecdis.8b00149

280. Barbachyn MR. *Oxazolidinone Antibacterial Agents*.; 2014. doi:10.1007/978-1-4614-1400-1_8

281. Shu JC, Kuo AJ, Su LH, et al. Development of carbapenem resistance in Pseudomonas aeruginosa is associated with OprD polymorphisms, particularly the amino acid substitution at codon 170. *J Antimicrob Chemother*. 2017;72(9):2489-2495. doi:10.1093/jac/dkx158

282. Farra A, Islam S, Strålfors A, Sörberg M, Wretlind B. Role of outer membrane protein OprD and penicillin-binding proteins in resistance of Pseudomonas aeruginosa to imipenem and meropenem. *Int J Antimicrob Agents*. 2008;31(5):427-433. doi:10.1016/j.ijantimicag.2007.12.016

283. Ochs MM, McCusker MP, Bains M, Hancock REW. Negative regulation of the Pseudomonas aeruginosa outer membrane porin OprD selective for imipenem and basic amino acids. *Antimicrob Agents Chemother*. 1999;43(5):1085-1090. doi:10.1128/aac.43.5.1085

284. Ochs MM, Lu CD, Hancock REW, Abdelal AT. Amino acid-mediated induction of the basic amino acid-specific outer membrane porin OprD from Pseudomonas aeruginosa. *J Bacteriol*. 1999;181(17):5426-5432. doi:10.1128/jb.181.17.5426-5432.1999

285. Kos VN, McLaughlin RE, Gardner HA. Identification of unique in-frame deletions in OprD among clinical isolates of Pseudomonas aeruginosa. *Pathog Dis*. 2016;74(4):ftw031. doi:10.1093/femspd/ftw031

286. Somboon K, Niramitranon J, Pongprayoon P. Probing the binding affinities of imipenem and ertapenem for outer membrane carboxylate channel D1 (OccD1) from P. aeruginosa: simulation studies. *J Mol Model*. 2017;23(8). doi:10.1007/s00894-017-3400-2

287. Shen J, Pan Y, Fang Y, Sekaran SD. Role of the outer membrane protein OprD2 in carbapenem-resistance mechanisms of pseudomonas aeruginosa. *PLoS One*. 2015;10(10):1-9. doi:10.1371/journal.pone.0139995

288. Isabella VM, Campbell AJ, Manchester J, et al. Toward the rational design of carbapenem uptake in pseudomonas aeruginosa. *Chem Biol*. 2015;22(4):535-547. doi:10.1016/j.chembiol.2015.03.018

289. Cooper SJ, Krishnamoorthy G, Wolloscheck D, et al. Molecular Properties That Define the Activities of Antibiotics in Escherichia coli and Pseudomonas aeruginosa. *ACS Infect Dis*. 2018;4(8):1223-1234. doi:10.1021/acsinfecdis.8b00036

290. Mwangi J, Yin Y, Wang G, et al. The antimicrobial peptide ZY4 combats multidrugresistant Pseudomonas aeruginosa and Acinetobacter baumannii infection. *Proc Natl Acad Sci U S A*. 2019;116(52):26516-26522. doi:10.1073/pnas.1909585117

291. Yasir M, Dutta D, Willcox MDP. Comparative mode of action of antimicrobial peptide melimine and its derivative Mel4 against Pseudomonas aeruginosa. *bioRxiv*. 2018;(March):1-12. doi:10.1101/450577

292. Ruden S, Rieder A, Chis Ster I, Schwartz T, Mikut R, Hilpert K. Synergy Pattern of Short Cationic Antimicrobial Peptides Against Multidrug-Resistant Pseudomonas aeruginosa. *Front Microbiol*. 2019;10(November). doi:10.3389/fmicb.2019.02740

Johanna Viola Ude

+41 78 247 14 76 | johanna.ude@live.de | Basel, Switzerland | Johanna Ude

Education

PhD, Biozentrum, University of Basel, 2016 - 2021

Master of Science in Life Science, University of Konstanz, 2011 - 2014

Bachelor of Science in Life Science, University of Konstanz, 2008 - 2011

Abitur, St. Ursula Gymnasium, Freiburg, 2007

Fellowships

Fellowships for Excellence for PhD studies at the Biozentrum, University of Basel

Doktoranden-Stipendium der Heinrich-Böll-Stiftung (declined)

Soft Skills

Independent working style

Creative and curious approach to problem-solving

High emotional intelligence

Excellent writing and presentation skills

Excellent communication skills

Key Skills

- Recombinant protein expression in *E. coli*, isotopic labelling
- Protein purification (FPLC based chromatography methods, protein refolding)
- SDS-PAGE and Westernblot
- NMR spectroscopy of proteins (sample preparation, experimental setup, backbone and side chain assignment, analysis, structure calculation)
- Biophysical and biochemical methods (MST, SEC MALS, Fluorescence Anisotropy Measurements, Protein Aggregation Assays, DLS, Thermostability tests, colorimetric assays)
- Mutagenesis and expression vector/construct design

Additional Skills

- Microscopy (Live Cell Imaging, Fluorescence Correlation Spectroscopy, Transmission Electron microscopy)
- bacterial and human cell cultures (*E. coli, P. aeruginosa,* HeLa cells)
- Python Scripting for data analysis and visualisation
- Proficiency with Apple and Windows devices, MS Office, electronic lab books

Research Experience

PhD in the research group of Prof. Sebastian Hiller, 2016 - 2021: *"Solution NMR studies of J-domain co-chaperones and bacterial outer membrane permeability"*

Project 1: Characterisation of J-domain co-chaperones

Conceptualisation of the project from scratch ranging from forming the research question to finalising a publication. Characterisation of three different J-domain proteins and their interaction with the ubiquitous chaperone Hsp70 including the elucidation of protein structures, dynamics, biophysical and biochemical characteristics, ATPase activities and their regulation and liquid-liquid-phase separation behaviour. Supervision of students during their internship.

Project 2: Investigation of nutrient and antibiotic uptake in *P. aeruginosa*

Our integrative approach combined extensive mutagenesis with NMR spectroscopy and microbiological experiments to unravel pathways of antibiotic and nutrient uptake across the outer membrane in *P. aeruginosa*. This project evolved as collaboration with the research group of by Prof. Dirk Bumann (Biozentrum Basel).

Language Skills

German (native)

English (fluent)

French (advanced)

Italian (basic)

Spanish (basic)

Extracurricular Activities

Organisation of public scientific events:

- lecture series on structural biology and biophysics (SBBS)
- international conference held at the Biozentrum Basel

Active participation in the PhD representative board:

- student representation
- organisation of monthly student talks and social activities

Teaching assistant at the University of Basel and Konstanz

Invited talks

Dr. Mathias Feige, TU München, 2020:

"GF-linkers of J-domain proteins as regulatory element for Hsp70-J-domain interactions"

Prof. Paolo De Los Rios, EPFL Lausanne, 2018:

"NMR studies of the J-domain protein ERdj3 and its interaction with client proteins"

Project 3: Exploration of inflammasome regulation

Establishment of an *in vitro* assay to develop inhibitors against the filament formation of the ASC-protein during inflammation. It included the screening of a library of small molecules and the investigation of several inhibitory proteins.

Research Assistant, University of Potsdam, Research Group of Prof. Heiko Möller 2014 - 2015:

Expression, purification and NMR experiments of proteins involved cytoskeletal dynamics. Supervision of one Bachelor and Master thesis.

Master of Science in Life Science, University of Konstanz, 2011 - 2014, Master thesis, Research Group of Dr. Heiko Möller: **"**NMR studies with the Na^+-translocating NADH:quinone oxido-reductase from *V. cholerae"*

Research Internship at Centre d'Immunologie de Marseille-Luminy, Research group of Dr. D. Marguet, 2013:

Application of Advanced microscopy methods such as Fluorescence Correlation Spectroscopy, single molecule technologies to study membrane dynamics in Natural Killer cells.

Bachelor of Science in Life Science, University of Konstanz, 2008 - 2011, Bachelor Thesis, Research group Prof. Zumbusch:
"Investigations of transport and fusion processes of lipid droplets in living human cells by fluorescence microscopy"

Conferences and Courses

- Zoom@Novartis (Career Coaching program at Novartis) , 2020
- EMBO Young Investigator Program for Science Communication and Career Development, 2019
- Euromar Conference, 2019 (poster presentation)
- Communication and Negotiation, 2018
- EMBO course for theoretical practical protein NMR spectroscopy, 2016 and 2018
- FASEB conference on protein folding, 2017 (poster presentation)
- Project Management, 2017
- PhD retreat, internal at the Biozentrum, 2016 and 2018 (poster presentation)

Publications

Ude, J., Mas, G. And Hiller, S. The endoplasmatic reticulum-specific regulation of a Hsp40 GF-region drives its LLPS, *in preparation*

Ude, J. et al. Outer membrane permeability: Antimicrobials and diverse nutrients bypass porins in Pseudomonas aeruginosa . Proc. Natl. Acad. Sci. 118, (2021).

Sborgi, L., Ude, J. and Hiller, S. Assay for high-throughput screening of inhibitors of the ASC-PYD inflammasome core filament, *Cell Stress*, 2, 82 – 91 (2017)